論文 / 著書情報
Article / Book Information

題目(和文)	
Title(English)	On the photostability of polythiophene based organic solar cells
著者(和文)	青山嘉憲
Author(English)	Yoshinori Aoyama
出典(和文)	学位:博士(工学), 学位授与機関:東京工業大学, 報告番号:甲第9496号, 授与年月日:2014年3月26日, 学位の種別:課程博士, 審査員:吉田　郵司,小田原　修,近藤　道雄,長井　圭治,和田　裕之
Citation(English)	Degree:Doctor (Engineering), Conferring organization: Tokyo Institute of Technology, Report number:甲第9496号, Conferred date:2014/3/26, Degree Type:Course doctor, Examiner:,,,,
学位種別(和文)	博士論文
Type(English)	Doctoral Thesis

On the photostabilty of polythiophene based organic solar cells

Yoshinori Aoyama

Interdisciplinary Graduate School of
Science and Engineering
Tokyo Institute of Technology

2014

Supervisors

Prof. Yuji Yoshida
Tokyo Institute of Technology
National Institute of Advanced Industrial Science and Technology (AIST)

Prof. Osamu Odawara
Tokyo Institute of Technology

Pre-examiners

Prof. Michio Kondo
Tokyo Institute of Technology
National Institute of Advanced Industrial Science and Technology (AIST)

Associate Prof. Hiroyuki Wada
Tokyo Institute of Technology

Associate Prof. Keiji Nagai
Tokyo Institute of Technology

Contents

Outline of thesis

Recently, the expectation for power generation by renewable energy has been dramatically increasing in terms of the world environmental preservation. Especially, solar cell has a big advantage because of infinite solar energy. As one of solar cells, polymer solar cells (PSCs) have many potential advantages such as low cost, mechanical flexibility, simple manufacturing, and improving power conversion efficiency. Therefore, an early commercialization is expected in these days. However, it is known that the PSCs rapidly degrade during irradiation. This degradation are very complicated and investigated conventionally by only physical approach such as power conversion characteristics by *I-V* measurement, charge traps by ESR or CELIV measurement, BHJ structure by AFM or TEM measurement, and so on. In contrast, these physical phenomenon has not been investigated in conjunction with

organic molecular chemical approach. Here, in this research, we are focusing on the photooxidation of organic layer and investigated these physical phenomenon by approaching from chemical review.

The thesis is based on four papers and divided into five chapters. In Chapter 1, a comprehensive PSCs degradation and my research approaches are provided. Chapter 2 shows PSC device performance deterioration by only initially photo-damaged organic layer. Chapter 3 highlights the elucidation of photoactive species in the p-type semiconductor polymer P3HT. In Chapter 4, based on the photooxidation mechanism triggered by the photoactive species, the challenge to photo-stable polythiophene derivatives are mentioned. Chapter 5 provides a summary of this thesis.

The research in this thesis has been done in the Research Center for PhotoVoltaic Technology (RCPVT) in National Institute of Advanced Industrial Science and Technology (AIST), Université de Mons (UMONS) and Materials R&D Centre (MateriaNova). RCPVT in AIST is japanese representative organization and researching some kind of solar cells including organic solar cells. UMONS and MateriaNova are also bellgium research organization and researching solid state physics of organic materials and organic electronics, respectively.

1. Introduction

This chapter provides a brief motivation to photodegradation of polymer solar cells and its material research in terms of general view. The brief backgroud of energy sociey and solar cells is given in 1.1.,1.2 The general photodegradation of polymer solar cells is explained in 1.3. Following the section, my research approach is mentioned in 1.4.

1.1 Background

Recently, the expectation for electrical power generation by renewable energy has become rising in terms of the world environmental preservation. Renewable energy is generally defined as energy that comes from resources which are continually replenished on a human timescale such as sunlight, wind, rain, tides, waves and geothermal heat. (**Figure 1.1**) [1] Solar energy has a big advantage because of its infinite energy and therefore solar power has been attracted and has already used as some kind, for example, solar heat and solar light. Solar cell

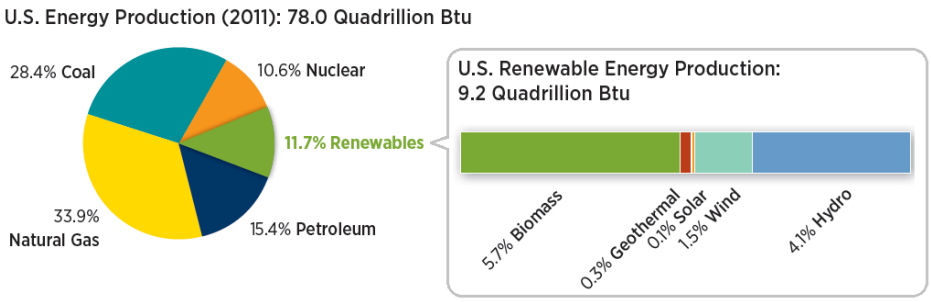

Figure 1.1 *U. S. Energy production (2011) (by http://www.nrel.gov/docs/fy13osti/54909.pdf).*

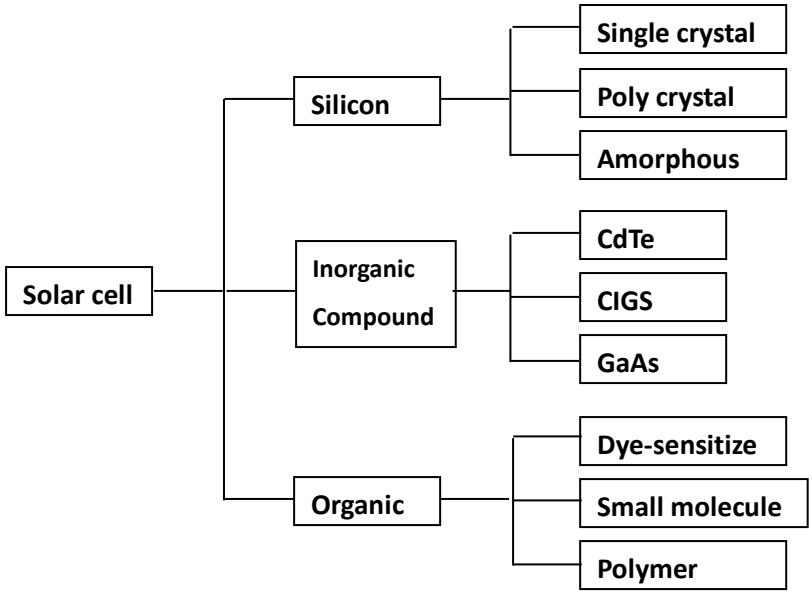

Figure 1.2 *The classification of general solar cells.*

voltaic is based on a absorption of solar light and this is more complicated voltaic mechanism than solar heat voltaic. Solar cell is diveded into two main cells by kinds of photovoltaic materials by light absorption. One cell is composed of inorganic materials such as silicone, GaAs, CIGS (Cu, In, Ga, Se), CdTe and so on.(**Figure 1.2**) The other cell is composed of organic materials such as organic dye, π-conjugated low molecule, and conductive polymer. Inorganic solar cells was fully researched, and have already began to contribute to our society by commercialization. In contrast, organic solar cell has a short history and is still the research stage.[2] One of the most researched organic solar cells for commercialization is polymer solar cells (PSCs). One of advantages of PSCs is easy fabrication, which can mainly be fabricated by printable wet process without vacuum process, and therefore relatively spend lower cost than that of small molecule solar cells. This easy process can make PSCs large-scale production, and production research of PSCs has began to be progressed (**Figure 1.3**) [3,4].

Furthermore, researches on power conversion efficiencies of PSCs has been conducted a lot all over the world, and power conversion efficiency has been improved in the recent decade (Figure 1.3). On the other hand, PSCs has a big problem to degrade rapidly during illumination, and the performance decrease by the degradation prevents commercialization (Figure. 1.3) [5]. In contrast to the progress in process tequnique and efficiency, research about stability has not progressed yet. For stable PSCs, it is important to clear the degradation mechanism in order to develop the encapsulation technique and to realize photostable polymer in the next stage. Detailed photo-degradation problems of

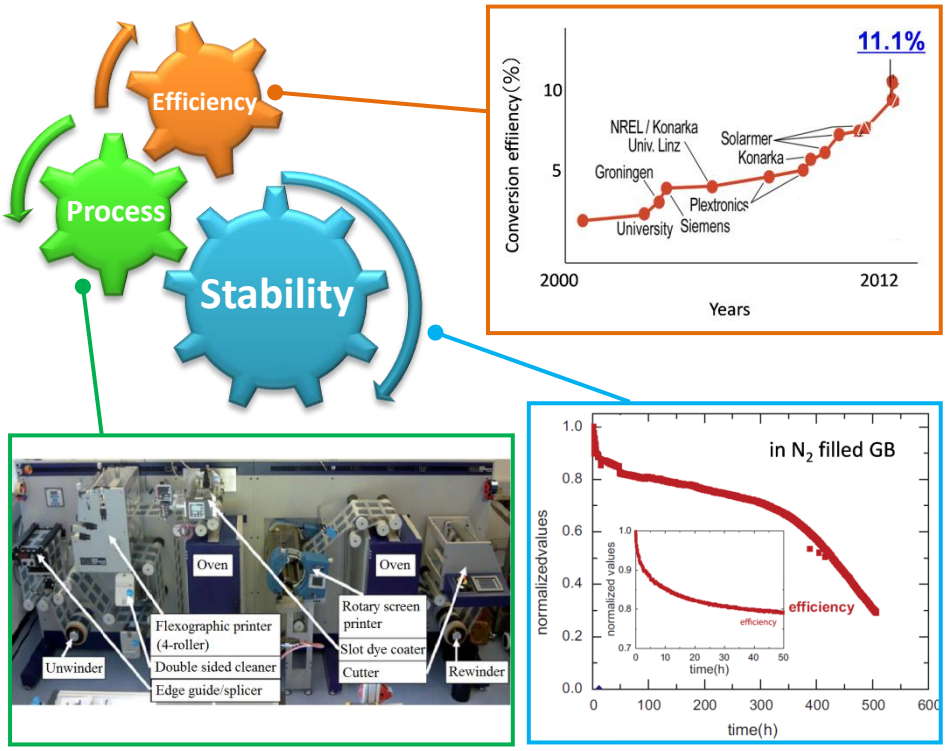

Figure 1.3 *The three approaches for commercialization of PSCs, and present situation of highly efficiency chart of OPV[3], process technique[4] and efficiency decrease.[5]*

PSCs will be described in 1.3 section.

1.2 Polymer solar cells and its photovoltaic principle

Before explaining the degradation problem, general sturucture of PSCs and its photovoltaic principle are mentioned, which are shown in **Figure 1.4**. In the device, glass, transparent electrode, buffer layer, organic layer, metal electrode are stacked. Indium tin-oxide (ITO) is used as transparent electrode, poly(3,4-ethylenedioxythiophene) / polystylene sulfonate (PEDOT-PSS) is used as buffer layer. These materials needs high transparency in visible light because of the light pass for organic material to absorb the light. In the organic layer, Poly(3-hexyl thiophene) (P3HT) and [6,6]-phenyl-C61-butyric acid methyl ester (PCBM) are one of the most used p-type semiconductors (Donor) and n-type semiconductors (Acceptor), respectively. These materials are blended uniformly and forms bulk heterojunction

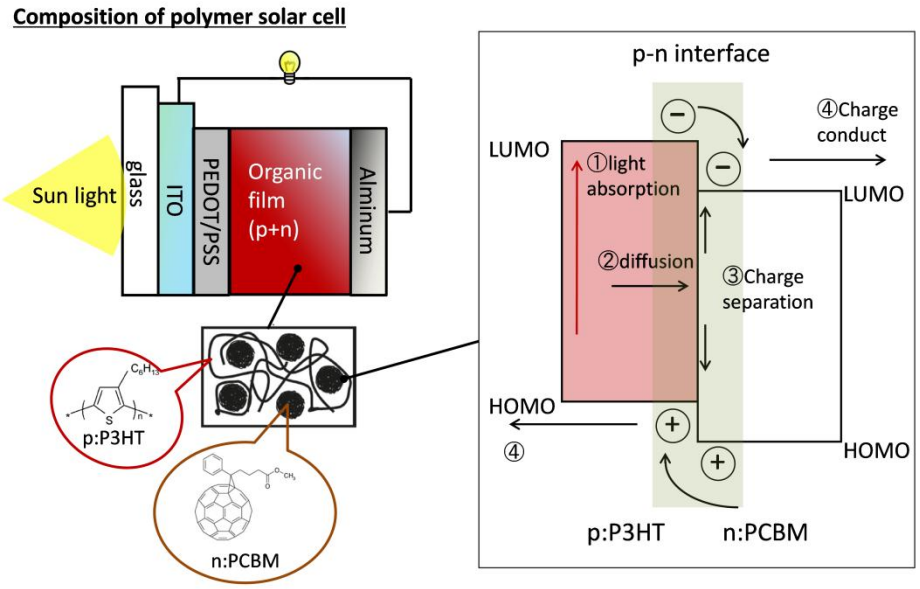

Figure 1.4 *The general composition of polymer solar cells (PSCs) and power conversion mechanism of PSCs.*

structure in which each material aggregates moderately in nano size and forms electron passway. At p-n interface, firstly P3HT (and PCBM) absorbs visible light and become excited state ([P3HT*]) in which hole-electron weakly binded pair (called exciton) are formed. Secondly, the exciton diffuses and then only the exciton reaching the p-n interface can separate to hole and electron by internal electrical field power. Fourthly, each charge conduct though each material and this charge stream forms current and electrical power. Alminum is used as metal electrode on top of the organic layer. Next, the electrical power by using the equivalent cirquit and *I-V* curve is shown in **Figure. 1-5**.[6,7]

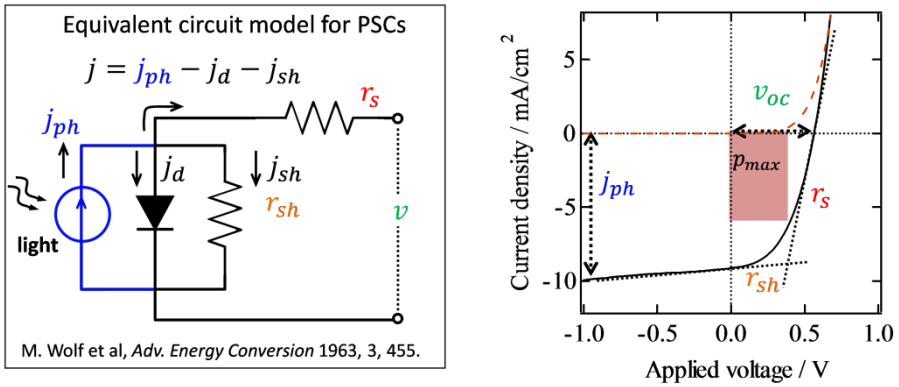

Figure 1.5 *The equivalent circuit model of PSCs which is denoted in M. Wolf et al*[6]*, and I-V curve with (--) dark and (−) light.*

This equivalent circuit is mentioned by the combination of constant current source (j_{ph}), parallel diode (j_d), series resistance (r_s), and shunt resistance (r_{sh}). Ideally, output power (J) is equal to the constant current source (J_{ph}), but in fact internal loss arises because solar cell is p-n diode device. This internal current loss (J_d) is dependent on operating voltage (v) and mentioned by the below equation (1.1).

$$j_d = j_0 \left\{ \exp\left(\frac{q(v+jr_s)}{n_d kT}\right) - 1 \right\}. \quad (1.1)$$

In this equation, j_o is inversed sirtulated current, q is elementary charge, n_d is diode factor, k is Boltzman constant, and T is absolute temperature. The inversed sirtulated current is derived from a diffusion of a few carrier in diode, and estimated by the dark current (when $v < 0$, exponential term is apporoximated by 0). The diode factor is coefficient to decide the diode characteristics which is close to 1 when the diode is ideal p-n junction. In addition, leak current loss (j_{sh}) also arises because of the mismatch among materials in device, which is mentioned by the below equation (1.2).

$$j_{sh} = \frac{v+jr_s}{r_{sh}}. \quad (1.2)$$

Therefore, real output power (J) is mentioned by the below equation (1.3), (1.4).

$$j = j_{ph} - (j_d + j_{sh}). \quad (1.3)$$

$$= j_{ph} - \left(j_0 \left\{ \exp\left(\frac{q(v+jr_s)}{n_d kT}\right) - 1 \right\} + \left(\frac{v+jr_s}{r_{sh}}\right) \right). \quad (1.4)$$

In equation (1.3), (j_d + j_{sh}) is dark current. As the photodiode current and leakage current have also a small current when it is reversed biased near 0 (v), the extra current caused by the light in this reversed bias is called the photocurrent (j_{ph}), as shown in I-V curves. In addition, the current when the device was short-circuited (v = 0) is called short circuit current (j_{sc}) , and this means the highest hole and electron stream formed by the light without the vias. But the j_{sc} is not necessarily equal to the j_{ph} because of a small leakage current, and therefore this

defference is mainly dependent on the r_{sh} and the slope ($\delta j/\delta v$) ($v \rightarrow 0$) is approximated by ($1/r_{sh}$). Furthermore, the voltage when the device was open-circuited ($j = 0$) is called open circuit voltage (v_{oc}), and this means the power enough to stop the hole and electron stream formed by the light. Therefore, this value is dependent on the energy difference between the hole stream energy (HOMO in p-type semiconductor) and the electron stream energy (LUMO in n-type semiconductor) (see fig. 1-4). But the value is also not necessarily equal to the energy difference because of a small hole and electron trap near the each energy level. In the V_{oc}, the slope ($\delta j/\delta v$) ($j \rightarrow 0$) is approximated by ($1/r_s$). At any given point (j, v) on *I-V* curve ($0 < j < j_{sc}$, $0 < v < v_{oc}$), generating max power output is mentioned by the below equation (1.5).

$$p_{max} = j_{max} v_{max}. \quad (1.5)$$

This means that p_{max} shows a largest rectangular area (see Fig. 1.4). This area is also mentioned by the below ratio (1.6).

$$\mathrm{FF} = \frac{j_{max} v_{max}}{j_{sc} v_{oc}} \leftrightarrow p_{max} = FF \cdot j_{sc} v_{oc}. \quad (1.6)$$

This FF is called Fill Factor and means area ratio. This value is highly dependent on r_s and r_{sh}, for example, when $r_s \rightarrow 0$, and $r_{sh} \rightarrow \infty$, the p_{max} rectangular area become close to the $j_{sc}v_{oc}$ area and FF become close to 1. FF is often used because max power output can be easily obtained by multipling it, j_{sc}, and v_{oc}. Then, this power conversion can be mentioned by using next equation (1.7).

$$\eta = \frac{p_{max}}{p_i S} \times 100[\%]. \quad (1.7)$$

where p_i is sun light energy density (W/m^2) and S is valid area (m^2) of PSCs, therefore the denominator shows sun light power. So, this equation means how much convert the sunlight energy to electrical energy.

1.3 Photodegradation of polymer solar cells

As it is mentioned above (1.2), to realize commercialization, it is important to clear PSCs degradation problem, in which general degradation factor is already proposed by one of the most famous researchers F. C. Krebs and M. Jørgensen et al, as shown in **Figure 1.9**.

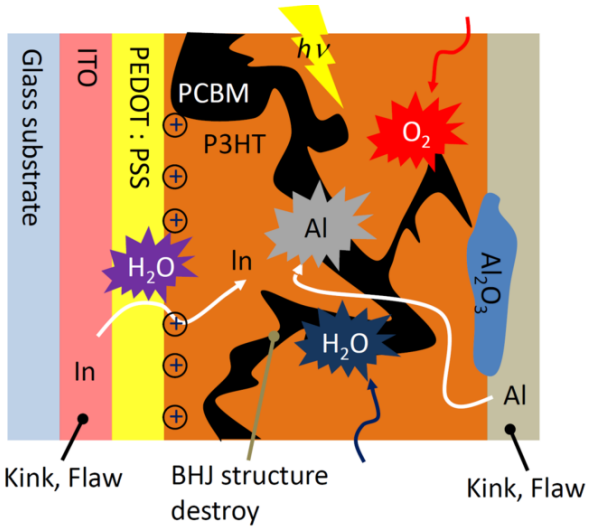

M. Jørgensen et al, *Sol. Energy Mater. Sol. Cells* 2008, 92, 686.

Figure 1.9 *General degradation factors proposed by F. C. Krebs and M. Jørgensen et al.*[8]

According to their report [8], the degradation factors were separated mainly as follows;

1) Organic material degradation by ultraviolet light, oxygen, water and so on

2) BHJ nanostructure break (change to bad p-n separation) in organic layer
3) Electrode break (Metal oxidation, ITO kink, Flaws)
4) Charge trap effect at the interface between each materials

In the device degradation, the effect of 1) and 2) to the device are only assumption because these investigation is not conducted in a complete device but in the state of an isolated simple organic film. This is because the organic layer was sandwiched between both anode and cathode electrodes and we can not investigate the layer directly. I will simply describe each phenomenon by using some reports[9] as follows;

1) Photochemical electroconductive polymer degradation is owing to the decomposition of the materials, which can lead to disruption of the π-conjugation. One of the widely accepted mechanisms of photo-oxidation and thermo-oxidation of P3HT claims that degradation originates from singlet oxygen photosensitisation. Once formed, the singlet oxygen undergoes a Diels–Alder cycloaddition with the thienyl unit of P3HT[10] (**Scheme. 1.1**), ultimately forming

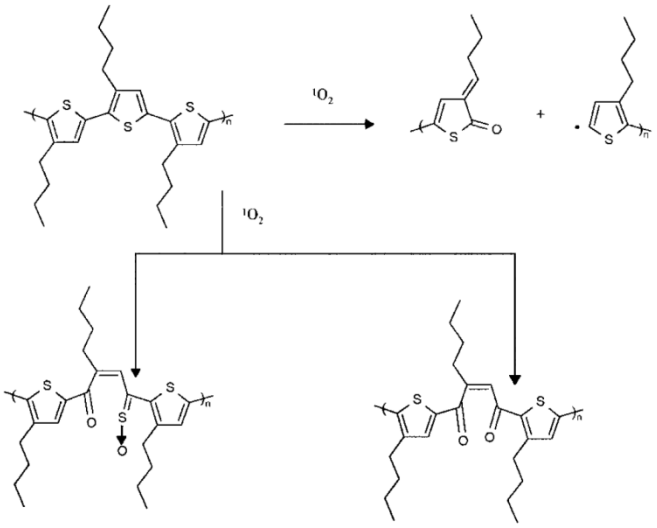

Scheme 1.1 *Typical thiophene oxidation by singlet oxygen by Carnona et al[10].*

an unstable endo-peroxide. The latter subsequently decomposes into sulfine and ketone, among others, which leads to disruption of the π-conjugation. Alternatively, the P3HT side chain can also be oxidized via a free-radical oxidation route, thus forming hydroxyl and carbonyl adducts. In contrast, as a recent report[11], these carbonyl- and sulfur moieties come from the degradation of the side chains (α-carbon atom of the hexyl group of P3HT which is the chemically weakest C–H bond) and of the backbone of the polymer, respectively. Manceau et al. list three types of degradation paths (**Scheme 1.2**): (i) the H-abstraction reaction of alkoxy radicals leading to the formation of an α-unsaturated alcohol, (ii) the cage reaction of alkoxy radicals with OH· leading to the formation of an aromatic ketone; the latter is unstable when irradiated at wavelengths lower than 400 nm and undergoes a Norrish photolysis, leading to the formation of aromatic carboxylic acid groups and

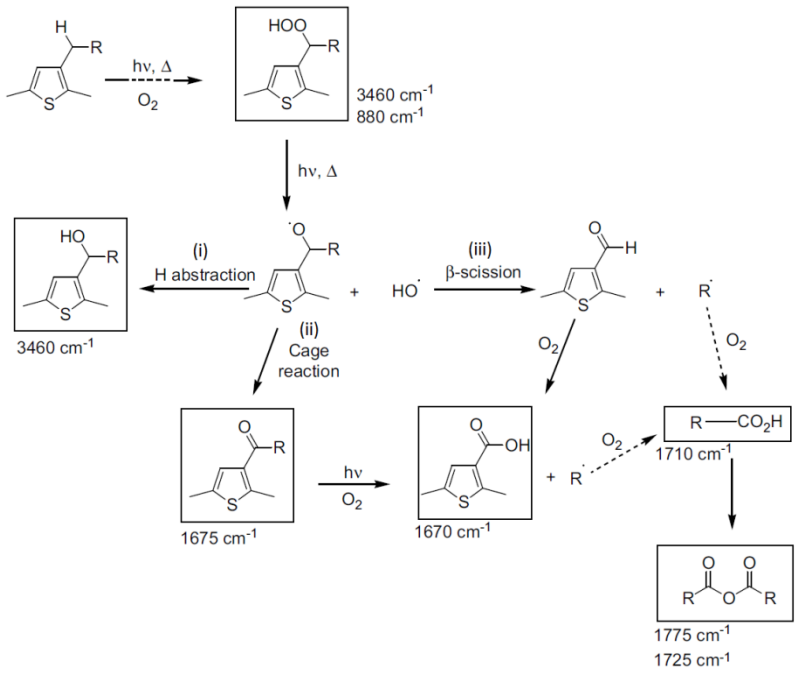

Scheme 1.2 *Initial reaction by H-abstraction and three types of degradation paths denoted by Manceau et al* [11].

alkyl radicals oxidized into aliphatic acids, and (iii) β-scission leading to the formation of an aromatic aldehyde that rapidly oxidizes into carboxylic acids. Additionally, the S atoms present in the polymer backbone can first be oxidized into sulfoxides, then to sulfones that decompose into carboxylic acids, see **Scheme 1.3**. On the other hand, as we can understand from scheme 1.1-1.3, the unified photooxidation mechanism are not realized, and under investigation.

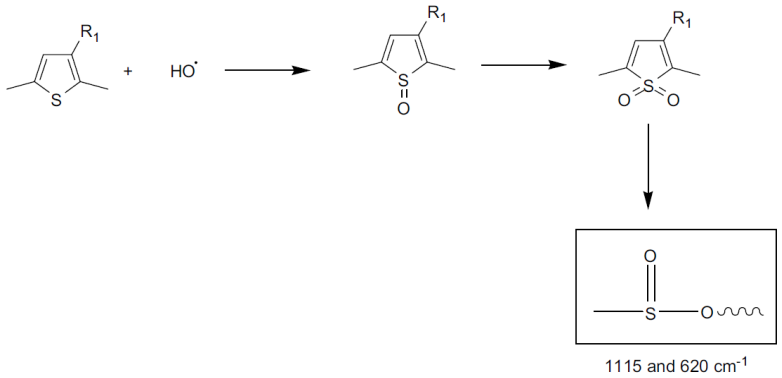

Scheme 1.3 *Thiophene ring oxidation reaction by OH・ denoted by Manceau et al* [11].

Fullerene derivatives are also decomposed by light and heat. But it is harder to be decomposed than that of polymer because HOMO energy was deeper (over 1.0 eV) than that of polymer. As example of report[12], oxidation proceeds via addition of oxygen to the fullerene molecules to form epoxidic species (C_{60} > O, i.e. two different C atoms, each of them linked to one O atom by a single bond) and C_{60}=O (C=O double bond), shown in **Figure 1.10**. C–O single bond formation was reported at temperatures in the range of 100 ^{o}C, which is higher than the expected device working temperatures, but which can possibly be reached during processing (it's no problem to prepare in GB). Fullerene cages which are linked with a single bond to atomic oxygen were reported to further

decompose and polymerize after 1000 h of heating at 80 ^{o}C, which may be similar to conditions when using these solar cells in hot climates and can be detrimental to cell performances.

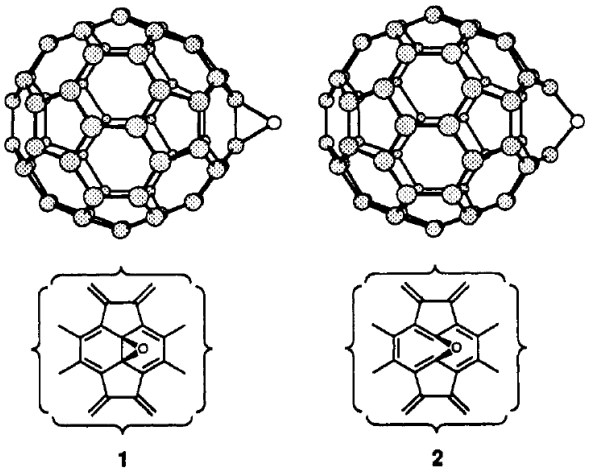

Figure 1.10 *Epoxidic species (C_{60} > O) on fullerene by oxidation by Wohlers et al* [12].

Importantly, it has been shown by several researchers that conjugated polymer photodegradation is mitigated and its kinetics seriously reduced up to a few orders of magnitude when the polymer is mixed with an acceptor fullerene derivative [9,13]. This behavior has been explained by both radical scavenging of the fullerene derivative molecule and its ability to quench the P3HT singlet state.

2) BHJ structure

In a bulk heterojunction cell, the organic film morphology is a key parameter to control the performance of the OPV cells. Photocurrent generation requires uniform A/D blending with domain sizes in the order of about twice the exciton diffusion length (~30 nm), whereas charge transport requires continuous paths from the D/A interface to the electrodes. Therefore, when the nanoscale morphology changes and p-n domain size and number decrease,

this means change to bad phase separation state and device performance become degraded. It is generally considered that the BHJ structure destroy is often triggered by the moving of molecules by heating (annealing) over the T_g (glass transition temperature) in the real device. Some example are shown in below[14] (**Figure. 1.11**).

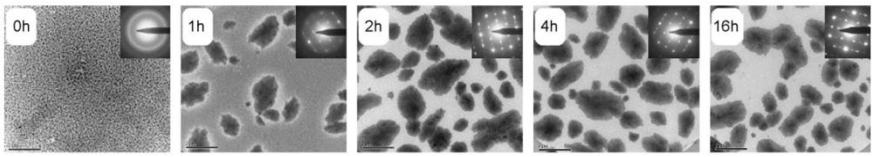

Figure 1.11 *Morphology changes in the active layer (MDMO-P PV:PCBM = 1:4) as a result of annealing at 110 ^oC for 0, 1, 2, 4, 16h denoted by Bertho et al[14].*

In the fig 1.11, the formation of large PCBM-clusters with annealing are observed. This is explained by the low T_g of polymer (MDMO-PPV), which becomes a little soft over the T_g , and then PCBM becomes easy to aggragate by its self-assemblization. This is a very extreme example for explanation of the BHJ structure destroy, but also in the real device degradation using P3HT, these phenomenon may happen to some extent. (the T_g of P3HT is higher (150 ^{o}C) than that of MDMO-PPV)

The organic monolayer degradation phenomenon in real device has not been shown. On the other hand, device degradation are generally investigated by mainly physical approach from the viewing of complete device, for example, I-V charasteristics (signal) change with phenomenon change (gas or temperature... with irradiation), material change (some buffer layer, electrode...), impedance spectroscopy signal with irradiation to find out some kind of resistance, electron spin resonance measurement (ESR) and Charge-carrier extraction by linearly increasing voltage measurement (CELIV) to observe charge trap signal, scanning electron microscope measurement (SEM) and

transmission electron microscope measurement (TEM) to get image of sterical structural change of organic layer (P3HT fibril structure, surface aggeragation size...) and some flaw like kink in electrode. One of examples are mentioned in below.

1) I-V measurement

The most popular investigation way is simply to trase the *I-V* characteristics with or without irradiation, of changing materials in device, and of changing gas atmosphere. The below figure (**Fig. 1.12**) shows I-V characteristics change with different gas atmosphe-

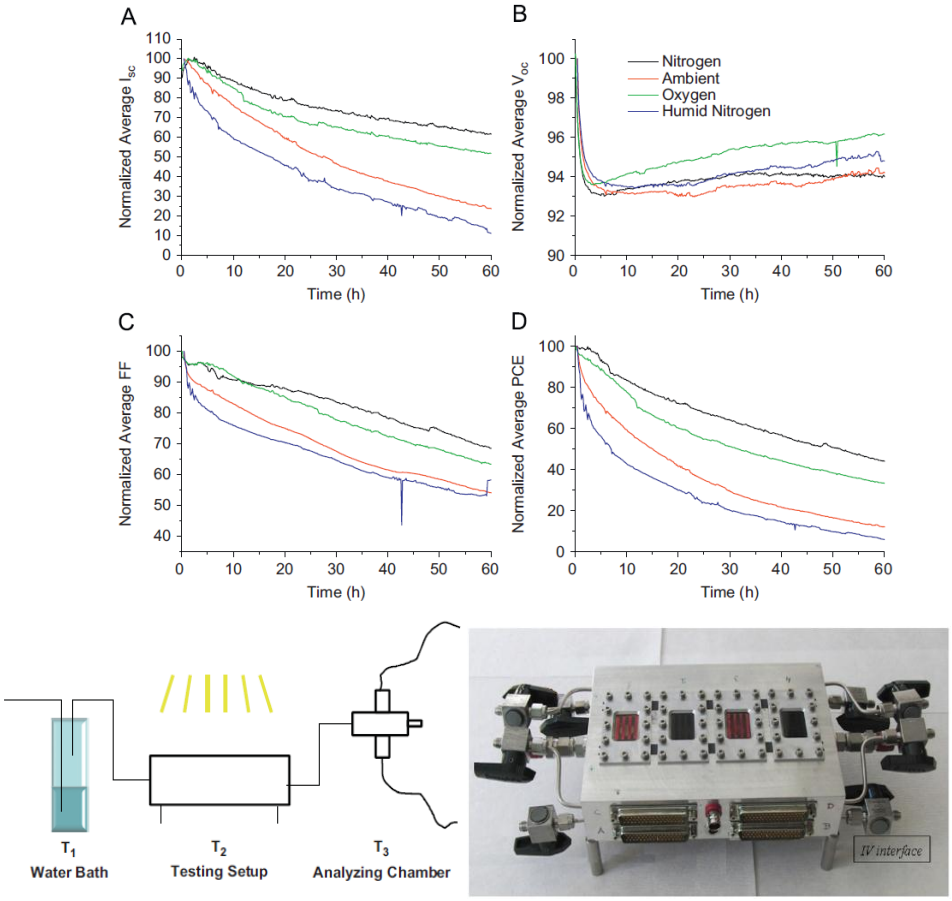

Figure 1.12 *I-V characteristics change during 60h irradiation with different gas atmosphere and experimental setup, denoted by Gevorgyan et al* [15].

re and experimental setup [15]. According to this report, in the initial irradiation performance, it really seems that the humidity in gas is key, and they explained the degradation reason is mainly because of the deactivation of PEDOT:PSS, whose PSS easily absorbs water molecule. In addition, oxygen may also become degradation reason which photooxidizes organic material. Regarding the effect of PEDOT:PSS, another research group also reported the degradation difference by changing buffer layer and comparing I-V characteristics with irradiation. They reported that the performance degradation was surpressed by changing PEDOT:PSS to inorganic MoOx.

2) Charge trap

Charge trap (cation and anion) are also generally observed in organic electronics, and this measurement is one of the most popular way. Normally, charge trap is formed at different material interface [16] where work function difference between each materials forms schottkey barrier, and some charges can not go over the barrier and therefore are trapped there during charge conduction. Because the charge trap quenches exciton, at the last, it is considered that the carrier decrease and result in device performance deteriolation [17]. Kawano et al. reported the phenomenon of charge trap in polymer solar cells by using Thermally Stimulated Current (TSC) measurement [18]. They focus on a release of charge trap by thermal annealing, and detect charge trap signal in photodegraded device. They explains that the most of the initial performance degradation is based on the charge trap effect, and especially deterioration of V_{oc} is because of charge trap at interface between P3HT and PCBM, which forms shallower energy levels (see **Fig. 1.13**).

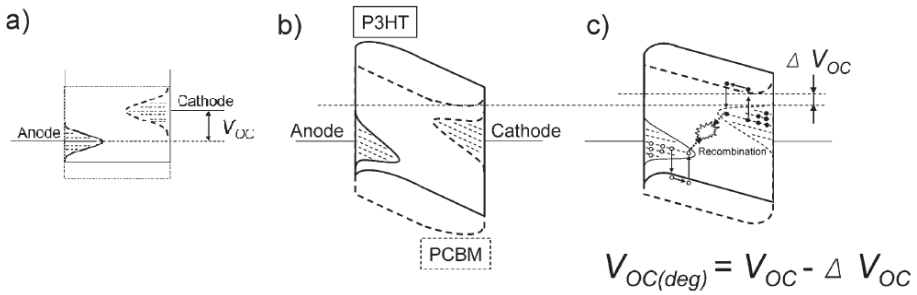

Figure 1.13 *Schematic energy diagram of bulk heterojunction organic solar cells a) under the initial open circuit condition, b) under the initial short circuit condition, and c) after degradation. The carriers are accumulated in two trap sites. Alleviation of the energy band slope occurs, resulting in a decrease of Voc, denoted by Kawano et al* [18].

On the other hand, the real identity of the charge trap signal is unknown, in other word, what is the electron binding state of atoms and what atoms form charge trap, and so on. Therefore, in order to realize it, researches to identify it are being conducted in these days. Nagamori et al. explained that the hole trap is formed at interface between PEDOT:PSS and P3HT by using LESR measurement [19], which is caused by an electron transfer from P3HT to PEDOT because of the energy difference between the HOMO of P3HT (4.7–5.1 eV) and the work function of PEDOT:PSS (5.3 eV). As an another opinion, Seemann et al.(Konarka) assumed that the charge trap exists as oxygen anion molecule which is formed by electron transfer reaction from P3HT and PCBM to oxygen molecule by using CELIV measurement (see **Fig. 1.14**) [20]. They focused on one of oxygen molecule‘s (may be singlet oxygen) energy level which is lower than that of P3HT and PCBM. In spite of much efforts, common philosophies about charge trap effect have not even been established yet. It is important to try to identify it.

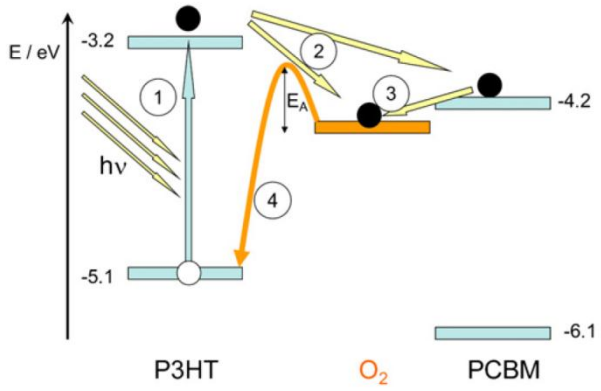

Figure 1.14 *Effects of oxygen doping on the charge transfer dynamics in a P3HT:PCBM blend. 1. Excitation of an electron in P3HT, 2. Electron transfer to PCBM, 3. Trapping of electron on oxygen, 4. Recombination, E_A. Activation barrier for charge carrier recombination, denoted by Seemann et al* [20].

3) Electrode (Metal and Transparent conductive oxide (TCO))
   Electrode has also been damaged by mechanical stress and oxidation. In the Al case, a part of Al electrode is oxidized by oxygen and changes to insulating oxidation material like Al_2O_3, which may cause resistance. It is generally agreed that oxygen and water can diffuse through the metalboundary and pinholes to cause modification of the inner interface of the electrode. As a result, a

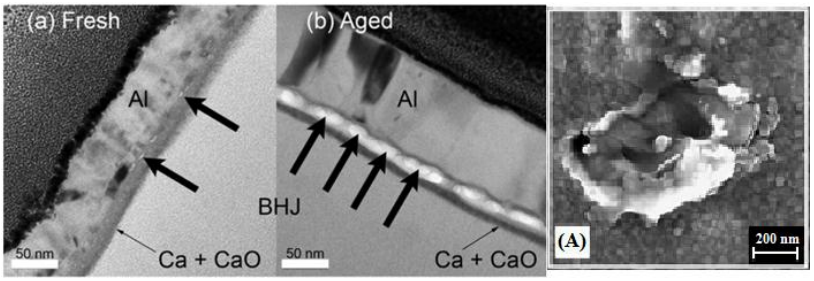

Figure 1.15 *TEM images for (a) freshly prepared, (b) aged ITO/BHJ/Ca/Al device and (A) 500 nm size flaw on Al after aged, denoted by Lloyd et al* [21].

chemical reaction with O_2 and H_2O takes place. In addition, some flaw and boid on Al electrode are reported, as shown in below **Figure 1.15** [21]. Bold arrows indicate regions of void formation at the Ca/Al interface. After aged (b), obiously void region (or insulating patches) increase are observed which may be triggered by the chemical reaction with H_2O. It is considered that this void can lead to mechanical disintegration and ultimately to delamination when longer exposure times (in the order of months) inducing a reduction of electrode/organic layer charge transfer. This reduction may be triggered by the large flaw on Al electrode (A). On the other hand, in the TCO case, it is a brittle material, meaning that it is vulnerable to cracks upon bending of the flexible substrate [22] (see **Fig. 1.16**). In the below (a) image, crack formation and its propagation in the ITO layer are observed after bending cycles, and it might hinder charge transport and increase the sheet resistivity. Though the crack may also lead to photodegradation of device, this is triggered mainly by mechanical bending stress, and therefore the effect of mechanical stress in the device may be next step.

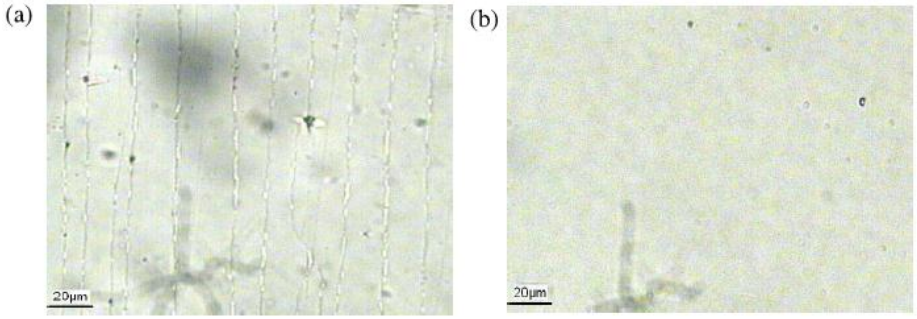

Figure 1.16 *Optical images of (a) ITO/PET and (b) polymer on PET after bending cycles, denoted by Wang et al.*

1.4 Original approach of the present research

A lot of investigation of device degradation have also been conducted without mentioned above in these days, and degradation mechanism have been cleared by slow degrees. However, the most important two things which we should note are that;

- ✓ The device degradation is very complicated because of these factors may happen at the same time, and nobody knows how much degree some observed causes affect to the device performance degradation. (i. e. if Al electrode oxidation are observed in a complete device, another degradation also cause performance decrease at the same time in a same device. Therefore, in this case, they can insist that Al electrode oxidation is one of reasons but can not insist how much it affect to the device performance. Perhaps, it does not affect to the device performance at all.)
- ✓ The investigation is comprehensively conducted by physical approach such as charge trap signal by ESR, current resistance signal by impedance, current-voltage signal by I-V. However, these physical signal has not been investigated in conjunction with chemical approach. (In other word, how the molecule changes during photodegradation, and how the molecular change affects to the device performance.) We see only the signal change of device.

Therefore, it is very important to separate these complicating problems in the device as much as possible, and investigate the effect to the device performance by the separated each factor. In addition, it is also important to try to realize a nanoscale molecular change in a complete device during photodegradation. In order to solve the complicating degradation problem, first of all, these viewing is very essential and important to realize a degradation mechanism in a real sense. Here, in

this research, I focused on the photooxidation of polymer in the photoelectric conversion layer and conducted further investigation of the physical degradation phenomenon by connecting with the chemical approach such as organic molecular structural change by using original way to separate other causes. (**Figure 1.17**)

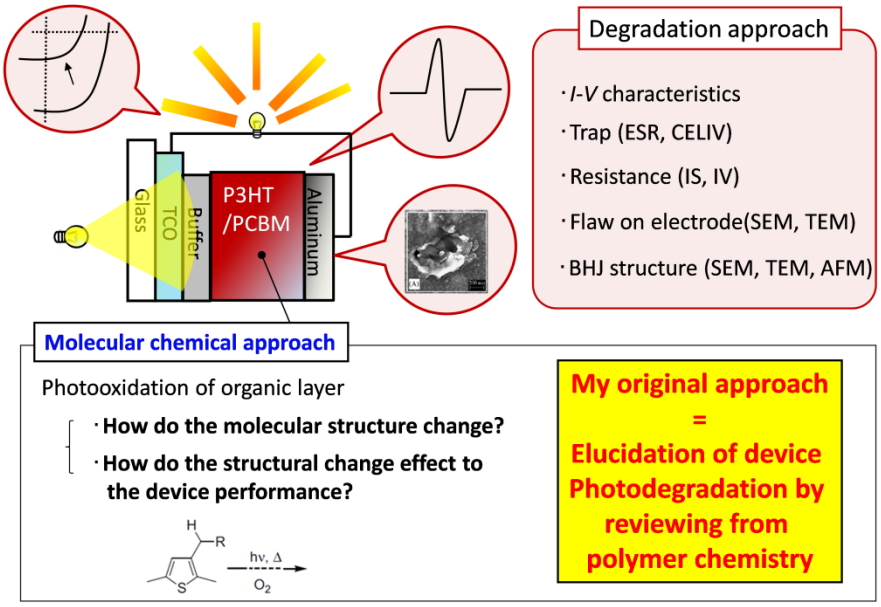

Figure 1.17 *My original research outline toward photodegradation of PSCs.*

The originality is briefly described as follows;

• I investigated direct effect of partially photo-oxidized poly(3-hexylthiophene) on the device characteristics in BHJ solar cell by using solution photooxidation technique. The advantage of this solution photooxidation method is that an evaluation of the device characteristics, excluding the i) degradation of the electrodes and interfacial buffer layers (directly study), and ii) a trapped charge accumulation, which is often observed in organic electronics. (detailed are in chapter 2) (**Figure 1.18**)

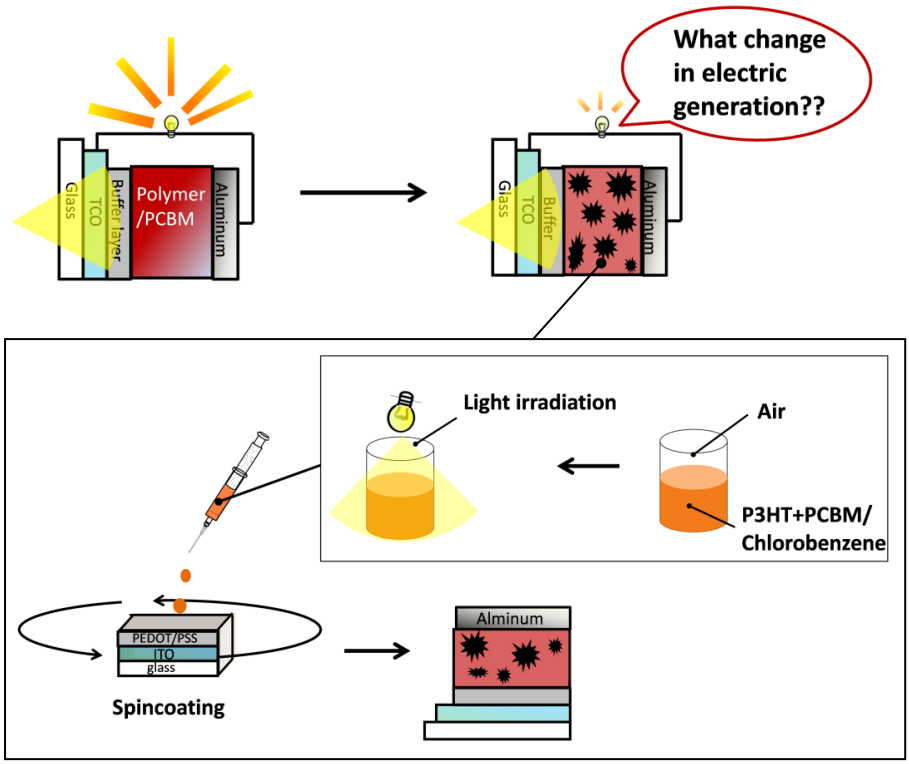

Figure 1.18 *The schematic image of my original research approach (chapter 2) .*

• In order to know the initial photooxidation mechanism and the photoactive species of P3HT, I investigated initial photooxidation reaction of poly(3-hexylthiophene) by focusing on the $[Polym]^{+}$ • $[O_2]^{-}$ CT state, which is formed by visible light irradiation in air. (detailed are in chapter 3) (**Figure 1.19**)

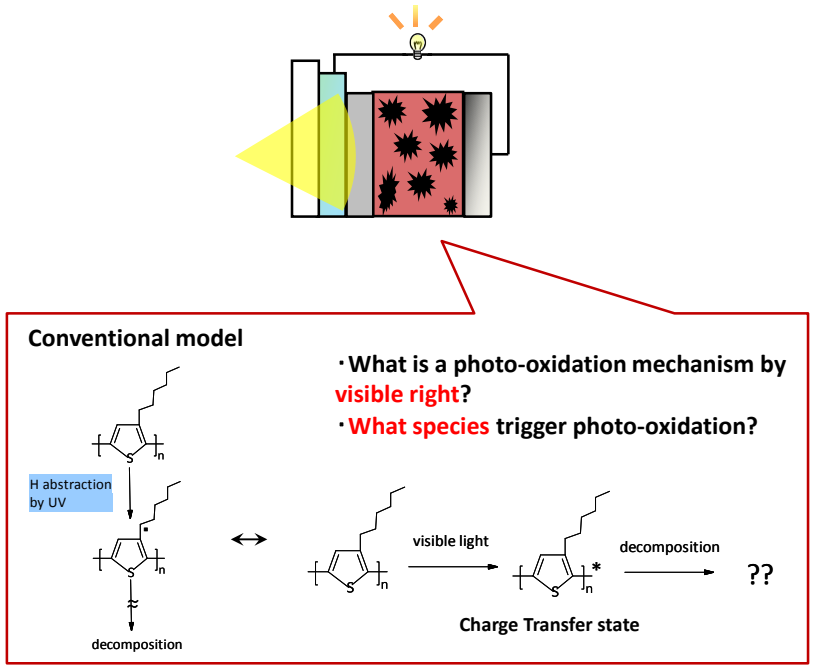

Figure 1.19 *The schematic image of my original research approach (chapter 3) .*

・In order to realize more photo-stabilized polythiophene derivatives than P3HT, I consider to prevent the photoactive species from reaction and design the polymer structure. As the design concept, I focused on the weak point (α-hydrogen in alkyl side chain) by the photo active species and changed the α-side chain structure to no α-hydrogen structure. (detailed are in chapter 4) (**Figure 1.20**)

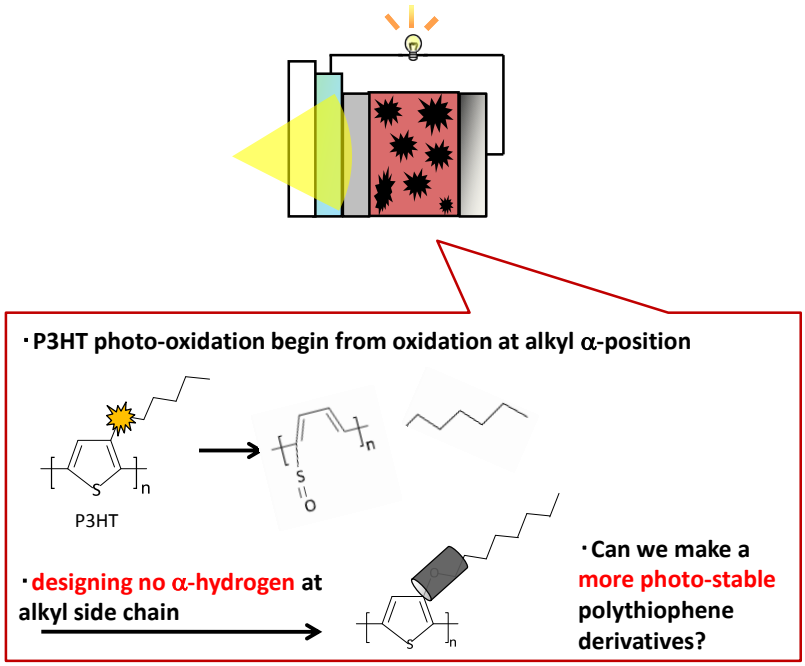

Figure 1.20 *The schematic image of my original research approach (chapter 4) .*

1.5 References

[1] U. S. Energy production (2011) in NREL internet site (by http://www.nrel.gov/docs/fy13ost i/54909.pdf)

[2] Present situation of highly efficiency chart of solar cells (by http://www.nrel.gov/ncpv/images/efficiency_chart.jpg)

[3] F C. Krebs. Polymer solar cell modules prepared using roll to roll methods: Knife-over-edge coating, slot-die coating and screen printing. *Sol. Energy Mater. Sol. Cells* **93** (2009) 465-475.

[4] F C. Krebs, J. Fvenbo, M. Jørgensen. Product integration of compact roll-to-roll processed polymer solar cell modules: methods and manufacture using flexographic printing, slot-die coating and rotary screen printing. J. Mater. Chem. **20** (2010) 8994-9001.

[5] E. Voroshazi, B. Verreet, T. Aernouts, P. Heremans, Long-term operational and degradation analysis of P3HT:PCBM photovlotaic cells. *Sol. Energy Mater. Sol. Cells* **95** (2011) 1303-1307.

[6] M. Wolf, H. Rauschenbach, Series resistance effects on solar cell measurements. *Adv. Energy Conversion* **3** (1963) 455-459.

[7] S.M. Sze, Semiconductor Devices: Physics and Technology, 2nd edition, John Wiley & Sons, Inc., (2001).

[8] M. Jørgensen, K. Norrman, F C. Krebs. Stability/degradation of polymer solar cells. *Sol. Energy Mater. Sol. Cells* **92** (2008) 686-714.

[9] N. Grossiord, J. Kroon, R. Andriessen, P. Blom, Degradation mechanism in organic photovoltaic devices. Org. Electron. **13** (2012) 432-456.

[10] T. Caronna, M. Forte, M. Catellani, S. Meille, Photodegradation and photostabilization studies of poly(3-butylthiophene) in the solid state. *Chem. Mater.* **9** (1997) 991-995.

[11] M. Manceau, A. Rivaton, J-L. Gardette, S. Guillerez, N. Lemaître. The mechanism of photo- and thermooxidation of poly(3-hexylthiophene) (P3HT) reconsidered. *Polym. Degrad. Stab*. **94** (2009) 898-907.

[12] M. Wohlers, H. Werner, D. Herein, T. S. Niedrig, A. Bauer, R. Schlögl. Reaction of C_{60} and C_{70} with molecular oxygen. Synth. Met. **77** (1996) 299-302.

[13] M. Reese, A. Nardes, B. Rupert, R. Larsen, D. Olson, M. Lloyd, S. Shaheen, D. Ginley, G. Rumbles, N. Kopidakis. Photoinduced degradation of polymer and polymer-fullerene active layers: Experiment and theory. Adv. Funct. Mater. **20** (2010) 3476-3483.

[14] S. Bertho, G. Janssen, T. Cleij, B. Conings, W. Moons, A. Gadisa, J. D'Haen, E. Goovaerts, L. Lutsen, J. Manca, D. Vanderzande. *Sol. Energy Mater. Sol. Cells* **92** (2008) 753-760.

[15] S. Gevorgyan, M. Jørgensen, F. C. Krebs, K. O. Sylvester-Hvid. A compact multi-chamber setup for degradation and lifetime studies of organic solar cells. *Sol. Energy Mater. Sol. Cells* **95** (2011) 1389-1397.

[16] D. Schlettwein, T. Oekermann, N. Jaeger, N. R. Armstrong, D. Wöhrle. Interfacial trap states in junctions of molecular semiconductors. *Chem. Phys.* **285** (2002) 103-112.

[17] J. M. Hodgkiss, S. A. Seifried, a. Rao, A. J. Barker, A. Camobell, R. Marsh, R. H. Friend. Exciton-Charge anihilation in organic semiconductor films. *Adv. Funct. Mater.* **22** (2012) 1567-1577.

[18] K. Kawano, C. Adachi, Evaluating carrier accumulation in degraded bulk heterojunction organic solar cells by a thermally stimulated current technique, *Adv. Funct. Mater.* **19** (2009**)** 3934-3940.

[19] T. Nagamori, K. Marumoto, Direct observation of hole accumulation in polymer solar cells during device operation using light-induced electron spin resonance, *Adv. Mater*. **25** (2013) 2362-2367.

[20] A. Seemann, T. Sauermann, C. Lungenschmied, O. Armbruster, S. Bauer, H.-J. Egelhaaf, J. Hauch, Reversible and irreversible degradation of organic solar cell performance by oxygen, *Sol. Energy* **85** (2011) 1238-1249.

[21] M. T. Lloyd, D. C. Olson, P. Lu, E. Fang, D. Moore, M. White, M. Reese, D. Ginley, J. Hsu. Impact of contact evolution on the shelf life of organic solar cells. J. Mater. Chem. **19** (2009) 7638-7642.

[22] G. Wang, X. Tao, R. Wang. Flexible organic light-emitting diodes with a polymeric nanocomposite anode. Nanotec. **19** (2008) 145201-145206.

2. Direct effect of partially photo-oxidized poly(3-hexylthiophene) on the device characteristics in BHJ solar cell

2.1 Introduction

Polymer solar cells (PSCs) have many potential advantages in their mechanical flexibility, portability, and low manufacturing costs [1,2]. Among the conducting polymers used, poly(3-hexylthiophene) (P3HT) is one of the most commonly employed materials for photoactive layers. According to recent studies on PSCs utilizing P3HT, the power conversion efficiency has been drastically improved [3-7], and large-scale production can be expected imminently [8]. On the other hand, it is well known that a PSC based on P3HT degrades with long-term solar light irradiation [9,10]. In order to realize and improve the problem for long-term durability, the photo-degradation of PSCs has been investigated [11-14].

Device degradation can be divided into reversible and irreversible types, as reported by Seeman et al [15]. Reversible degradation is defined as a drop in device performance that is recoverable through thermal annealing. Kawano et al. reported that reversible degradation is mainly caused by the accumulation of a charge carrier at the trap site, as investigated through thermally stimulated current (TSC) measurements [16]. Schafferhans et al. reported that the exposure of solar cells to synthetic air results in degradation, and oxygen doping increases the density of the deeper charge traps when investigated using TSC and charge extraction from linearly increasing voltage (CELIV) measurements [15,17].

Irreversible degradation is defined as a drop in device performance that cannot be restored using thermal annealing. Jorgensen et al. assumed that the main cause of irreversible degradation is the dramatic decomposition of organic materials such as P3HT and [6,6]-phenyl-C61-butyric acid methyl ester (PCBM) through photooxidation [9,10]. However, because it is difficult to directly evaluate an organic layer sandwiched between the transparent electrode and metal electrode of a device, the photodecomposition effect of organic materials on the drop in device performance has remained undetermined [9,10]. In addition, it is also another problem that the complete device degradation can not exclude some factors such as degradation of electrodes and interfacial buffer layers, and an accumulation of trapped charge. Chang et al. recently reported on the correlation between photooxidized P3HT and the photovoltaic performance of PSCs by using a pre-prepared solution of photooxidized P3HT [18]. The solution of degraded P3HT was prepared by irradiating for 10 h in air at an intensity of 100 $mWcm^{-2}$ using a mercury light, and the drastic photo-decomposition of P3HT was observed by UV-vis, photoluminescence (PL), and Fourier transform- infrared (FT-IR) spectroscopy. They found that the decrease in performance could be attributed to a drop in hole mobility, light absorption, and an increase in the carrier quencher concentration upon the degradation of P3HT. Although they investigated the effect of drastic structural changes of P3HT on the device, details on the initial effect of photooxidation on the device is yet to be investigated.

In this research, we attempt to make the correlation between the details of the initial effect of organic material (P3HT, PCBM) photooxidation and the photovoltaic performance of PSCs clear. We investigated the device characteristics based on the *I–V*, incident photon-to-current efficiency (IPCE), and impedance spectroscopy (IS) measurements by employing a slightly oxidized organic material. A slightly photooxidized material was prepared through the irradiation of

solar-simulated light in air for less than 1 h at the solution state. We then focused on the structual change based on UV-vis, FT-IR, AFM, and matrix-assisted laser desorption ionization time-of-flight (MALDI-TOF) mass measurements. Degradation of the organic layer was not carried out for a complete PSC, and whose mechanism might not be completely identical to that in a thin film state [10], however, the advantage of this solution photooxidation method is that an evaluation of the device characteristics, excluding the i) degradation of the electrodes and interfacial buffer layers, and ii) a trapped charge accumulation, can be made.

2.2 Experimental Details

2.2.1 Device fabrication

The device structure was [glass / transparent electrode / buffer layer / organic layer / Al] (see **Figure 2.1**). Indium tin oxide (ITO), Poly(3-hexylthiophene) (P3HT) (Merck), and [6,6]-Phenyl-C61-ButyricAcid Methyl Ester (PCBM) (Solenne) was used as transparent electrode, p-type organic semiconductor, and n-type organic semiconductor, respectively. ITO coated (2 mm × 26 mm, sheet resistance = ~10 Ω/□) glass substrates were cleaned by O_2 plasma treatment (Harrick Plasma Inc.) for 30 min. To deposit the interfacial buffer layer poly(3,4-ethylenedioxy thiophene) : poly(styrenesulfonate) (PEDOT : PSS) (H. C. Starck Baytron PVP. AI 4083) was dropped onto grass substrate using a 0.45 μm filter. Then, the substrate was spin-coated at 3000 rpm for 185 sec (~30 nm) and dried at 135 ^{o}C on hot plate for 10 min. To prevent water adsorption into the PEDOT : PSS films, the substrates were immediately transferred to a glove box (N_2 99.99%, H_2O is under 10 ppm, O_2 is under 5 ppm) after annealing.

For the active layer, 8 different P3HT : PCBM solutions were prepared. P3HT and PCBM were dissolved in anhydrous

chlorobenzene (Sigma-Aldrich) to yield P3HT = 1.8 wt%, PCBM = 1.2 wt% solution in the glove box. All materials were used as recieved. The solution was stirred overnight in the glove box. The next day, half of the solution was transferred into an air-filled transparent glass bottle. The remaining half of the solution was transferred into a nitrogen-filled transparent glass bottle. The oxygen concentration of the air and solution in the former bottle were estimated by Henry's law to be 3.75×10^{-5} mol and 1.63×10^{-6} mol, respectively [19]. Then, the two bottled solutions were illuminated with AM1.5G solar simulated light irradiation of 100 mW cm^{-2} intensity for 0, 20, 40, and 60 min to form partially photooxidized 8 different organic solutions (0, 20, 40, 60 min in air and 0, 20, 40, 60 min in nitrogen). We confirmed that the volatilization of solvent in solutions did not occur after the irradiation.

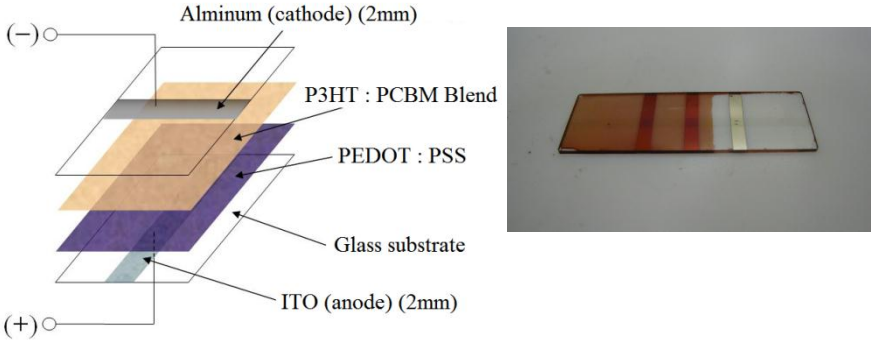

Figure 2.1 *The P3HT / PCBM normal solar cell structure in this research .*

Each solution was dropped onto a PEDOT : PSS-coated ITO substrate, and the substrate was spin-coated at 2,000 rpm for 120 sec (~100 nm) in the glove box. Finally, Al electrode were deposited (~100 nm) on top of the active layers by vacuum evaporation through a shadow mask onto each film. The active area of the cell was 0.04 cm^{-2}. Then, the substrates were post-annealed at 110 ^{o}C on hot plate for 10 min and then at 135 ^{o}C for 15 min.

Regarding encapsulated device fabrication, encapsulation treat was conducted by using typical encapsulation epoxy resin after above procudure. First, liquid encapsulation resin was lined a square shape around the device by using dispenser mathine (see **Figure 2.2**), and then another glass was mounted on top of the liquid resin. Next, UV-light was irradiated to the resin, and the device was heated at 120 ^{o}C on hot plate for 30 min for enough encapsulation. These treat was conducted in a nitrogen filled glove box (N_2 99.99%, H_2O is under 5 ppm, O_2 is under 5 ppm).

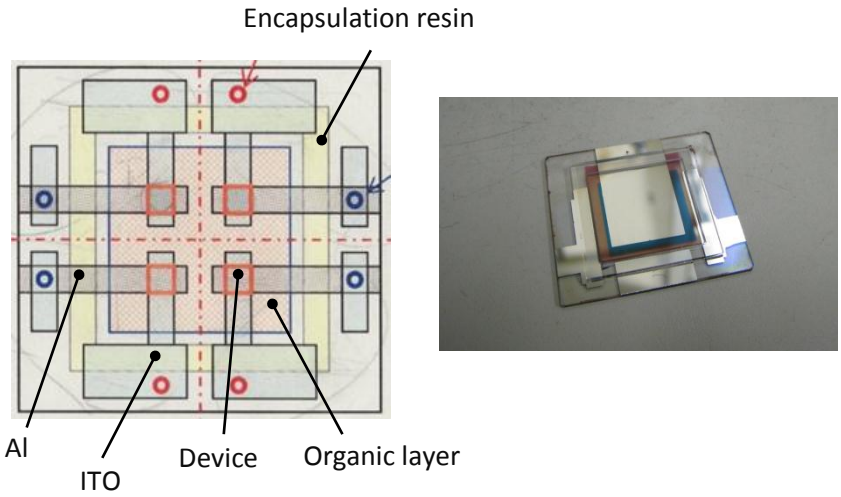

Figure 2.2 *(left) The encapsulated P3HT / PCBM solar cell structure used in this research . (Right) One of encapsulated devices.*

2.2.2 Evaluation of organic film

Organic films were characterized by UV-vis-NIR (Shimadzu Co., LTD.), FT-IR (JASCO Co.), AFM (Bruker-AXS). After the mesurement, a sample solution were prepared by extraction from each organic films by $CHCl_3$ using an ultrasonic cleaning machine. A complete extraction of material and no-effect of ultrasonic were confirmed. The solution was mixed into 2-[(2*E*)-3-(4-tert-butylphenyl)-2-methylprop-2-enyli

dene] malononitrile (DCTB) [20] / $CHCl_3$ as matrix solution. Then, the samples were characterized by MALDI-TOF mass (Bruker Daltonics Inc.) by use of nitrogen laser (λ = 337 nm). The calibration was conducted by using peptide standard purchased from Bluker. In addition, the extracted solution were used to conduct Gel Permeation Chromatography (GPC) (Waters Corp.) measurement.

2.2.3 Characterization of device performance

After the fabrication of devices, each device was placed in a sample holder which was sealed in the glove box (see **Figure. 2.3**), and then

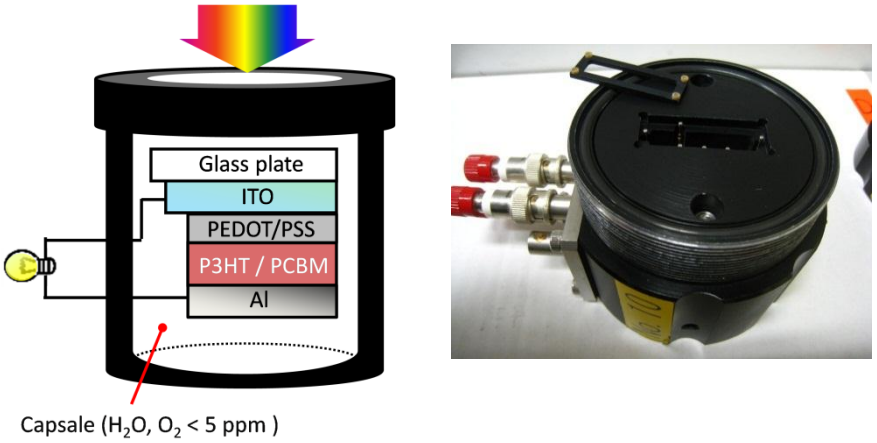

Figure 2.3 *(left) The capsule image and (Right) real capsule for encapsulation of P3HT / PCBM solar cell structure used in this research.*

the devices were removing from the glove box. All the device characterization is conducted under the condition at room temperature. The current density-volage (*I-V*) curves were obtained using a source meter (Keithley Instruments Inc.) under AM1.5G solar simulated light irradiation of 100mW cm^{-2} intensity. The solar simulator equipped with a Xe arc lamp and an AM1.5G filter (Bunkoukeiki Co., LTD.). The irradiation intensity was calibrated using a standard cell for a-Si solar cells (Bunkoukeiki Co., LTD.). The power conversion efficiency (η)

was calculated from the *I-V* characteristics. The space charge limited current (J_{sclc}) were obtained by *I-V* measurement (0.1~10 V) of the same device with Au deposition. The incident photon-to-electron conversion efficiency (IPCE) were measured under illumination with monochromatic light from a Xe lamp (1-7 mW cm^{-2} at each wavelength) (Bunkoukeiki Co., LTD.). The impedance spectra were measured with impedance / gain-phase analyzer (Solartron Co., LTD.) The impedance response were measured over the range of 1Hz to 1MHz with an oscilation amplitude of 30 mV under dark during DC bias (0.0, 0.2, 0.4, 0.6, 0.8 V). The C-AFM measurements of the devices without Al deposition were performed using a Dimension Icon equipped with a Nanoscope V controller (Bruker-AXS) [21]. To adjust chip energy level to the P3HT HOMO energy level (5.0 eV), Si coated Pt/Ir (5.1 eV) chip were used.

2.3 Result and Discussion

2.3.1 Solar cell device characteristics

The I-V curves and changes in device characteristics of photovoltaic cells are shown in **Figure 2.4**. Before fabricating the organic film, a P3HT and PCBM blend solution was irradiated for 0, 20, 40, and 60 min in air using simulated solar light (AM 1.5 G) at an intensity of 100 mW/cm^2. The devices were then fabricated using this solution. The device using a non-photooxidized organic film showed a photovoltaic behavior comparable to those previously reported [9,10,19] with an open-circuit voltage (V_{oc}) of 0.56 V, short-circuit current density (J_{sc}) of 9.13 mA cm^{-2}, fill factor (FF) of 0.48, and power conversion efficiency (η) of 2.45. The values of η, J_{sc}, and FF were reduced, whereas V_{oc} increased as the irradiation time increased. In addition, the series resistance also increased (see **Figure S1** in the supporting information). In particular, the decrease in η reached by 40% of the initial value after

60 min of irradiation. The decrease in FF and J_{sc} clearly contribute to the decline in device efficiency. It is known that the charge trap accumulation at a material interface decreases the V_{oc} during photodegradation of the complete device [15,17]; however, no decrease in the V_{oc} was observed in the image in **Figure 2.4**, which confirms that

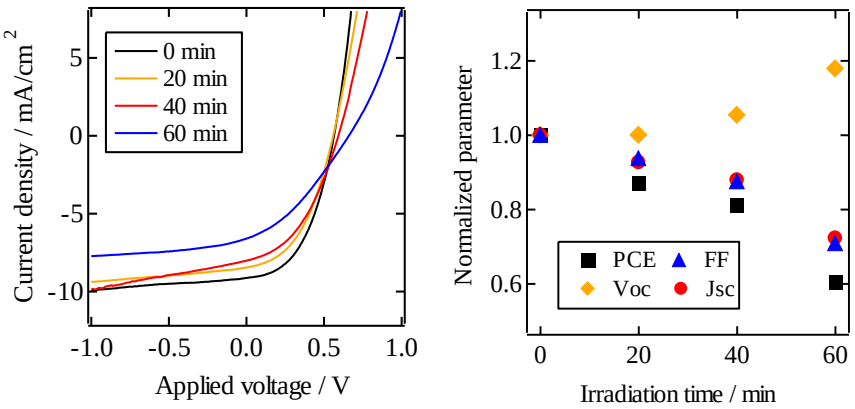

Figure 2.4 *I-V curves for (—) 0, (—) 20, (—) 40, and (—) 60 min, and the changes in (■) PCE, (▲) FF, (◆) Voc, and (●) Jsc of the ITO/PEDOT:PSS/P3HT:PCBM/Al device. Before fabrication of the organic film, the blended solution was irradiated in air using simulated solar light (AM 1.5 G) at an intensity of 100 mW/cm^2.*

the effect of the charge trap accumulation in the device is small. The performance degradation was also observed by IPCE measurements, where the spectra showed that the overall intensity dropped as the irradiation time increased (see **Figure 2.7**). Since hardly any changes in η, J_{sc}, FF, V_{oc}, and the series resistance were observed when using a photo-irradiated organic material in nitrogen gas (see **Figure S1** in the supporting information), it is thought that these parameter changes were caused by the changes in the organic material through photooxidation.

To determine the reason for the performance deterioration, impedance spectra (IS) of the photovoltaic cells were examined.

Cole-Cole plots of the device using non-photooxidized and 60-min photooxidized materials under dark, 0.0 V conditions are shown in **Figure 2.5**. The spectrum of the device using a non-photooxidized organic material showed the same tendency as those previously reported [19]. In the measurements (dark, 0 vias), the semicircle diameter may be highly dependent on the bulk resistance of the organic thin film because this equivalent circuit is considered simply an R-C parallel

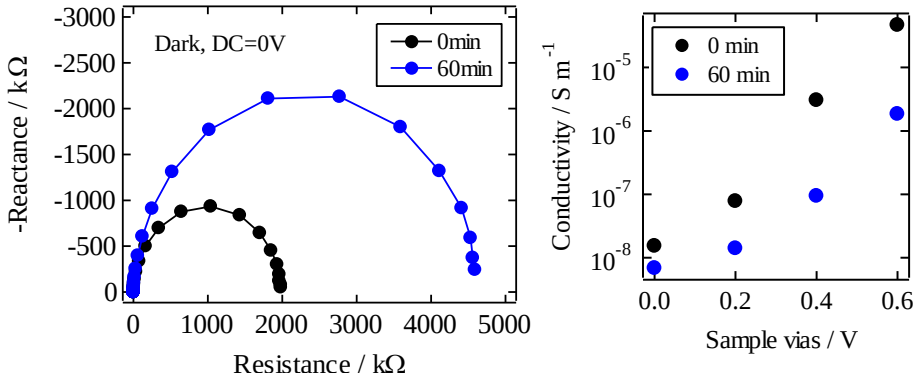

Figure 2.5 *(Left) Cole-Cole plots and (Right) Electro-conductivity changes estimated by R-C parallel circuit for (—) 0 and (—) 60 min of the ITO/PEDOT:PSS /P3HT:PCBM/Al device at 0.0 V under dark conditions.*

circuit, as based on a previously reported equivalent circuit [19], and an increase in capacitance is excluded because the charge carrier trap is thermally released through annealing during the device fabrication. This tendency was also confirmed through the fitting of an equivalent circuit over the range of 1 Hz to 40 kHz (Z View). An increase in the diameter was clearly observed in the device measurement using a 60-min photooxidized material as compared with a measurement using a non-photooxidized material. In addition, a decrease in the electroconductivity in the 60-min photooxidized organic film was also observed (see **Figure 2.5**). It can therefore be considered that the performance deterioration, such as in the FF, J_{sc}, and series resistance, is mainly due to the increase in organic bulk resistance. The reasons for

the increase in organic film resistance are discussed in the following section.

2.3.2 Evaluation of the partially photooxidized P3HT : PCBM organic thin films

To realize an increase in resistance of an organic film, the morphological changes of the photooxidized organic films were first investigated using atomic force microscope (AFM) measurements. The grain size could be determined through an AFM topographic image and the surface roughness of the material based on the root mean square (RMS). The exciton diffusion range in the organic material is on the order of 10 nm, thereby limiting the optimum grain size (~100 nm), which is formed through the self-organization of the P3HT and PCBM

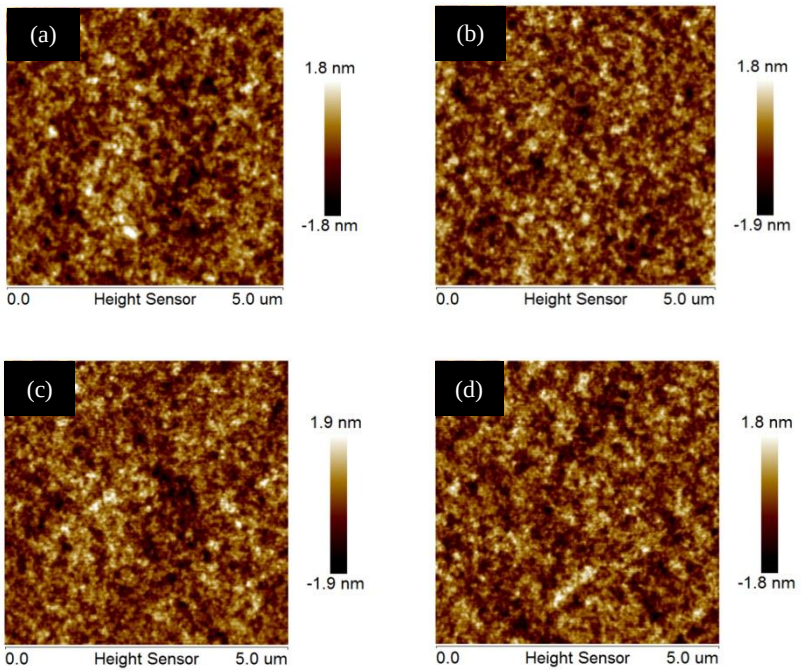

Figure 2.6 *AFM topographic images of P3HT:PCBM organic films. Before fabrication, the blended solution was irradiated for (a) 0, (b) 20, (c) 40, and (d) 60 min in air.*

blend [22]. For example, Li et al. reported that a larger grain size (peak height of 10 to 100 nm, and RMS of 0.87 to 9.5 nm), generated by a performance [22]. In contrast, the topographic images in **Figure 2.6** show that the peak heights and RMS ((a)–(d)) have differences of about 3.5 ±0.1 nm and 0.52±0.01 nm, which are normal values in the typical spincoating of P3HT and PCBM, and are not dependent on the irradiation time. It is therefore considered that the significant differences in grain size were not observed during the duration of photooxidation. In addition, differences in the P3HT microfibril structures or blend aggregation were not observed in the phase images of the samples (see **Figure S2** in the supporting information), and such differences were also not observed when using photo-irradiated organic materials in nitrogen gas. Next, before investigating the local conductivity of the BHJ blend film in the above region (5μm×5μm) of topographic image, the local *I-V* curve were firstly obtained, as shown in **Figure 2.7.** In this figure, we can see the current under both negative vias and positive vias which is dissymmetric against original point.

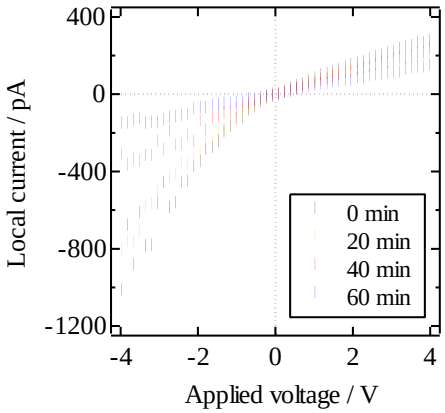

Figure 2.7 *Local I-V curves of ITO/PEDOT:PSS/P3HT:PCBM/Pt/Ir tip device. Before fabrication, the blended solution was irradiated for (•) 0, (•) 20, (•) 40, and (•) 60 min in air using simulated solar light (AM 1.5 G) at an intensity of 100 mW/cm^2.*

This current change is similar to the local P3HT current reported by Desbief et al [21]. In addition, it is noted that the current also arises under negative vias, which does not show arise in the case of p-n diode (rectification). Furthermore, we can confirmed that the current does not arise on PCBM aggeragation domain (data not shown). Therefore, we can confirmed that the local current is not derived from p-n diode but P3HT. The differences of the current behavior under positive and negative vias may be based on the vias effect difference to the organic layer which is formed from Pt/Ir tip and ITO plane, respectively. Then, we obtain the current mapping (under +2V) on the region in topographic image, as shown in **Figure 2.8**.

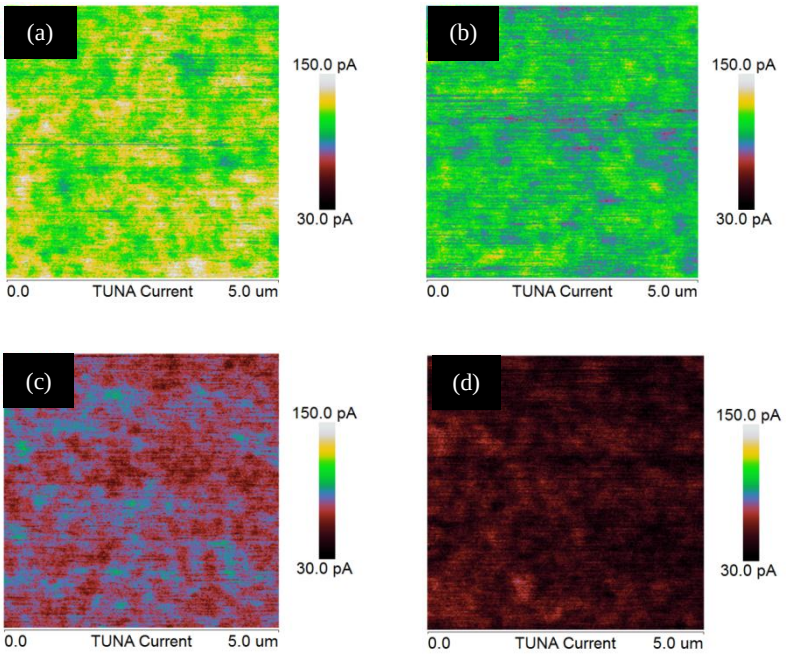

Figure 2.8 *AFM conductive images of P3HT:PCBM organic films. Before fabrication, the blended solution was irradiated for (a) 0, (b) 20, (c) 40, and (d) 60 min in air.*

Contrary to the topographic image, absolute currents show large difference among the samples, and obviously it decrease with

irradiation time. Therefore, it can be confirmed that the P3HT local current decrease with irradiation time. On the other hand, this current is not correspond to the topographic image, and there are no domains of zero current which is considered as PCBM. So, we can find out that the BHJ film is very homogeneous, and we can not distinguish the region between P3HT and PCBM because of the measure limit of conductivity by the tip size (10 nm). In the next figure (**Figure 2.9**), to study further investigation of P3HT solid state, statistics versus current under negative vias are shown. The reason why we use the current is that the *I-V* curve under minus vias shows exponential function which change is

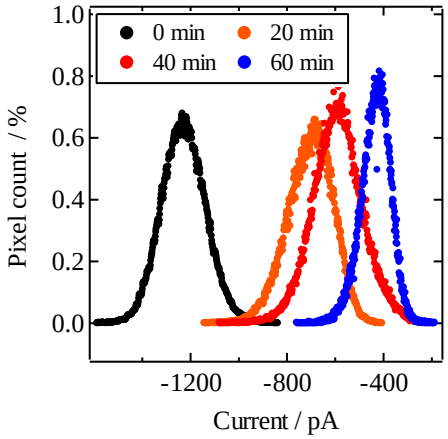

Figure 2.9 *Statistics of current obtained by the conductive images of P3HT:PCBM organic films.*

Table 2.1 *Peak currents, Full width half maximum (FWHM) current in the above statistics and crystallinity estimated by UV-vis.*

Time (min)	Peak current (pA)	FWHM (pA)	Crystallinity (%)
0	-1235	224	44
20	-687	217	40
40	-596	209	36
60	-416	133	32

typical in space charge limited current. This statistics information (each information is shown in **Table 2.1**) were obtained by the conductive mapping image. In the Fig. 2.9, we can see clear current distribution state in which it is considered that the higher the current, the more the number of P3HT crystal region [23]. In addition, from the value of FWHM, we can find out the distribution of the crystal size [23] in which the value changes little by little from 0 min to 40 min and then shows large decrease. Therefore, these results indicates that both the crystal region number and the crystal size distribution decrease with irradiation time.

Next, to examine the deterioration of J_{sc}, the photoabsorption spectra of photooxidized organic films were investigated using UV-vis absorption measurements, and IPCE measurement were investigated, as shown in **Figure 2.10**. This figure shows that the total absorption amount decreases slightly, within 5% of the initial absorption, against the 25% decline of the initial J_{sc}. In addition, the peak top of P3HT (515 nm) shifted 10 nm to a short wavelength after 60 min of irradiation.

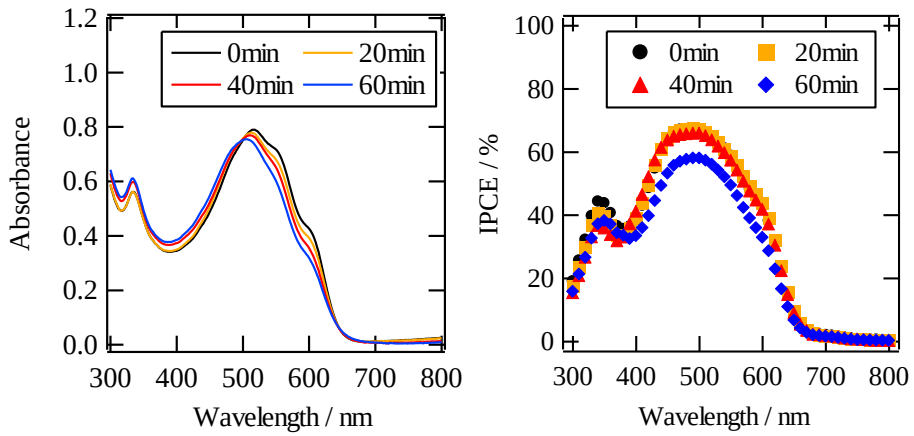

Figure 2.10 *(Left) UV-vis spectra of P3HT:PCBM organic films and (Right) IPCE spectra of P3HT:PCBM organic solar cells. Before fabrication, the blended solution was irradiated for (—) 0, (—) 20, (—) 40, and (—) 60 min in air using simulated solar light (AM 1.5 G) at an intensity of 100 mW/cm^2.*

This blue shift indicates that the photo-induced effect reduces the conjugation length of P3HT. In addition, we can see the absorption decrease of P3HT shoulders (550 nm and 600 nm) which is derived from P3HT aggregate 0-0 transition (crystal region) [23,24]. From the absorbances at 0-0 transition and 459 nm absorbances which is derived from amorphous P3HT, we estimates the crystallinity of P3HT with irradiation [23,24], as shown in **Table 2.1** (shown with C-AFM characteristics). As we already found out in current statics by C-AFM, we can confirm by UV-vis measurement that the crystal region number (crystallinity) decrease with irradiation time. Furthermore, it was noted that an absorption increase newly appeared at 400–500 nm based on a blue shift, but that the absorption increase did not contribute to the photocurrent, as shown in the IPCE spectra. It is therefore considered that the decrease in J_{sc} is mainly due to the photoconductive process after light absorption. In addition, the shrinking of the P3HT absorption band was confirmed through a blueshift. It is therefore considered that the decrease in π-conjugation length shrunk the HOMO bandwidth, and therefore slightly lowered (0.10 eV) the HOMO level and increased by 0.10 (V) of V_{oc}.(See **Figure S3**)

Variations in the FT-IR spectra of photooxidized organic films are shown in **Figure 2.11.** The formations of a carbonyl species (1660 cm^{-1}), carbonyl compound or alkene (1620 cm^{-1}), and sulfoxide derivative (1420 cm^{-1}) [25] were slightly observed. These signals relatively increase as the irradiation time increases. It is therefore considered that the structural change partially occurred as the photooxidation progressed. In contrast, in a previous report by Chang et al., the alkyl peak of P3HT disappeared, and broad and strong signals of the hydroxyl group, carbonyl species, and sulfoxide derivatives appeared after 10 h of irradiation, which is considered to be a severely photooxidized film [18,25]. The authors reported that the performance deterioration was caused by a change when using a photooxidized P3HT film. In our research, however, it was deduced that the partial

change of P3HT within a 1-h irradiation period had already caused an increase in the organic film resistance and a deterioration of the device performance. On the other hand, if the photooxidation of PCBM occurs, a peak derived from ketone on fullerene (1782 cm^{-1}) must be appear; [26] however, no peak was observed during this photooxidation time. This is because the LUMO level of PCBM is deeper by 1.0–eV than that of P3HT, and the photooxidation of PCBM is more difficult to occur than that of P3HT [27].

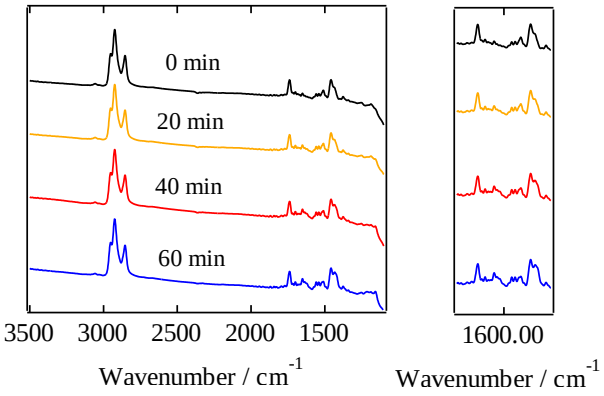

Figure 2.11 *FT-IR spectra of P3HT:PCBM organic films. Before fabrication, the blended solution was irradiated for (—) 0, (—) 20, (—) 40, and (—) 60 min in air using simulated solar light (AM 1.5 G) at an intensity of 100 mW/cm*^{2}.

Since it seems difficult to investigate the more detailed changed in the degradation using only FT-IR measurements, we focused on MALDI-TOF mass measurements,[28] and examined the detailed changes in conjunction with the results of the FT-IR measurements. The results are shown in **Figure 2.12**. The spectrum of the non-photooxidized organic film showed a signal of over 2,500 mass (m/z), which was based on the P3HT molecules. However, as the irradiation time increased, the intensity under a 2,500 mass (m/z) appeared and then increased relatively. This result indicates that the molecular scission of P3HT molecules easily occurred. A detailed

analysis from the expanding spectra revealed that a strong peak of m/z values can be expressed as 166*n* (repeat unit) + 2 (2H), and another peak of m/z values can be expressed as 166*n* (repeat unit) + 1 (1H) + 79 (Br), where *n* is equal to the number of repeated units. As the irradiation time increased, new peaks whose m/z values were expressed

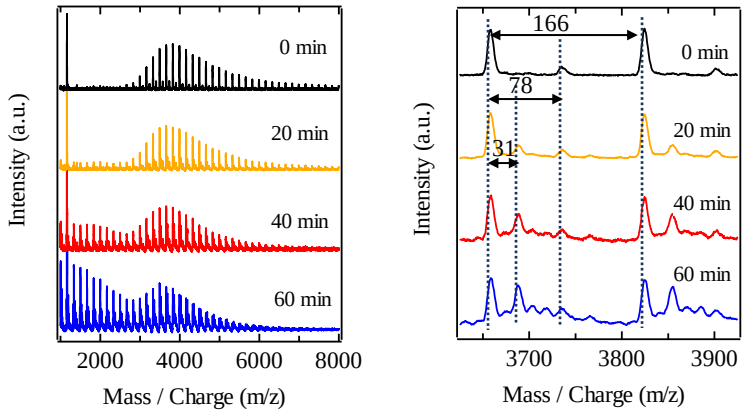

Figure 2.12 *MALDI-TOF-mass spectra of P3HT:PCBM organic films. Before fabrication, the blended solution was irradiated for (—) 0, (—) 20, (—) 40, and (—) 60 min in air using simulated solar light (AM 1.5 G) at an intensity of 100 mW/cm*^{2}.

as 166*n* (repeat unit) + 2 (2H) + 31 and 166*n* (repeat unit) + 2 (2H) + 46, and 166*n* (repeat unit) + 2 (2H) + 61 appeared, which were considered to be from a combination of added oxygen atoms (+16) and/or the elimination of hydrogen atoms (-1). Based on the FT-IR spectra results, these oxygen atoms were deduced to be present in the form of a carbonyl species (1660 cm^{-1}, 1620 cm^{-1}) and sulfoxide derivative (1420 cm^{-1}) accompanied by the molecular scission of a P3HT chain. We are currently investigating the detailed molecular scission mechanism of P3HT [29].

In the MALDI-TOF mass spectra, it is considered that a sufficient ionization of high molecules of P3HT (M_n=11,200 g/mol) did not occur. Thus, Gel permeation chromatography (GPC) measurements

of the photooxidized organic films were also conducted (see **Figure 2.13**.). The results show a small change in the overall spectral shape,

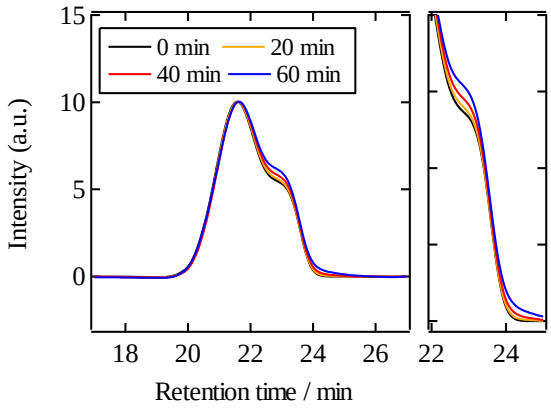

Figure 2.13 *GPC spectra of P3HT:PCBM organic films. Before fabrication, the blended solution was irradiated for (—) 0, (—) 20, (—) 40, and (—) 60 min in air using simulated solar light (AM 1.5 G) at an intensity of 100 mW/cm*^{2}.

but based on a detailed examination, high molecules disappeared and small molecules newly appeared, and M_n decreased. This therefore shows that a molecular scission of P3HT partially occurred with the irradiation. From the results, we estimated the small oxide morecule number (mol%) by using below equation [30] and values in **Table 2.2**.

$$N_{low\,x}(\text{mol\%}) = \left(\frac{M_{n\,0}}{M_{n\,x}} - 1\right) \times 100. \quad (2.1)$$

where $N_{low\,x}$ is small oxide molecule number (mol%) which is triggered by molecular scission. M_{no} and M_{nx} are the initial and final number-average molecular weights (shown in Table 2.2).

Table 2.2 *P3HT molecular characteristics (Mn) calculated by GPC spectra and small oxide molecule number calculated by using the equation (2.2).*

Time (min)	Mn (g)	N_{low} (mol%)
0	12510	0
20	12228	2.3062
40	11917	5.0013
60	11578	8.0917

Furthermore, if most of the polymer molecules change into low molecules, as shown in Fig. 2.12, a P3HT fibril structure should be formed more easily, which would be confirmed in an AFM phase image [22]. However, this phenomenon was not observed in **Figure S2** (see supporting information). This is because the molecular scission is limited, and a large segment of polymer left without a scission determined the morphological structure.

Kline et al. investigated the correlation between the molecular weight of P3HT and mobility using a field-effect transistor [31]. In their report, when the average molecular weight decreased from 11,600 to 3000 (GPC), the mobility drastically decreased from 10^{-3} ($cm^2V^{-1}s^{-1}$) to 10^{-6} ($cm^2V^{-1}s^{-1}$). Furthermore, Hiorns et al. investigated the correlation between the molecular weight of P3HT and the photovoltaic performance of PSCs using P3HT and PCBM [32]. In their report, when the average molecular weight decreased from 8600 to 2800 (GPC), the device characteristics of J_{sc}, FF, and η decreased from 6.5 (mA cm^{-2}), 0.53, and 2.2 (%) to 2.4 (mA cm^{-2}), 0.37, and 0.6 (%), respectively. Therefore, in the deterioration of J_{sc}, FF, and η, as one of reasons for the deterioration, it is considered that the very low molecular weight fragments generated by the molecular scission behave as impurities, and increase the resistance of the organic layer, thereby causing the device degradation. In previous reports, major changes in the UV-vis spectra, FT-IR spectra, and AFM images have only focused on

P3HT-based solar cell device degradation analyses [9,10,17,18]. However, the results showed that a MALDI mass measurement is an effective analysis tool for examining the polymer degradation in detail.

Here, from these datas, we will consider the nanoscale P3HT solid state change in the organic layer. In the films with initial irradiation time, we have already found out that the crystal region number (crystallinity) and the crystal size distribution decrease as irradiation time increase, and this phenomenon results in the absolute conductivity decrease. Then, in this initial photooxidation time, we can find out that the P3HT molecular scission occurs and P3HT small molecule oxide are forms (~8 mol%). From the MALDI-MS spectra, the chemical structural change on the main chain (one molecule) is only S=O on the thiophene ring. Therefore, it is hard to think that the main chain's stacking were prevented by only 2oxygen atoms (S=O) on polythiophene. So, in the research, I establish a hypothesis of the stacking formation of P3HT, as shown in the below figure (**Figure 2.14**)

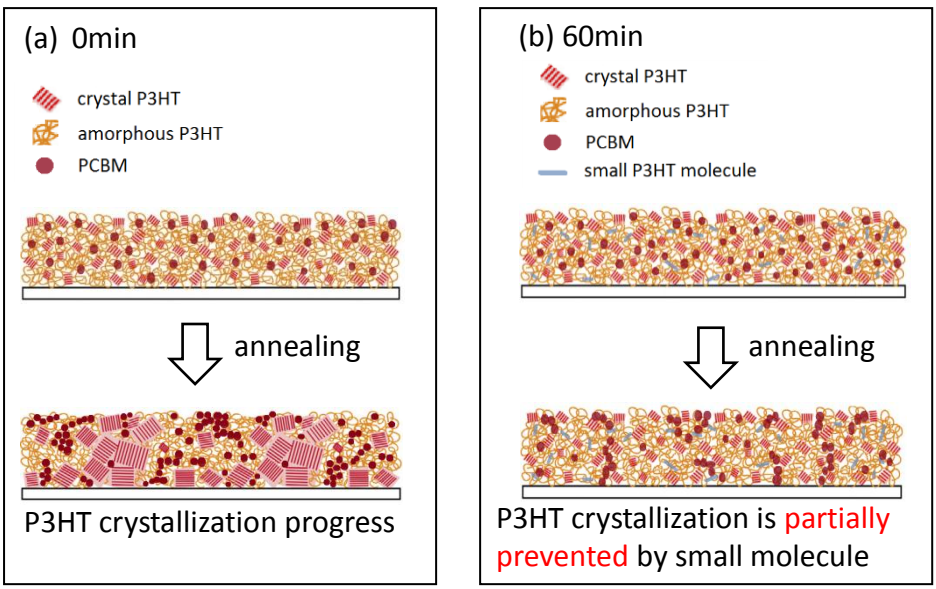

Figure 2.14 *Hypothesis about the P3HT stacking formation way.*

Before irradiation, crystallization normally progress during annealing. However, after irradiation, crystalization is prevented by uneven length small oxide molecule and make the film remained to be amorphous state. Next, in order to verify the hypothesis, we measure hole mobility and try to relate the correlation between μ (hole mobility) and N_{low} (small molecule number) by using equation. *I-V* curve and hole mobility data is shown in **Figure 2.15**.

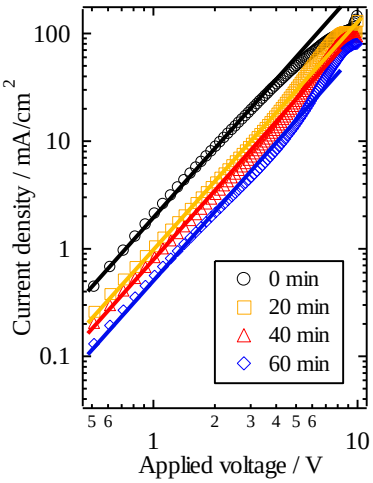

P3HT hole mobility and its inverse

Time (min)	μ (cm^2/Vs)	1/μ
0	1.2×10^{-5}	8.27×10^{4}
20	6.2×10^{-6}	1.61×10^{5}
40	4.4×10^{-6}	2.28×10^{5}
60	3.2×10^{-6}	3.07×10^{5}

Figure 2.15 *(left) I-V curve for (—) 0, (—) 20, (—) 40, and (—) 60 min of the ITO/PEDOT:PSS/P3HT:PCBM/Au device. (Right) P3HT hole mobility given by the Mott-Gurney law,* $J_{sclc} = \frac{9}{8}\varepsilon_0\varepsilon_r\mu\frac{V^2}{L^3}$. *Before fabrication of the organic film, the blended solution was irradiated in air using simulated solar light (AM 1.5 G) at an intensity of 100 mW/cm*^{2}.

In the figure, space charge limited current was appered in which the slope is equal to 2 (shown in real line) and the current density is given by the Mott-Gurney law

$$J_{sclc} = \frac{9}{8}\varepsilon_0\varepsilon_r\mu\frac{V^2}{L^3}. \quad (2.2)$$

where ε_0 is the vacuum permittivity, ε_r is dielectric constant of the film (ε_r = 3 was assumed for P3HT), and μ is hole mobility. The thickness of

the films is 120 nm. As the irradiation time increase, the mobility decrease can also be observed like in conductive decrease. Here, it can be considered that inverse number of the hole mobility ($\frac{1}{\mu}$) shows resistivity. In addition, it can also be considered that the N_{low} affects to the resistivity. Therefore, we will check the correlation between $\frac{1}{\mu}$ and N_{low} (mol%), as shown in **Figure 2.16**.

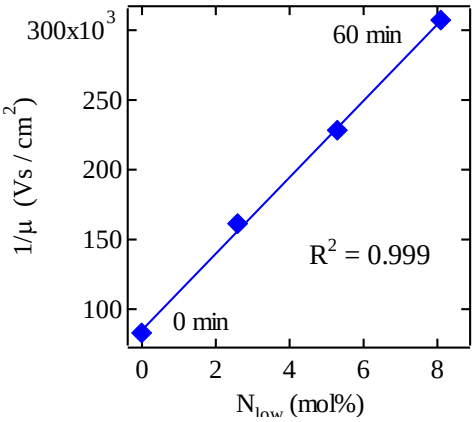

Figure 2.16 *The correlation between* $\frac{1}{\mu}$ *and* N_{low} *(mol%).*

From the figure we can completely find out that the relationship between $\frac{1}{\mu}$ and N_{low} (mol%) is really propotionate as below line function (R^2 = 0.999) (2.3) and therefore we can completely verify the involvement of small oxide molecule to the resistivity.

$$\frac{1}{\mu(t)} = aN_{low}(t) + \frac{1}{\mu(0)} \quad (2.3^*)$$

* where a = 2.7×10^4 (Vs/mol% cm^2), t = 0, 20, 40, 60 (min)

This resistivity $(\frac{1}{\mu})$ in organic layer is owing to the increase of small oxide molecule. Therefore, some relationship between $\frac{1}{\mu}$ and Rs in device parameter (Ωcm^2) is indicated, and confirmed as proportionate relationship (R^2 = 0.980) (2.4). These results supports that the formation of small oxide molecule affects to the increase of series resistance, resulting in the deteriolation of device characteristics.

$$Rs \propto \frac{1}{\mu} \quad (2.4)$$

In this research, photooxidized organic films, which were prepared using solution photooxidation, show a slight 5% decay in the amount of photo-absorption, as can be seen in the UV-vis spectra.

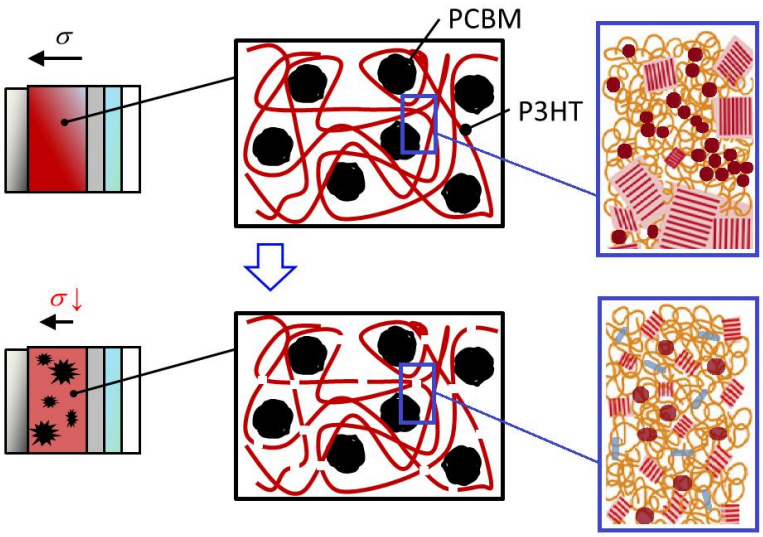

Figure 2.17 *Graphical abstract image in this chapter 2.*

In addition, no difference in the surface morphology was observed in the AFM images. On the other hand, the partial molecular scission of P3HT occurred and then formed a small oxide molecule in which conductivity were obviously decreased. These oxide is carbonyl species and sulfoxide derivative observed in the MALDI-TOF mass spectra and FT-IR spectra. These structural changes were also observed as a decrease in π-conjugation length and the number of crystallinity region decrease in the UV-vis spectra. The oxide fragments after molecular scission did not contribute to an increase in the photocurrent, but prevented the P3HT from stacking to make good crytal and therefore did reduce the total cell performance in the IPCE spectra. These molecular changes increased the resistance of the organic films, and the device characteristics (J_{sc}, FF, and η) were deduced to have decreased.

2.3.3 Investigation of P3HT : PCBM organic thin films in an encapsulated solar cells during photodegradation

In the former section, direct effect of partialy photooxidized organic materials to solar cell performance is described. In this section, an oxidation of organic film in an encapsulated solar cells during photodegradation is investigated by MALDI-TOF-MS measurement. This measurement is conducted by archiving direct extraction of the photovoltaic organic region (2mm × 2mm). Detailed method is described in the experimental section (4-1). The changes of *I-V* curves and device characteristics (J_{sc}, V_{oc}, FF, and η) in an encapsulated BHJ solar cell is shown in **Figure. 2.18**. No-degraded device preformance was comparable values (J_{sc}, V_{oc}, FF, and η are 7.50 (mA cm^{-2}), 0.58 (V), 0.45, and 2.01 (%)). Although the device was completely encapsulated, it was confirmed that all the device characteristics dropped as reported during light irradiation (~9,000 min). Firstly, in the initial irradiation time (~2000 min), rapid performance drop were observed. This drop is mainly because of the drop of FF, V_{oc}. The degradation of this initial

time is refered to as "Burn-in" [33], and explained by the hole trap at the interface between P3HT and PEDOT:PSS layer [34], which increased internal resistance and made P3HT HOMO energy level high. In the latter degradation time (2,000 min ~), power conversion efficiency showed gradual drop. In contrast to the burn-in time, the drop of FF were hardly observed, and the little drop of V_{oc} were observed. Therefore, this degradation was mainly because of the drop of J_{sc}.

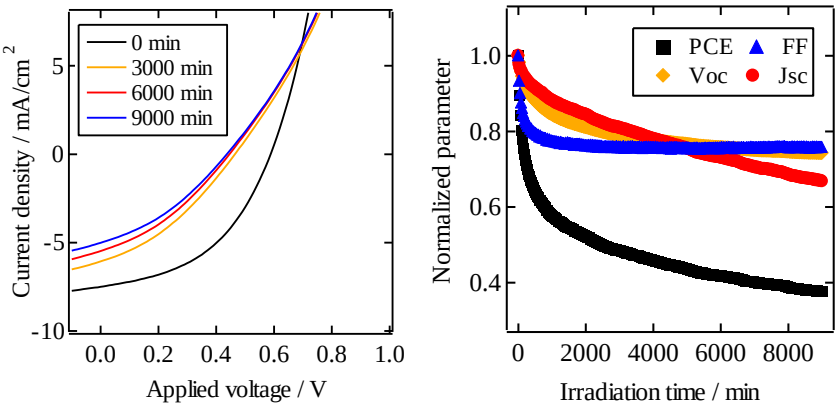

Figure 2.18 *I-V curves for (—) 0, (—) 3000, (—) 6000, and (—) 9000 min, and the changes in (■) PCE, (▲) FF, (◆) Voc, and (●) Jsc of the ITO/PEDOT:PSS/P3HT:PCBM/Al encapsulated device during 1sun irradiation.*

To realize these degradation phenomena, MALDI-TOF-MS measurement of organic materials in (a) burn-in degradation (3,000 min) and (b) subsequent degradation (9,000 min) was conducted, and the formation of the low molecular chains and oxides fragments are investigated. The MALDI-TOF-MS spectra of (a) burn-in degradation (3,000 min) and (b) subsequent degradation (9,000 min) is shown in **Figure 2.19**. After 3000 min irradiation, the photooxidation of P3HT was certainly observed a little as shown in the Figure. Thus, it is confirmed that the formation of low molecular chains and oxides fragments by chain scission was observed even in the burn-in scale degradation in an encapsulated solar cells. In addition, after the 9000

min irradiation, the low molecules signal increased, which is similar to the results in solution photooxidation method (after 60 min irradiation). This low molecules may trigger the performance drop, such as *Jsc*. The factors of the photo-degraded device are very complicated, however, it is at least considered that the photooxidation of P3HT is certainly related even in the encapsulated device performance drop.

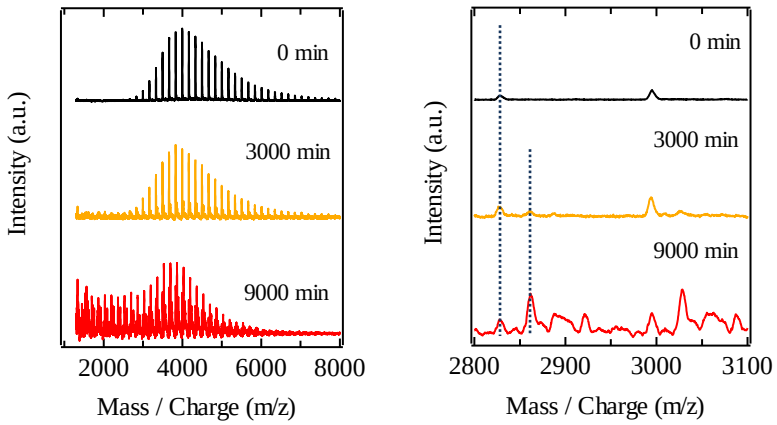

Figure 2.19 *MALDI-TOF-MS spectra of the (—) 0, (—) 3000, and (—) 9000 min of P3HT:PCBM organic films in the ITO/PEDOT:PSS/P3HT:PCBM/Al encapsulated device during 1sun irradiation. The organic layer was extracted by using $CHCl_3$, and the extracted region was only sandwiched place (2*2 mm^2) between Al and ITO.*

2.4 Conclusion

To realize the effect of the initial photooxidation of organic films on a device, we fabricated different devices using degraded organic materials, which had been photooxidized in the solution state. We observed the correlation between the structual change of the film and the device characteristics. In the UV-vis spectra, a 10 nm blue shift was observed, indicating that the conjugation length of P3HT decreased during this initial photooxidation period. A slight decrease (8 mol%) in the amount of photoabsorption was also observed. The AFM images

did not show a significant change in the surface morphology of the organic films. FT-IR spectra confirmed the formation of a carbonyl species (1660 cm^{-1}, 1620 cm^{-1}) and sulfoxide derivative (1420 cm^{-1}). MALDI-TOF mass spectra indicated the partial molecular scission of P3HT in the organic films. Significant degradation of the device characteristics was observed from the *I–V* and IPCE spectra, and an increase in the resistance of the organic films was observed through IS measurements. These results indicate that the oxide fragments formed on partial molecular scission of P3HT increased the resistance of the organic films, and it was deduced that the decrease in the device characteristics was one reason for the complete device degradation.

2.5 References

[1] G. A. Chamberlain, Organic solar cells: A review, *Sol. Cells* **8** (1983**)** 47-83.

[2] C. J. Brabec, Organic photovoltaics: technology and market, *Sol. Energy Mater. Sol. Cells* **83** (2004) 273-292.

[3] N. C. Das, P. E. Sokol, Hybrid photovoltaic devices from regioregular polythiophene and ZnO nanoparticles composites, *Renew Energy* **35** (2010) 2683-2688.

[4] S-Y. Chuang, C-C. Yu, H-L. Chen, W-F. Su, C-W. Chen, Exploiting optical anisotropy to increase the external quantum efficiency of flexible P3HT:PCBM blend solar cells at large incident angles, *Sol Energy Mater Sol Cells* **95** (2011) 2141-2150.

[5] W. Zhang, Y. Xu, H. Wang, C. Xu, S. Yang, Fe_3O_4 nanoparticles induced magnetic field effect on efficiency enhancement of P3HT:PCBM bulk heterojunction polymer solar cells, *Sol Energy Mater Sol Cells* **95** (2011) 2880-2885.

[6] S. K. Jang, S. C. Gong, H. J. Chang, Effects of various solvent addition on crystal and electrical properties of organic solar cells with P3HT:PCBM active layer, *Synth. Met*. **162** (2012**)** 426-430.

[7] L. N. S. A. Thummalakunta, C. H. Yong, K. Ananthanarayanan, J. Luther, P3HT based solution-processed pseudo bi-layer organic solar cell with enhanced performance, *Org. Electron.* **13** (2012**)** 2008-2016.

[8] F. C. Krebs, Polymer solar cell modules prepared using roll to roll methods: Knife-over-edge coating, slot-die coating and screen printing, *Sol. Energy Mater. Sol. Cells* **93** (2009**)** 465-475.

[9] M. Jørgensen, K. Norrman, F. C. Krebs, Stability/degradation of polymer solar cells, *Sol. Energy Mater. Sol. Cells* **92** (2008**)** 686-714.

[10] N. Grossiord, J. M. Kroon, R. Andriessen, P. W. M. Blom, Degradation mechanism in organic photovoltaic devices, *Org. Electron.* **13** (2012**)** 432-456.

[11] A. Moujoud, S. H. Oh, J. J. Hye, H. J. Kim, Improvement in stability of poly(3-hexylthiophene-2,5-diyl)/[6,6]-phenyl-C61-butyric aicd methyl ester bulk heterojunction solar cell by using UV light irradiation, *Sol. Energy Mater. Sol. Cells* **95** (2011**)** 1037-1041.

[12] J. Li, S. Kim, S. Edington, J. Nedy, S. Cho, K. Lee, A, Heeger, M. C. Gupta, J. T. Yates Jr, A study of stabilization of P3HT/PCBM organic solar cells by photochemical active TiOx layer, *Sol. Energy Mater. Sol. Cells* **95** (2011**)** 1123-1130.

[13] L. Yang, H. Xu, H. Tian, S. Yin, F. Zhang, Effects of cathode buffer layer on the stability of polymer bulk heterojunction solar cells, *Sol. Energy Mater. Sol. Cells* **94** (2010**)** 1831-1834.

[14] B. Zimmermann, U. Würfel, M. Niggemann, Longterm stability of efficient inverted P3HT:PCBM solar cells, *Sol. Energy Mater. Sol. Cells* **93** (2009**)** 491-496.

[15] A. Seemann, T. Sauermann, C. Lungenschmied, O. Armbruster, S. Bauer, H.-J. Egelhaaf, J. Hauch, Reversible and irreversible degradation of organic solar cell performance by oxygen, *Sol. Energy* **85** (2011) 1238-1249.

[16] K. Kawano, C. Adachi, Evaluating carrier accumulation in degraded bulk heterojunction organic solar cells by a thermally stimulated current technique, *Adv. Funct. Mater.* **19** (2009**)** 3934-3940.

[17] J. Schafferhans, A. Baumann, A. Wagenpfahl, C. deibel, V. Dyakonov, Oxygen doping of P3HT:PCBM blends: Influence on trap states, charge carrier mobility and solar cell performance, *Org. Electron*. **11** (2010**)** 1693-1700.

[18] Y-M. Chang, W.-F. Su, L. Wang, Influence of photo-induced degradation on the optoelectronic properties of regioregular poly(3-hexylthiophene), *Sol. Energy Mater. Sol. Cells* **92** (2008) 761-765.

[19] R. Battino, T. R. Rettich, T. Tominaga, The solubility of oxygen and ozone in liquids, *J. Phys. Chem.* **12** (1983) 163-178.

[20] L. Ulmer, J. Mattay. H. G. T.-Garcia, H. Luftmann, The use of 2-[(2*E*)-3-(4-*tert*-butylphenyl)-2-methylprop-2-enylidene]malononitrile as a matrix for matrix-assisted laser desorption/ionization mass spectrometry, *Eur. J. Mass Spectrom.* **6** (2000) 49-52.

[21] S. Desbief, N. Hergué, O. Douhéret, M. Surin, P, Dubois, Y. Geerts, R. Lazzaroni, P. Leclère. Nanoscale investigation of the electrical properties in semiconductor polymer-carbon nanotube hybrid materials, *Nanoscale*. **4**

(2012) 2705-2713.

[22] B. J. Leever, C. A. Bailey, T. J. Marks, M. C. Hersam, M. F. Durstock, In situ characterization of lifetime and morphology in operating bulk heterojunction organic photovoltaic devices by impedance spectroscopy, *Adv. Energy Mater.* **2** (2012) 120-128.

[23] M. Osaka, H. Benten, L. Lee, H. Ohkita, S. Ito, Development of highly conductive nanodomains in poly(3-hexylthiophene) films studied by conductive atomic force microscopy, *Polymer* **54** (2013) 3443-3447.

[24] J. Clark, J-F. Chang, F. Spano, R. Friend, C. Silva, Determining exciton bandwidth and film microstructure in polythiophene films using linear absorption spectroscopy, *Appl. Phys. Lett.* **94** (2009) 163306-163310

[25] M. Manceau, A. Rivaton, J.-L. Gardette, S. Guillerez, N. Lemaître, The mechanism of photo- and thermooxidation of poly(3-hexylthiophene) (P3HT) reconsidered, *Polym Degrad Stab* **94** (2009) 898-907.

[26] S. Chambon, A. Rivaton, J.-L.. Gardette, M. Firon, Photo- and thermal degradation of MDMO-PPV:PCBM blends, *Sol. Energy Mater. Sol. Cells* **91** (2007) 394-398.

[27] E. T. Hoke, I. T. S.-Quintana, M. T. Lioyd, I. Kauvar, W. R. Mateker, A. M. Nardes, C. H. Peters, N. Kopidakis, M. D. McGehee, The role of electron affinity in determining whether fullerenes catalyze or inhibit photooxidation of polymers for solar cells, *Adv. Energy Mater.* **11** (2012) 1351-1358.

[28] J. Liu, R. S. Loewe, R. D. MuCullogh, Employing MALDI-MS on poly(alkylthiophenes): Analysis of molecular weights, molecular weight distributions, end-group structures, and end-group modifications, *Macromol*. **32** (1999) 5777-5785.

[29] Y. Aoyama, T. Yamanari, N. Koumura, H. Tachikawa, M. Nagai, Y. Yoshida, Photo-induced oxidation of polythiophene derivatives: dependence on the side chain structures, *Polym. Degrad. Stab*. **98** (2013) 899-903.

[30] M. Abdou, S. Holdcroft, Mechanisms of photodegradation of poly(3-alkylthiophenes) in solution, *Macromol*. **26** (1993) 2954-2962.

[31] R. J. Kline, M. D. Mcgehee, E. N. Kadnikoza, J. Liu, J. M. J. Fréchet, Controlling the field-efect mobility of regioregular polythiophene by changing the molecular weight, *Adv. Mater.* **15** (2003) 1519-1522.

[32] R. C. Hiorns, R. d. Bettignies, J. Leroy, S. Bailly, M. Firon, C. Sentein, A. Khoukh, H. Preud'homme, C. D.-Lartigau, High molecular weights, polydispersities, and annealing temperatures in the optimization of bulk-heterojunction photovoltaic cells based on poly(3-hexylthophene) or poly(3-butylthiophene), *Adv. Funct. Mater*. **16** (2006) 2263-2273.

[33] C. H. Peters, I. T. Sachs-quintana, W. Mateker, T. Heumueller, J. Rivnay, R. Noriega, Z. Beiley, E. Hoke, A. Salleo, M. McGehee, The mechanism of burn-in loss in a high efficiency polymer solar cell, *Adv. Mater*. **24** (2012) 663-668.

[34] T. Nagamori, K. Marumoto, Direct observation of hole accumulation in polymer solar cells during device operation using light-induced electron spin resonance, *Adv. Mater*. **25** (2013) 2362-2367.

3. Role of superoxide anions in the photooxidation of polythiophene derivatives

3.1 Introduction

Polymer solar cells (PSCs) have potential advantages in various applications because of their mechanical flexibility, portability, colorful, and low fabrication cost. Poly(3-hexylthiophene) (P3HT) is one of the most widely employed p-type materials for the photoactive layer of PSCs [1–4]. Furthermore, it is also known that the use of P3HT degrades PSCs on long-term irradiation of solar light [5–11]. Jørgensen et al. recently proposed that the degradation mechanism of PSCs was related to the photooxidation of P3HT [11,12]. Therefore, the lifetime of PSCs could be increased by preventing the photooxidation of P3HT.

The mechanism for the photooxidation of P3HT has been reported to involve a singlet oxygen, which directly undergoes a Diels-Alder cycloaddition with a thienyl unit of P3HT [10.13–14]. However, this has been beginning to be reviewed. For example, Hintz et al. recently reported that the photooxidation of P3HT was initiated by the oxidation of the hexyl side chains [15]. In addition, Manceau et al. also reported that the sulfur atom of the thiophene ring was oxidized into sulfur oxide by hydroxyl radicals, which arose through hydrogen abstraction from the hexyl side chain at the α-position [16]. These findings implied that these photooxidation mechanism is different from direct cycloaddition of a singlet oxygen to the thiophene ring and involves another active species, which can attack the α-position of the alkyl side chain and form radicals. Furthermore, Manceau et al. also reported that a singlet oxygen did not react with P3HT [17].

On the basis of these findings, we review the photooxidative degradation mechanism of poly(3-alkylthiophene). Aguirre et al. reported that the $[Polym]^{+}\cdot[O_2]^{-}$ complex was formed by photoirradiation during initial stages of photooxidation [18]. Furthermore, Hoke et al. also reported that the superoxide anions were involved in the photooxidation of P3HT and fullerene derivatives by changing the electron affinities of fullerene [19].

We previously reported that poly(3-octyloxythiophene) (P3OOT) showed substantial stability and hardly any structural change was observed after simulated solar light irradiation [20]. It was explained by the low reactivity of the oxidation of the sulfur atom in the thiophene ring to by the hydroxyl radical [20]. Although the cationic state of photostable P3OOT was observed by light irradiation in air, the cationic state of P3HT was not observed. It is likely that the stable counter anion exists in P3OOT. The polymer cation and the counter anion would also have an influence on the photooxidation reaction.

To understand the role of another active species in the photooxidation of the polythiophene derivatives and the mechanism of radical formation by the species, P3HT and photostable P3OOT were irradiated by light. The differences in the photochemical behavior of P3HT and P3OOT were observed by light-induced electron spin resonance (LESR), ultraviolet-visible-near infrared (UV-vis-NIR) spectroscopy, Fourier transform infrared (FT-IR) (attenuated total reflectance [ATR]) spectroscopy, and density functional theory (DFT) calculation.

3.2 Experimental Details

3.2.1 Preparation of polythiophene derivatives

We used two polythiophene derivatives with different side chains: $–C_6H_{13}$ (P3HT) and $–OC_8H_{17}$ (P3OOT). P3HT (regioregularity >95%) was purchased from Merck. The weight-averaged molecular

weight (M_w) and polydispersity (M_w/M_n) of P3HT were determined by Gel Permeation Chromatography (GPC; Waters Co., Ltd.) 18,000 and 1.60, respectively. P3OOT was prepared by polymerization using the Grignard metathesis method [21]. 3-Octyloxythiophene was synthesized from 3-methoxythiophene and octanol in the presence of sodium hydrogen sulfate as the catalyst. After dibromination, P3OOT was synthesized from 2,5-dibromo-3-octyloxythiophene by a Kumada coupling reaction with 0.5 mol% $NiCl_2$(dppp) [dppp = 1,3-bis(diphenylphosphino)propane]. A bright blue powder was obtained in approximately 20% yield. The M_w and M_w/M_n of the polymer were 12,000 and 1.72, respectively. The M_w and M_w/M_n values of the polymer were determined as 12,000 and 1.72, respectively. ^{1}H NMR of P3OOT (400 MHz, $CDCl_3$): δ (ppm) 0.95 (t, 3H), 1.40 (broad, 10H), 1.80 (q, 2H), 4.00 (t, 2H), 6.80 (s, 1H), regioregularity > 95%.

3.2.2 Sample preparation and measurement

Polymer films were fabricated by spin coating on CaF_2 substrates. The thickness of each polymer film was 120 ± 10 nm, which was measured by the stylus-type film thickness meter (ULVAC E. S., Inc., Dektak). Solar-simulated light (AM 1.5 G) was used to irradiate the polymer films. The intensity was 100 mW/cm^2, and the device was calibrated by a standard cell for a-Si solar cells (Bunkoh-Keiki Co., Ltd). The temperature on the films was about 60 ^{o}C. To observe the effect of visible light, two kinds of color filters were put between sample and light source, respectively. UV-pass filter (SIGMA KOKI Co., LTD. UTVAF-50S-34U) passes only ultraviolet rays (under 400nm) and UV-cut filter (Toshiba Co., LTD. L-42) shuts out only ultraviolet rays (over 400 nm). To observe the effect of the surrounding gas atmosphere, samples were illuminated in several atmospheric environments, such as dry nitrogen (99.99%, H_2O is under 20 ppm, O_2 is under 5 ppm), dry oxygen (99.99%, H_2O is under 20 ppm) and dry

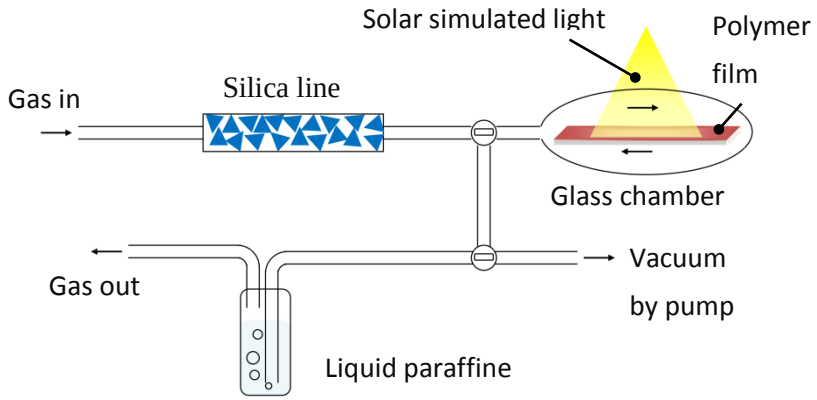

Figure 3.1 *The experimental setup for gas perge.*

air (H_2O is under 120 ppm) in glass chamber (See **Figure 3.1**). To investigate the temporal change of the polymer cation upon light irradiation, LESR spectra of films were measured by a X-band electron spin resonance (ESR) spectrometer (JEOL JES-FA200) with solar-simulated light (AM 1.5 G) irradiation (100 mW/cm^2) in ambient air. The sample was inserted into an ESR quartz tube with an inner diameter of 3.5 mm and mounted into a cavity, where an ESR spectrum was measured with light irradiation [22]. To confirm the influence of the superoxide anion radical, samples were dipped in (copper–zinc) superoxide dismutase (SOD) (Wako Pure Chemical Industries, Ltd.; activity; 2500 U/mg) aqueous solution (1.44 mg/mL). Then, these samples were rinsed with distilled water. In addition, P3HT film was also irradiated with ascorbic acid, which was superoxide anion quencher. Spectral measurements were performed using a UV-vis-NIR spectrophotometer (Shimazu Co., Ltd.; UV-3600) and an FT-IR Spectrometer (Perkin Elmer Co., Ltd.; Spectrum one).

These SOD and ascorbic acid were purchased from Wako chemical. These structures is as follows (**Figure. 3.2**). SOD is a redox enzyme that disproportionates from superoxide anion to hydrogen

peroxide and oxygen. This disproportionation reaction is triggered by metal ion such as copper ion (II) and zinc ion (II) which present in the active center on the enzyme. The reaction equation is as follows:

- M^{2+}-SOD + O_2^- → M^{1+}-SOD + O_2
- M^{1+}-SOD + O_2^- + $2H^+$ → M^{2+}-SOD + H_2O_2

(M=Cu or Zn)

Ascorbic acid is generally known as Vitamin C, which totally supports our health. One of support functions is the antioxidant function which prevents active oxygen species such as superoxide anion, singlet oxygen, and hydroxyl radical from oxygenating our body tissue. The ascorbic acid catches the lone pair electron of superoxide anion.

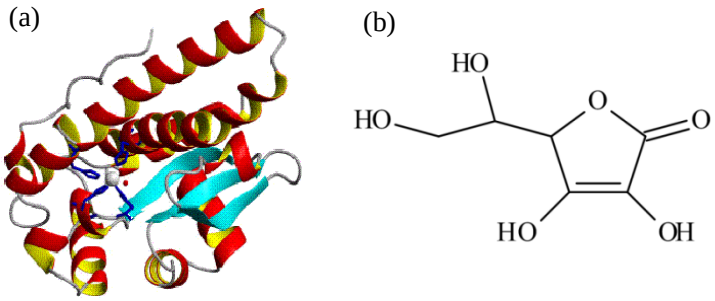

Figure 3.2 *Molecular structure of (a) SOD and (b) ascorbic acid.*

3.2.3 Density functional theory calculations

In the DFT calculations, 3′-hexyl-2,2′:5′,2″’-terthiophene was chosen as the model compound of P3HT. First, the geometries of neutral P3HT were calculated by means of the DFT method with Becke 3-Parameter (exchange), and Lee, Yang, and Parr (correlation) B3LYP function with 6-311G(d,p) basis set. Then, the geometries of the cation radical of P3HT (denoted by $[P3HT]^+$) were optimized from the neutral

structures. In addition, we also optimized polymers whose proton or hydrogen was abstracted by the superoxide anion. The proton or hydrogen atom was abstracted from the α-position of the side chain of the model compounds. The energy diagram was developed from these energy values. The structures were fully optimized using the energy gradient method without symmetry restriction. The calculations were performed using a Gaussian program package (Gaussian09).

3.3 Result and Discussion

3.3.1 Effects of the visible light or surrounding gas on photooxidation of P3HT

To confirm the effect of the wavelength for irradiation light, changes of absorbance at absorption peak of P3HT (530 nm) during light irradiation was observed, as shown in **Figure 3.3**. The irradiated solar simulated light was divided by color filters. Both of the UV light and the UV-cut light triggered the photooxidation of P3HT. Especially, the irradiation to P3HT with UV-cut filter was more degradated by photooxidation than that with UV-pass filter. The photooxidation by

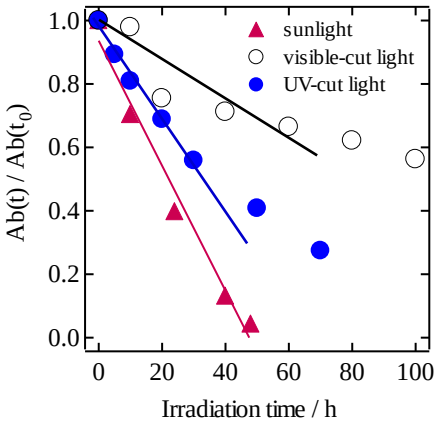

Figure 3.3 *Normalized UV-visible absorption of P3HT (at 530 nm) films (▲) with sunlight, (○) with visible-cut light and (●) with UV-cut light.*

UV light is explained by the strong energy of ultraviolet light which can break C-H bond [19-21]. However, the photooxidation can not be explained by only the dissociation of chemical binding due to the ultraviolet light, and the visible light certainly related to the photooxidation reaction of P3HT.

In order to investigate effect of the surrounding gas on P3HT photooxidation, P3HT films were illuminated in several gas, such as dry nitrogen, dry oxygen and dry air. Relative decays of absorption peak (530 nm) of P3HT are shown in **Figure 3.4**. In dry nitrogen gas, the decrease in absorption spectra of P3HT was hardly observed even after 100h irradiation. Thus, the nitrogen is not the main agent of the photooxidation of P3HT. Also, the light irradiation for 100h could not decompose P3HT. In dry air and normal air, the decrease in absorption of P3HT was similar. Therefore, the moisture does not affect to the photooxidation of P3HT. On the other hand, in dry oxygen, the decrease in absorption of P3HT was acceralated compared with irradiation in dry and normal air. The variations of the chemical structure of P3HT under light irradiation was also acceralated in

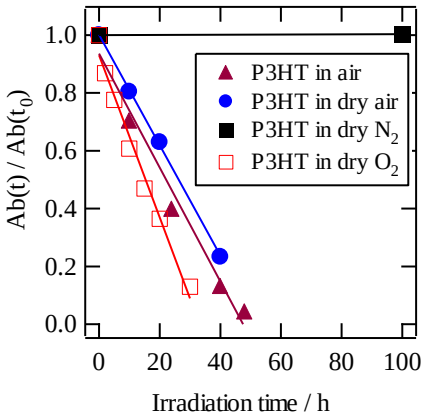

Figure 3.4 *Normalized UV-visible absorption peaks of P3HT (at 530 nm) samples during AM1.5G light irradiation. Atmospheres are (▲) air, (●) dry air, (■) dry nitrogen and (□) dry oxygen. Polymer films were illuminated with solar simulated light (AM 1.5 G) irradiation of 100 mW/cm^2 intensity.*

oxygen atmosphere (data not shown). Therefore, it can be considered that the oxygen species mainly triggers the photooxidation of P3HT.

Variations of UV-vis-NIR spectra of P3HT and P3OOT during light irradiation in dry oxygen are shown in **Figure 3.5**. The absorbance at visible light region of both of these polymers (1.8eV~3.0eV) decreased, and the absorbance of the near-infrared region (0.5-1.8 eV) appeared at the same irradiation time. This absorbance is based on the absorption of the polymer cation (polaron) [23-25]. Changes in absorbance of P3HT (at 1.6 eV) and P3OOT (at 1.3 eV) [23,25] upon light irradiation in air or in dry oxygen are shown in the inset figure 3. The absorbance of polaron in P3HT and P3OOT in dry oxygen was obviously higher than that in air. These results indicated that the polymer cation arisen by electron transfer from polymer to oxygen as the complex of polymer cation $[Polym]^+$ and oxygen anion $[O_2]^-$ [16, 23-25].

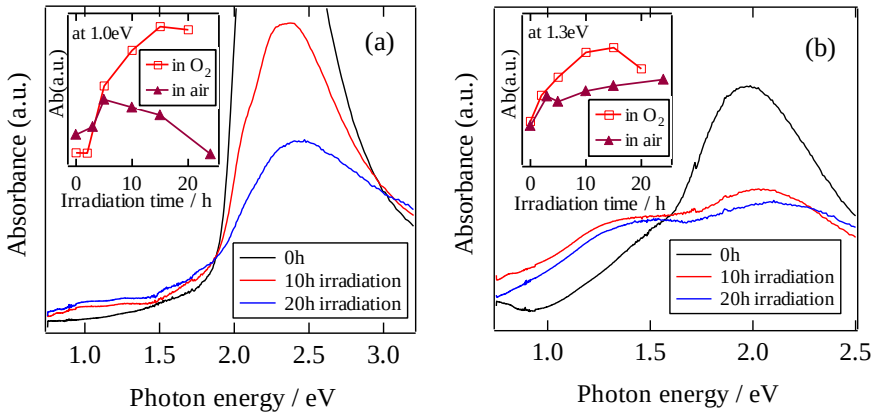

Figure 3.5 *Photoabsorption spectra of (a) P3HT films and (b) P3OOT films of (—) 0 h, (—) after 10 h irradiation and (—) after 20 h irradiation in dry oxygen atmosphere. Inset: Temporal changes in the absorbances of (a) P3HT film (at 1.0 eV) and (b) P3OOT film (at 1.3 eV) during AM1.5G light irradiation (□) in dry oxygen atmosphere and (▲) in air.*

3.3.2 Elucidation of photoactive species on photooxidation of P3HT

To further investigate the oxygen-doped polymer cation upon light irradiation,[18,19] LESR of P3HT and P3OOT were measured (see **Figure S4**). One signal was observed in the ESR spectra of P3HT and P3OOT measured after 20 h light irradiation in air, and the *g* factors of P3HT and P3OOT were determined to be 2.00218 (321.33 mT) and 2.00369 (321.16 mT), respectively. These ESR characteristics were in good agreement with those of P3HT and P3OOT after iodine doping [24,25]. Therefore, these ESR signals upon light irradiation were ascribed to the polymer cations.

Temporal changes in the ESR peak intensities of P3HT and P3OOT thin films in air and vacuum are shown in **Figure 3.6**. The data were measured from 0 to 20 h of illumination. Then, the data were measured from 20 to 27 h after turning off the light. The spin concentrations hardly increased in vacuum (<10^{-4} Pa) compared with the case in air, because oxygen, which accepts π-electron from polymers, hardly existed in vacuum. The spin concentrations increased in air during light irradiation. Thus, changes occur in the cationic state

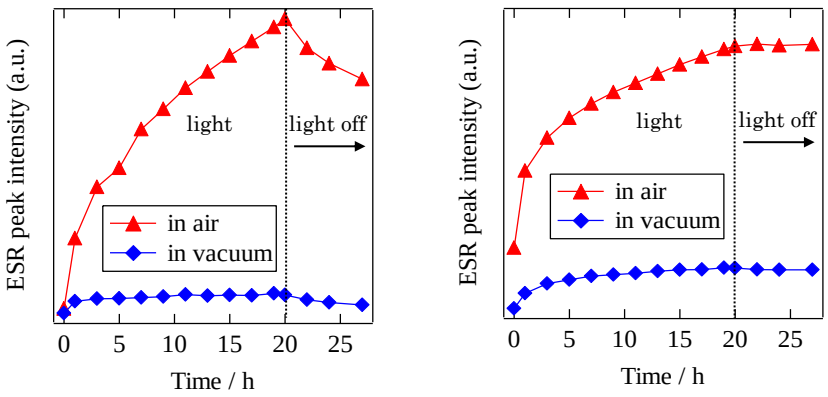

Figure 3.6 *Temporal changes in the ESR peak intensities of (a) P3HT and (b) P3OOT films (▲) in air and (◆) in vacuum. The light condition: 0–20 h. The dark condition: 20–27 h.*

on oxygen doping. Under dark conditions (20–27 h), which followed the 20 h-light illumination, the spin concentration of P3HT decayed, whereas that of P3OOT remained. The changes in the ESR spectra of P3HT and P3OOT after 4 h in the dark are shown in the supporting information. These results indicated that the $[P3HT]^{+}\cdot[O_2]^{-}$ complex was unstable, whereas the $[P3OOT]^{+}\cdot[O_2]^{-}$ complex was stable.

As can be seen in ESR measurements, the $[P3HT]^{+}\cdot[O_2]^{-}$ complex seems to decrease. This decrease could be explained in two possible ways. One way is a reversible reaction in which the $[P3HT]^{+}\cdot[O_2]^{-}$ complex returns to neutral P3HT and O_2 [13,24] The other way is the decomposition of $[P3HT]^{+}$ by the $[O_2]^{-}$ (superoxide anion radical). If the former pathway were the predominant mode, then the photoabsorption of irradiated P3HT would partially recover after turning off the light. **Figure 3.7** shows the UV-visible absorbance changes of P3HT. First, the P3HT film was irradiated for 5 h, and then the film was kept in the dark for 20 h. However, contrary to our expectations, a decrease in absorption was observed after turning off the light Thus, it is appears that the decomposition of $[P3HT]^{+}$ by $[O_2]^{-}$ occurs in preference to the reversible reaction of the $[P3HT]^{+}\cdot[O_2]^{-}$ complex. It is known that the superoxide anion radical is one of the

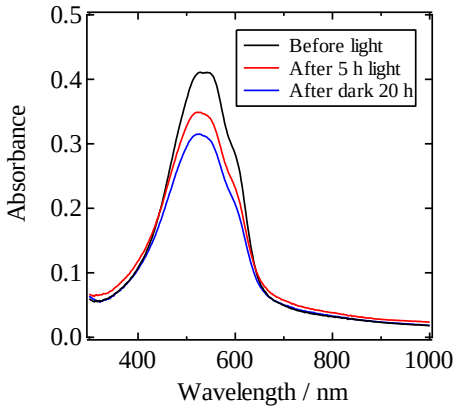

Figure 3.7 *UV-vis/NIR spectra of P3HT films before irradiation (—), after 5 h irradiation (—), and 20 h under dark conditions after 5 h irradiation (—).*

strongest oxidants among oxygen species and triggers hydrogen or proton abstraction reactions.[26–29] Therefore, if the superoxide anion radical affects to the reaction, the photooxidation will be suppressed by adding a superoxide quencher. SOD, a redox enzyme, selectively quenches the superoxide anion radical.[29,30] We focused on the irradiated state of P3HT and examined the UV-visible absorbance changes of P3HT using SOD (**Figure 3.8**) to confirm the effect of the superoxide anion. First, the P3HT films were irradiated for 12 h, and then the films were dipped in SOD aqueous solution or distilled water in the dark for 20 h. In Figure 3.6(a), the decrease in absorbance observed is similar to that observed in Figure 3. However, in Figure 3.6(b), no change in the absorbance is observed. Therefore, the decrease in P3HT absorbance is suppressed with SOD, confirming that the superoxide anion is one of active species in P3HT oxidation. This suppression of the photooxidation was also confirmed by irradiation of P3HT in an ascorbic acid aqueous solution, which is a superoxide anion radical quencher[30] (See **Figure S5**).

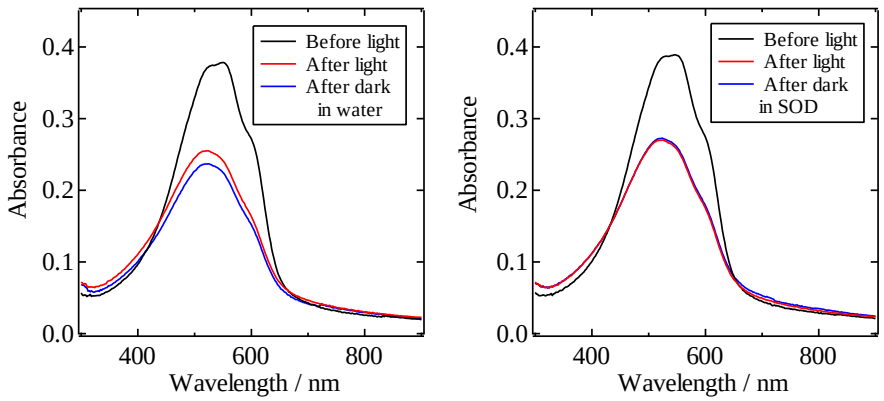

Figure 3.8 *UV-vis/NIR spectra of P3HT films in presence/absence of SOD: (a) before irradiation (—), after 12 h irradiation (—), and 20 h under dark conditions in water (without SOD) after 12 h irradiation (—); (b) Before irradiation (—), after 12 h irradiation (—), and 20 h under dark conditions in SOD aqueous solution (with SOD) after 12 h irradiation (—).*

3.3.3 Initial photooxidation mechanism by superoxide anion

In the oxidation reaction with the superoxide anion, the superoxide anion radical shows an ionic reaction with the proton[26,27,29] and a free-radical reaction with the hydrogen.[26–30] Therefore, in the present study, we assumed that the superoxide anion radical can trigger an oxidation reaction to abstract either a hydrogen atom or a proton at the α-position of the hexyl side chain in $[P3HT]^+$.The reaction was simulated by the DFT calculation (see **Figure 3.9**) to examine which reaction occurs. The reaction of the superoxide anion with the α-proton in $[P3HT]^+$ is an exothermic reaction, which produces a heat of reaction of 121.1 kcal/mol. In contrast, the reaction of the superoxide anion with the α-hydrogen in $[P3HT]^+$ is an endothermic reaction, which gives a

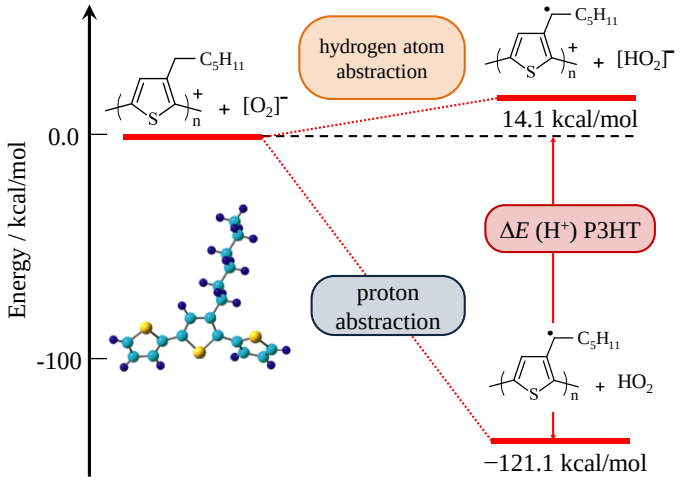

Figure 3.9 *Energy diagram of $[P3HT]^+ + [O_2]^-$, $[P3HT\cdot] + [HO_2]^-$, and $[P3HT\cdot] + HO_2$. Superoxide anion $[O_2]^-$ reacts with the α-hydrogen and α-proton of P3HT. Inset; model compound (3′-hexyl-2,2′:5′,2″-terthiophene) structure of P3HT.*

negative heat of reaction of 14.1 kcal/mol. Therefore, the DFT calculation confirmed that the superoxide anion could easily abstract the α-proton of P3HT. On the other hand, the hydrogen abstraction was

less favored. This means that the superoxide anion abstracts the α-proton, which proceeds by cation movement from the π-orbital on the thiophene main chain to the α-hydrogen.

On the other hand, $[P3OOT]^+$ has no α-protons. Therefore, the superoxide anion cannot abstract the α-proton. Moreover, Hatakeyama et al. reported that the deprotonation reaction of poly(3-alkyl thiophene)$^+$ $[P3AT]^+$ occurred easily at the α-position in side chain

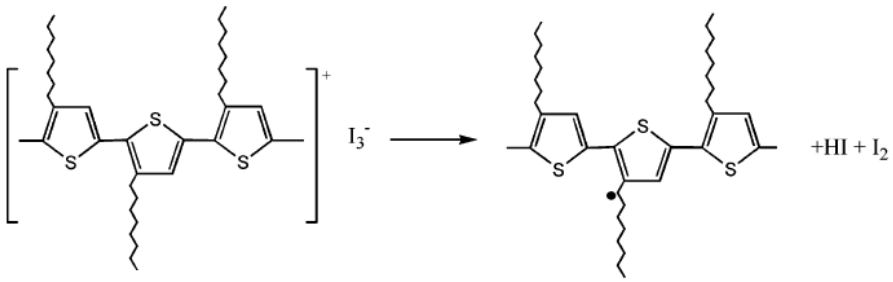

Scheme 3.1 *Deprotonation reaction of [poly(3-alkylthiophene)]˙, which is denoted in Koizumi et al.*[31].

(**Scheme 3.1**), but the deprotonation of $[P3OOT]^+$ did not take place, and the cationic state of P3OOT was stable.[25,31] This tendency was also observed in ESR spin changes after continuous irradiation (Figure 3.4). Thus, these results indicated that the photooxidation of P3HT progresses through the deprotonation reaction in the presence of a superoxide anion. The deprotonation is caused by an electron transfer from the excited polymer to oxygen.

We proposed the initiation step photooxidation of polythiophene derivatives, as shown in **Scheme. 3.2**. The polythiophene derivative is excited by absorption of visible light. The energy of the excited state of polythiophene derivatives transfer to a triplet oxygen yielding a singlet oxygen. While some of singlet oxygen is directly involved in the cycloadditional reaction to polythiophene double bond, other singlet oxygen withdraw the π-electron from polythiophene derivative, and then a charge transfer complex ($[Polym]^+ \cdot [O_2]^-$) was formed (Energy diagram is shown in **Table 3.1**).

Table 3.1. *Energy diagrams of oxygen species and polythiophene derivatives. The energies of oxygen species were calculated at the B3LYP/6-311G(d,p) level of theory. *The energies of polythiophene derivatives were measured by Photoelectron Yield Spectroscopy (PYS).*

		E LUMO (eV)	*E* HOMO (eV)
$^1O_2$		-4.88	-6.81
*Polymers	P3HT	-3.30	-5.10
	P3OOT	-3.50	-4.95

The $[O_2]^-$ is strong oxidant and exist unstably in P3HT. The $[O_2]^-$ trigger proton abstraction at α-position at the hexyl side chain of $[P3HT]^+$ (polaron) yielding the [P3HT] radical and $[HO_2]$. The localized radical at α-position at the hexyl side chain in P3HT quickly react with a triplet oxygen, and the chain reaction of the photooxidation progressed [16]. The $[HO_2]^-$ may trigger hydrogen abstraction and yield hydroperoxide.

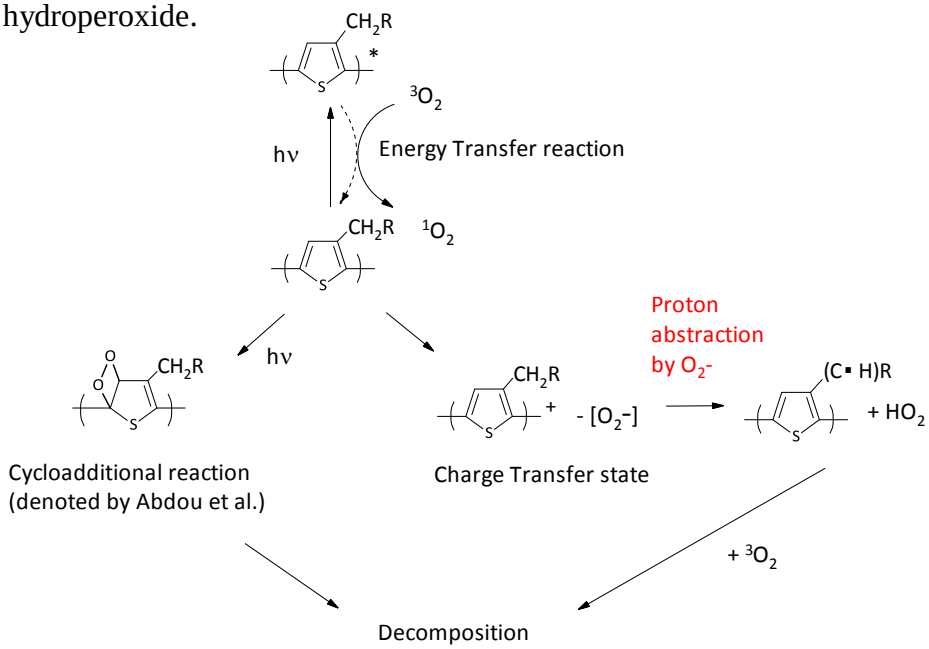

Scheme 3.2 *The proposed initiation step photooxidation mechanism of polythiophene derivatives. Cycloadditional reaction by a singlet oxygen is denoted by Abdou et al.*[14]

3.4 Conclusion

To understand the role of another active oxygen species in photooxidation of P3HT, we have investigated the photostable P3OOT, and have investigated the differences in the photochemical behavior of P3HT and P3OOT by means of LESR and UV-vis-NIR analysis. In air, both the $[P3HT]^{+}\cdot[O_2]^{-}$ and $[P3OOT]^{+}\cdot[O_2]^{-}$ charge transfer complexes were formed by oxygen doping upon light irradiation. Although the $[P3HT]^{+}\cdot[O_2]^{-}$ complex was unstable, $[P3OOT]^{+}\cdot[O_2]^{-}$ was found to be stable. This instability of the $[P3HT]^{+}\cdot[O_2]^{-}$ complex is mainly due to the decomposition of $[P3HT]^{+}$ by the superoxide anion radical $[O_2]^{-}$, which was confirmed by addition of SOD. The superoxide anion is one of the strongest known oxidants of oxygen species and triggers hydrogen or proton abstraction reactions. DFT calculations revealed that the superoxide anion reacts more easily with the α-proton than the α-hydrogen in the hexyl side chain of P3HT. These results indicated that the part of photooxidation of P3HT started from the reactive α-proton abstraction by $[O_2]^{-}$. Our results suggest that the photooxidation of polythiophene derivatives can be partially prevented by quenching the superoxide anion. We are now conducting quantitative investigations by means of ESR to further expand on the photooxidation of polythiophene derivatives.

3.5 References

[1] Iwan A, Palewicz M, Ozimek M, Chuchmala A, Pasciak G, Influence of aluminium electrode preparation on PCE values of polymeric solar cells based on P3HT and PCBM. *Org. Electron.* **13** (2012) 2525–2531.

[2] Das N C, Sokol P E. Hybrid photovoltaic devices from regioregular polythiophene and ZnO nanoparticles composites. *Renew Energy* **35** (2010) 2683-2688.

[3] Wang M, Wang X. P3HT/ZnO bulk-heterojunction solar cell sensitized by a perylene derivative. *Sol Energy Mater Sol Cells* **92** (2008) 766-771.

[4] Shen Y.-M, Chen C.-S, Yang P.-C, Ma S.-Y, Lin C.-F. Improvement of surface morphology of thin films and performance by applying electric field on P3HT:PCBM based solar cells. *Sol Energy Mater Sol Cells* **99** (2012) 263–267.

[5] Manceau M, Rivaton A, Gardette J.-L, Guillerez S, Lemaître N. Light-induced degradation of the P3HT-based solar cells active layer. *Sol Energy Mater Sol Cells* **95** (2011) 1315–1325.

[6] Rivaton A, Chambon S, Manceau M, Gardette J.-L, Lemaître N, Guillerez S. Light-induced degradation of the active layer of polymer-based solar cells. *Polym Degrad Stab* **95** (2010) 278–284.

[7] Guerrero A, Boix P. P, Marchesi L. F, Ripolles-Sanchis T, Pereira E. C, Garcia-Belmonte G. Oxygen doping-induced photogeneration loss in P3HT:PCBM solar cells. *Sol Energy Mater Sol Cells* **100** (2012) 185–191.

[8] Jin H, Olkkonen J, Tuomikoski M, Kopola P, Maaninen A, Hast J. Thickness dependence and solution-degradation effect in poly(3-hexylthiophene) :phenyl-C61-butyric acid methyl ester based solar cells. *Sol Energy Mater Sol Cells* **94** (2010) 465–470.

[9] Voroshazi E, Verreet B, Aernouts T, Heremans P. Long-term operational lifetime and degradation analysis of P3HT: PCBM photovoltaic cells. *Sol Energy Mater Sol Cells* **95** (2011) 1303–1307.

[10] Grossiord N, Kroon J. M, Andriessen R, Blom P. W. M. Degradation mechanisms in organic photovoltaic devices. *Org. Electron.* **13** (2012) 432–456.

[11] Jørgensen M, Norrman K, Gevorgyan S. A, Tromholt T, Andreasen B, Krebs F. C. Stability of polymer solar cells. *Adv. Mater.* **24** (2012) 580–612.

[12] Jørgensen M, Norrman K, Krebs F C. Stability/degradation of polymer solar cells. *Sol Energy Mater Sol Cells* **92** (2008) 686-714.

[13] Sperlich A, Kraus H, Deibel H, Blok H, Schmidt J, Dyakonov V. Reversible and irreversible interactions of poly(3-hexylthiophene) with oxygen studied by spin-sensitive methods. *J. Phys. Chem. B* **115** (2011) 13513–13518.

[14] Abdou M S A, Holdcroft S. Mechanism of photodegradation of poly(3-alkylthiophenes) in solution. *Macromol.* **26** (1993) 2954-2962.

[15] Hintz H, Egelhaaf H.-J., Peisert H, Chassé T. Photo-oxidation and ozonization of poly(3-hexylthiophene) thin films as studied by UV/VIS and photoelectron spectroscopy. *Polym. Degrad. Stab.* **95** (2010) 818-825.

[16] Manceau M, Rivaton A, Gardette J-L, Guillerez S, Lemaître N. The mechanism of photo- and thermooxidation of poly(3-hexylthiophene) (P3HT) reconsidered. *Polym. Degrad. Stab*. **94** (2009) 898-907.

[17] Manceau M, Rivaton A, Gardette J.-L. Involvement of singlet oxygen in the solid-state photochemistry of P3HT. *Macromol. Rapid Commun*. **29** (2008) 1823–1827.

[18] Aguirre A, Meskers S. C. J, Janssen R. A. J, Egelhaaf H.-J. Formation of metastable charges as a first step in photoinduced degradation in π-conjugated polymer:fullerene blends for photovoltaic applications. *Org. Electron*. **12** (2011) 1657–1662.

[19] Hoke E. T, Sachs-Quintana I. T, Lloyd M. T, Kauvar, I, Mateker W. R, Nardes A. M, Peters C. H, Kopidakis N, McGehee M. D. The role of

electron affinity in determining whether fullerenes catalyze or inhibit photooxidation of polymers for solar cells. *Adv. Energy Mater.* **2** (2012) 1351–1357.

[20] Aoyama Y, Yamanari T, Koumura N, Tachikawa H, Nagai M, Yoshida Y. Photo-induced oxidation of polythiophene derivatives: Dependence on side chain structure. *Polym. Degrad Stab*. **98** (2013) 899–903.

[21] McCullough R D, Lowe R D, Jayaraman M, Anderson D L. Design, synthesis, and control of conducting polymer architectures: Structurally homogeneous poly(3-alkylthiophenes). J. Org. Chem. **58** (1993) 904-912.

[22] Marumoto K, Fujimori T, Ito M, Mori T. Charge formation in pentacene layers during solar-cell fabrication: Direct observation by electron spin resonance. *Adv. Funct. Mater.* **2** (2012) 591–597.

[23] Furukawa, Y. Electronic absorption and vibrational spectroscopies of conjugated conducting polymers. *J. Phys. Chem.* **100** (1996) 15644-15653.

[24] Abdou M. S. A, Orfino F. P, Son Y, Holdcroft S. Interaction of oxygen with conjugated polymers: Charge transfer complex formation with poly(3-alkylthiophenes). *J. Am. Chem. Soc*. **119** (1997) 4518–4524.

[25] Hatakeyama K, Koizumi H, Ichikawa T. Stability of a conductive state of Poly(3-alkoxyth iophene)s. *Bull. Chem. Soc. Jpn*. **82** (2009) 202-205.

[26] Chemical Society of Japan. Chemistry of active oxygen species. KIKAN KAGAKU SOSETSU. Japan: Scientific Societies Press **7** (1990) 3-28.

[27] Crank G, Makin M. I. H. Oxidations of aromatic amines by superoxide ion. Aust. J. Chem. **37** (1984) 845–855.

[28] Eberhardt M. K. Reactive oxygen metabolites: Chemistry and medical

consequences. CRC Press LLC: USA (2001) 51–53.

[29] Moro-Oka Y, Chung P. J, Arakawa H, Ikawa T. Chemistry of superoxide ion. Reaction of superoxide ion with substrates having labile hydrogens. *Chem. Lett.* (1976) 1293–1296.

[30] Takeo O, Chemical Society of Japan. Active oxygen species. Maruzen Press: Japan, (1999) 27.

[31] Koizumi H, Dougauchi H, Ichikawa T. Mechanism of dedoping processes of conducting poly(3-alkylthiophenes). J. Phys. Chem. B **109** (2005) 15288–15290.

4. Photo-induced oxidation of polythiophene derivatives: Dependence on side chain structure

4.1 Introduction

Polymer solar cells (PSCs) have many potential advantages in their mechanical flexibility, portability, and low manufacturing cost. Among the conducting polymers used, poly(3-hexylthiophene) (P3HT) is one of the most commonly employed materials for the photo-active layer because of its high conductivity [1,2]. According to recent studies on PSCs utilizing P3HT, the power conversion efficiency has been drastically improved [3-10] and large-scale production can be expected imminently [11]. On the other hand, it is well known that a PSC based on P3HT degrades with long-term solar light irradiation. Jørgensen et al. recently proposed that photooxidation of the polymer was related to the mechanism of degradation of PSCs [12].

The photooxidation of P3HT has been investigated [13-19]. Hintz et al. reported that the photooxidation of P3HT was initiated by the oxidation of the hexyl side chains [18]. In addition, Manceau et al. reported that the sulfur atom of the thiophene ring was oxidized into sulfur oxide by hydroxyl radicals, which arose through hydrogen abstraction from the hexyl side chain at the α-position [19]. The photooxidation of poly(3-butylthiophene) and poly(3-octylthiophene) has also been investigated [20-22]. On the other hand, Rivaton et al. reported that polythiophene (PT) had substantial stability, even after long-term light irradiation [16]. In addition, poly(3-carboxydithiophene) (P3CT), which has a carboxyl side chain, was shown to have good stability under light illumination [23,24]. Thus, it is hypothesized that the

photooxidation of polythiophene derivatives is dependent on the structures of their side chains.

In this paper, in order to investigate the photooxidation of polyalkylthiophene derivatives, the side chain at the α-position was varied and three different polythiophene derivatives with no α-hydrogen were synthesized (phenyl, alkoxy, and *tert*-pentyl). The differences in photochemical behavior of the derivatives and the previously studied P3HT were investigated by UV-vis-NIR and FT-IR (ATR) spectroscopy during simulated solar light irradiation.

4.2 Experimental Details

4.2.1 Synthesis of polythiophene derivatives

Three polythiophene derivatives with different side chains were prepared: $-C_6H_5$ poly(3-phenyl)thiophene (P3PhT), $-C(CH_3)_2C_2H_5$ poly(3-(1,1-dimethylpropyl) thiophene) (P3DMPT), and $-OC_8H_{17}$ poly(3-octyloxy)thiophene (P3OOT), as shown in **Figure 4.1**. The P3PhT was prepared by polymerization using the Grignard metathesis method (See supporting information) [25]. 3-Phenylthiophene was dibrominated with *N*-bromosuccinimide (NBS) in tetrahydrofuran (THF) to afford 2,5-dibromo-3-phenylthiophene. This was then polymerized using a Kumada coupling reaction catalyzed by $NiCl_2$(dppp) [dppp = 1,3-bis(diphenyl phosphino)propane]. A bright red powder was obtained with ca. 20 % yield, which was soluble in organic solvents such as chloroform and THF. ^{1}H NMR (400 MHz, $CDCl_3$): δ 7.10 ppm (s, 1H), δ 7.36 ppm (t, 1H), δ 7.43 ppm (t, 2H), δ 7.49 ppm (d, 2H). Regio-regularity > 95%. GPC (Waters Co., LTD.): M_w = 1.59 kg/mol, M_w/M_n = 1.39.

The P3DMPT was prepared by polymerization using the Grignard metathesis method [26]. 2,5-Dibromo-3-(1,1-dimethylpropyl) thiophene was synthesized from 2,5-dibromothiophene and

2-chloro-2-methylbutane by a Friedel-Crafts reaction using $AlCl_3$ as a catalyst. The final product was synthesized from 2,5-dibromo-3-(1,1-dimethylpropyl)thiophene by the same reaction as was used for P3PhT. A red brown powder was obtained with ca. 10 % yield. ^{1}H NMR (400 MHz, $CDCl_3$): δ 1.00 ppm (t, 3H), δ 1.35 ppm (q, 2H), δ 1.60 ppm (s, 6H), δ 6.80 ppm (s, 1H). Regio-regularity > 95%. GPC: M_w = 11.4 kg/mol, M_w/M_n = 2.30.

P3OOT was prepared by polymerization using the Grignard metathesis method [27]. 3-Octyloxythiophene was synthesized from 3-methoxythiophene and octanol with $NaHSO_4$ as a catalyst. 3-Octyloxylthiophene was dibrominated and the final product was synthesized from 2,5-dibromo-3-octyloxythiophene by the same reaction as was used for P3PhT. A bright blue powder was obtained with ca. 20 % yield. ^{1}H NMR (400 MHz, $CDCl_3$): δ 0.95 ppm (t, 3H), δ 1.40 ppm (broad, 10H), δ 1.80 ppm (q, 2H), δ 4.00 ppm (t, 2H), δ 6.80 ppm (s, 1H). Regio-regularity > 95%. GPC: M_w = 12.0 kg/mol, M_w/M_n = 1.72.

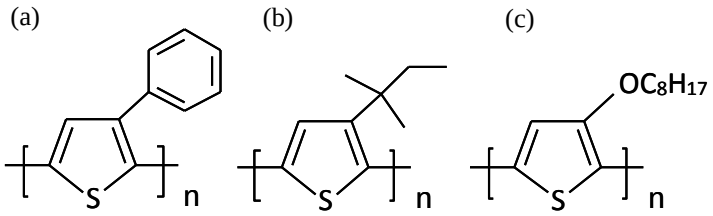

Figure 4.1 *The chemical structures of (a) poly(3-phenyl)thiophene (P3PhT) (b) poly(3-(1,1-dimethylpropyl)thiophene) (P3DMPT), and (c) poly(3-octyloxy)thiophene (P3OOT).*

4.2.2 Sample preparation and measurement

P3HT (M_w = 18.0 kg/mol, M_w/M_n = 1.60, Regio-regularity > 95%), which has similar molecular weight, polydispersity, and

regio-regularity, was purchased from Merck. We exclude the effect of the regio-regularity with four polymers [28]. Polymer films were fabricated by spin-coating onto CaF_2 substrates. All the thicknesses of polymer films were 120 nm, which were measured by stylus method film thickness meter (ULVAC E. S., Inc.). The effect of the thickness difference with four polymers was excluded [28-30]. These films were irradiated with simulated solar light (AM 1.5 G) of 100 mW/cm^2 intensity for up to 100 h in ambient air. The irradiation intensity was calibrated using a standard cell for a-Si solar cells (Bunkoukeiki Co., LTD.). UV-vis-NIR (Shimadzu Co., LTD.) spectra and FT-IR (ATR) (Perkin Elmer Co., LTD.) spectra of the polymer films were measured before and after the illumination.

4.2.3 Density functional theory (DFT) calculations

First, the geometries of thiophene and the thiophene radical were calculated by means of the DFT method with Becke 3-Parameter (exchange), Lee, Yang, and Parr (correlation) B3LYP function with 6-311G(d,p) basis set. The binding energy of the hydrogen atom was calculated from the energy difference between thiophene and the thiophene radical plus hydrogen atom. One unit model of thiophene and a thiophene radical was examined for the energy calculation. Hereafter, the structural models of P3HT and P3OOH are expressed as mP3HT and mP3OOH, respectively. The structures were fully optimized using the energy gradient method without symmetry restriction. The calculations were performed using a Gaussian program package (Gaussian09).

4.3 Result and Discussion

4.3.1 Photooxidation of polythiophene derivatives

Variations in the UV-vis-NIR spectra of P3HT, P3PhT, P3DMPT, and P3OOT thin films during AM 1.5G light irradiation are shown in **Figure 4.2**. The visible absorption intensities of P3HT, P3PhT, and P3DMPT decreased continuously during the irradiation and the peak wavelengths exhibited a blue shift (see **Figure. S6**).

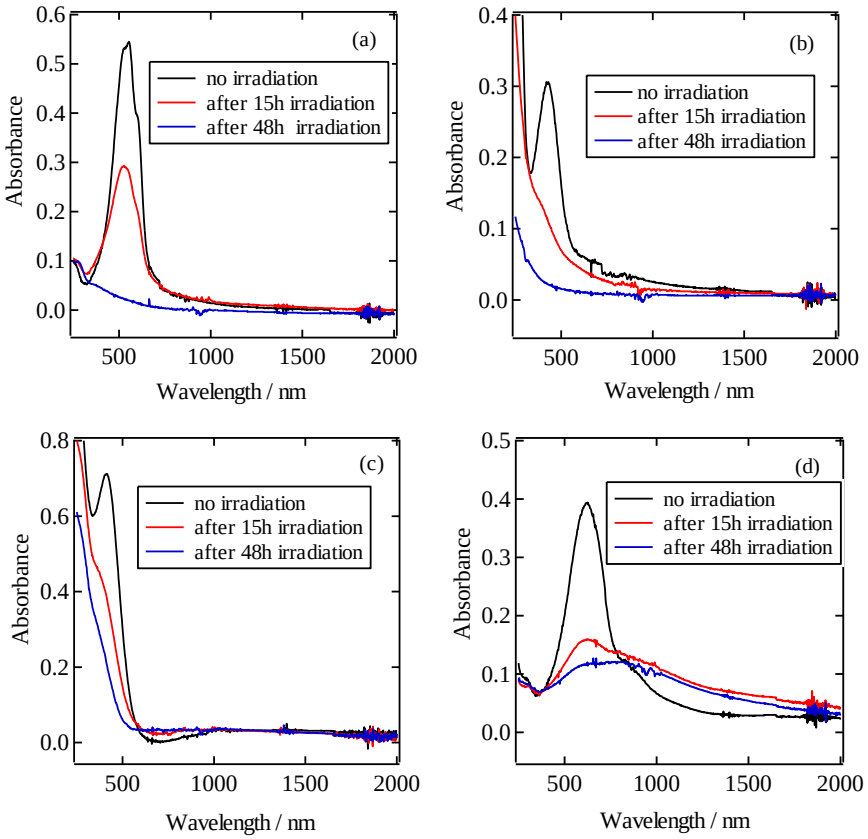

Figure 4.2 *UV-vis-NIR spectra of (a) P3HT, (b) P3PhT, (c) P3DMPT, and (d) P3OOT films after (—) no-irradiation, (—) 15 h irradiation, and (—) 48 h irradiation. Polymer films were irradiated with simulated solar light (AM 1.5 G) of 100 mW/cm^2 intensity.*

These results indicate a reduction in the conjugation length of the polymers [15]. On the other hand, for the P3OOT, the visible absorption intensity decreased but the blue shift in peak wavelength was not

observed. In addition, absorbance of the NIR region appeared at the same time. Therefore, it was deduced that the scission of π-conjugation of P3OOT did not occur. Relative decays in absorption peak intensity for each of the polythiophenes are shown in **Figure 4.3**, with the wavelengths being 530 nm, 430 nm, 410 nm, and 630 nm for P3HT, P3PhT, P3DMPT, and P3OOT, respectively. The decreases in absorption for P3PhT, P3DMPT, and P3OOT were clearly faster than that for P3HT. The absorptions of P3HT and P3PhT were completely decreased within 50 h, on the other hand, those of P3DMPT and P3OOT remained to some extent even after 50 h light irradiation. The remaining absorbance for the P3DMPT (410 nm) would mainly be derived from the absorbance of photooxidized materials [31] and that for P3OOT (630 nm) would be derived from the absorbance of the cationic state [27,32].

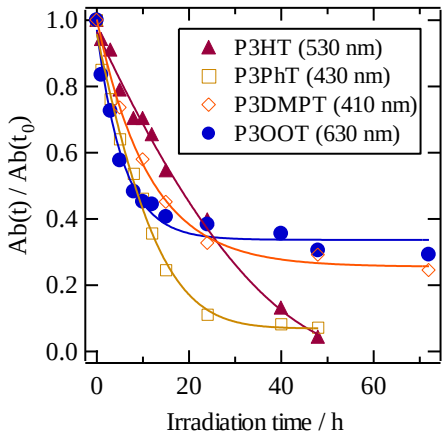

Figure 4.3 *Normalized UV-visible absorption of P3HT(at 530 nm(▲)), P3PhT(at 430 nm(□)), P3DMPT(at 410 nm(◊)) and P3OOT(at 630 nm(●)) samples during AM1.5G light irradiation.*

Variations in FT-IR (ATR) spectra of P3HT, P3PhT, P3DMPT, and P3OOT thin films upon AM 1.5G light irradiation are shown in **Figure 4.4**. The variations in the spectra of P3PhT and P3DMPT were

similar to those of P3HT [13,19]. The formation of carbonyl species (1700 cm^{-1}), sulfoxide derivative (1400 cm^{-1}), sulfone species (1335, 1190 cm^{-1}), sulfonate ester (1115 cm^{-1}), and sulfoxide (1050 cm^{-1}) were all observed, and the thiophene ring (820 cm^{-1}) and dimethyl propyl

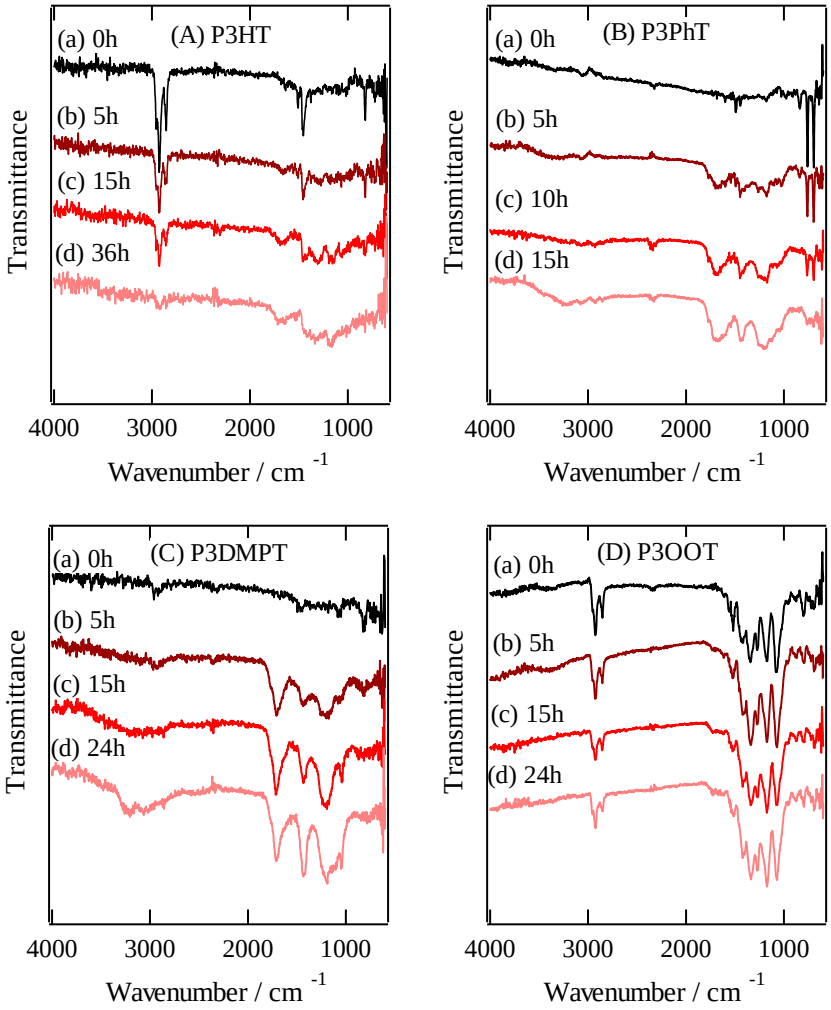

Figure 4.4 *FT-IR (ATR) spectra of (A) P3HT films irradiated for (a) 0 h, (b) 5 h, (c) 15 h, and (d) 36 h; (B) P3PhT films irradiated for (a) 0 h, (b) 5 h, (c) 10 h, and (d) 15 h; (C) P3DMPT films irradiated for (a) 0 h, (b) 5 h, (c) 15 h, and (d) 24 h; and (D) P3OOT films for (a) 0 h, (b) 5 h, (c) 15 h, and (d) 24 h. Polymer films were irradiated with simulated solar light (AM 1.5 G) of 100 mW/cm*^{2}

group (2800–2950 cm^{-1}) signals decayed as photooxidation progressed. This suggested that the photooxidation of P3PhT and P3DMPT occurred by a similar photooxidation mechanism to that of P3HT [19]. On the other hand, there was very little variation observed in the P3OOT spectra. There was a small amount of carbonyl species formation observed (1700 cm^{-1}), and the octyl side chain signal (2950 cm^{-1}) did not completely decay as photooxidation progressed, as shown in Figure 4d. It should be noted that sulfur oxides were not observed for P3OOT even after 72 h light irradiation.

4.3.2 Mechanism of polythiophene derivatives photooxidation

As shown in Figures 4a and 4d, the progress of the photooxidation of the octyloxy side chain of P3OOT was significantly slower than that of the hexyl side chain of P3HT. The binding energies of the hydrogen atoms of P3HT and P3OOT were therefore calculated using the DFT method in order to elucidate the reason for the difference in reactivity of the two thiophenes. The binding energies of hydrogen atoms are given in **Table 4.1**. For the mP3HT, the binding energies of the α- and β-hydrogen atoms in the side chain were calculated to be 3.92 and 4.41

Table 4.1 *Hydrogen binding energies from thiophenes (mP3HT and mP3OOT) calculated at the B3LYP/6-311G(d,p) level of theory.*

	ΔE(H) / eV		
thiophenes	α	β	γ
mP3HT	3.92	4.41	–
mP3OOT	–	4.32	4.54

eV, respectively, indicating that the C–H bond of the α-hydrogen atom is weaker than that of the β. As the P3OOH has no α-hydrogen atom, only the energies for the β- and γ-hydrogen atoms were calculated, and these were found to be 4.32 and 4.54 eV, respectively. The results indicate that the α-hydrogen atom of mP3HT is highly reactive. On the basis of the theoretical results, the effect of the molecular structures on the reactivity in the photooxidation are discussed in next section. For the photooxidation of P3HT, Manceau et al. reported that the sulfur atom of the thiophene ring was oxidized into sulfoxides, sulfones, and sulfonate esters by hydroxyl radicals, which arose through α-hydrogen abstraction from the hexyl side chain [19]. In this work, the variations in the chemical structures of P3PhT and P3DMPT that occurred on light irradiation were similar to that of P3HT. Thus, P3PhT and P3DMPT, which had no reactive hydrogen atoms at α-position, would be oxidized in a similar way to P3HT. In other words, the photooxidation of P3PhT and P3DMPT would be initiated by hydrogen abstraction from the side chain followed by hydroxyl radical oxidation of the sulfur atom of the thiophene ring. On the other hand, in the case of P3OOT, there was very little evidence of sulfur oxides in the FT-IR spectra (Fig. 4d). The hydrogen atoms of the side chain nearest to the thiophene ring are in the β-position (CH_2). In the DFT calculations, these hydrogens were shown to have relatively low reactivity. However, if these hydrogens did react and photooxidation progressed, the hydroxyl radical would arise further from the thiophene ring than for the P3HT. The hydroxyl radical would preferentially react with the nearest hydrogen atoms in the octyl side chain rather than with the sulfur atom of the thiophene ring owing to its short lifetime [33]. As a result, it would be likely that the sulfur atom of the thiophene ring is hardly oxidized by the hydroxyl radical. On the other hand, for P3DMPT, there are six hydrogens present in the side chain near the thiophene ring, making it much more likely that the hydroxyl radical would be produced near the thiophene ring by abstraction of one of these hydrogens. Therefore, P3DMPT

would be oxidized in a similar manner to P3HT. For P3PhT, the radical produced by hydrogen abstraction from the phenyl-group side chain can go into the main chain by the resonance effect, and the resulting carbon radical could react with oxygen, leading to progression of the oxidation [14]. Thus, as the hydroxyl radical is also near the thiophene ring, P3PhT would be oxidized in a similar manner to P3HT. (The closest distance between sufur atom and hydrogen atom in thiophene derivatives calculated by B3LYP is in **Table 4.2**)

Table. 4.2. *The closest distance between sufur atom and hydrogen atom in thiophene derivatives calculated by B3LYP. First, the optimized structure was calculated, and then distance was estimated.*

thiophenes	Distance between S and H (Å)
mP3HT	α 4.363
mP3OOT	β 5.059
mP3DMPT	β 4.481
mP3PhT	β 4.400

In the variations of UV-vis-NIR spectra of P3OOT upon light irradiation (Fig. 2(d)), the visible absorption band of P3OOT decreased but absorbance of the NIR region appeared at the same time. This spectral change in P3OOT was similar to a change previously described for iodine doping of P3OOT [29]. It is known that polythiophene doped by an oxidant such as an iodine, bromine, or $FeCl_3$ changes to a cationic state. In addition, Liu et al. reported that oxygen molecules in air act as oxidants upon polythiophenes [34]. Thus, it is possible that P3OOT was doped by oxygen upon light irradiation and formed a cationic state. To confirm this hypothesis, the photo-irradiated P3OOT film was dipped into a hydrazine solution (0.3 mol/L) [29] and further UV-vis-NIR spectra were measured, as shown in **Figure 4.5**. The NIR

absorbance of P3OOT disappeared and the visible absorbance recovered somewhat after the hydrazine treatment. Therefore, the state of P3OOT film after light irradiation was deduced to be the cationic state of polymer.

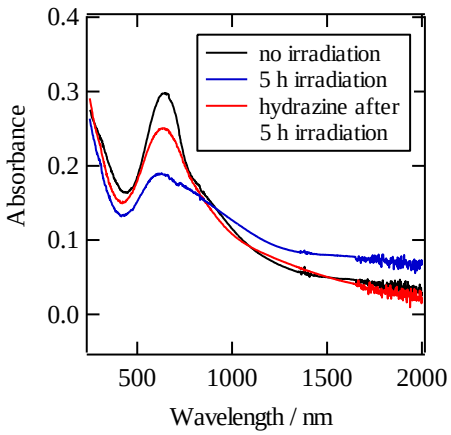

Figure 4.5 *UV-vis-NIR spectra of P3OOT films with (—) no-irradiation, (—) 5 h irradiation, and (—) hydrazine treatment after 5 h irradiation.*

4.4 Conclusion

Three polythiophene derivatives with no α-hydrogen in the side chains were synthesized and differences in their photochemical behavior were investigated using UV-vis-NIR and FT-IR (ATR) spectroscopy during simulated solar light irradiation. The various side chains contained either a phenyl group (P3PhT), *tert*-pentyl group (P3DMPT), or octyloxy group (P3OOT), in addition to the previously studied hexyl group derivative (P3HT). The results showed that the photooxidation of P3PhT and P3DMPT progressed in the same way as P3HT. On the other hand, the structural changes evident for P3OOT did not progress to the same extent as for P3HT. Because visible absorbance of photo-irradiated P3OOT was seen to recover after hydrazine treatment, P3OOT is thought to be doped by oxygen upon

light irradiation, resulting in the formation of a cationic state.

4.5 References

[1] Roncali J. Conjugated poly(thiophenes): Synthesis, functionalization, and applications. *Chem. Rev.* **92** (1992) 711-738.

[2] McCullough R D. The chemistry of conducting polythiophenes. *Adv. Mater.* **10** (1998) 93-116.

[3] Rait S, Kashyap S, Bhatnagar P K, Mathur P C, Sengupta S K, Kumar J. Improving power conversion efficiency in polythiophene/fullerene-based bulk heterojunction solar cells. *Sol. Energy Mater. Sol. Cells* **91** (2007) 757-763.

[4] Das N C, Sokol P E. Hybrid photovoltaic devices from regioregular polythiophene and ZnO nanoparticles composites. *Renew. Energy* **35** (2010) 2683-2688.

[5] Wang M, Wang X. P3HT/ZnO bulk-heterojunction solar cell sensitized by a perylene derivative. *Sol. Energy Mater. Sol. Cells* **92** (2008) 766-771.

[6] Vanlaeke P, Swinnen A, Haeldermans I, Vanhoyland G, Aernouts T, Cheyns D, Deibel C, D'Haen J, Heremans P, Poortmans J, Manca J V. P3HT/PCBM bulk heterojunction solar cells: Relation between morphology and electro-optical characteristics. *Sol. Energy Mater. Sol. Cells* **90** (2006) 2150-2158.

[7] Yamanari T, Taima T, Hara K, Saito K. Investigation of optimum conditions for high-efficiency organic thin-film solar cells based on polymer blends. *J. Photochem. Photobio. Chem.* **182** (2006) 269-272.

[8] Chuang S-Y, Yu C-C, Chen H-L, Su W-F, Chen C-W. Exploiting optical anisotropy to increase the external quantum efficiency of flexible P3HT:PCBM blend solar cells at large incident angles. *Sol. Energy Mater. Sol. Cells* **95** (2011) 2141-2150.

[9] Jin S-H, Naidu B V K, Jeon H-S, Park S-M, Park J-S, Kim S C, Lee J W, Gal Y-S. Optimization of process parameters for high-efficiency polymer photovoltaic devices based on P3HT:PCBM system. *Sol. Energy Mater. Sol. Cells* **91** (2007) 1187-1193.

[10] Zhang W, Xu Y, Wang H, Xu C, Yang S. Fe_3O_4 nanoparticles induced magnetic field effect on efficiency enhancement of P3HT:PCBM bulk heterojunction polymer solar cells. *Sol. Energy Mater. Sol. Cells* **95** (2011) 2880-2885.

[11] Krebs F C. Polymer solar cell modules prepared using roll to roll methods: Knife-over-edge coating, slot-die coating and screen printing. *Sol. Energy Mater. Sol. Cells* **93** (2009) 465-475.

[12] Jørgensen M, Norrman K, Krebs F C. Stability/degradation of polymer solar cells. *Sol. Energy Mater. Sol. Cells* **92** (2008) 686-714.

[13] Griffini G, Turri S, Levi M. Degradation and stabilization of poly(3-hexylthiophene) thin films for photovoltaic applications. *Polym. Bull.* **66** (2011) 211-222.

[14] Abdou M S A, Holdcroft S. Mechanism of photodegradation of poly(3-alkylthiophenes) in solution. *Macromol.* **26** (1993) 2954-2962.

[15] Chang Y-M, Su W-F, Wang L. Influence of photo-induced degradation on the optoelectronic properties of regioregular poly(3-hexylthiophene). *Sol. Energy Mater. Sol. Cells* **92** (2008) 761-765.

[16] Rivaton A, Chambon S, Manceau M, Gardette J L, Lemaître N, Guillerez S. Light-induced degradation of the active layer of polymer-based solar cells. *Polym. Degrad. Stab.* **95** (2010) 278-284.

[17] Manceau M, Chambon S, Rivaton A, Gardette J-L, Guillerez S, Lemaître. Effects of long-term UV-visible light irradiation in the absence of oxygen on P3HT and P3HT:PCBM blend. *Sol. Energy Mater. Sol. Cells* **94** (2010) 1572-1577.

[18] Hintz H, Egelhaaf H.-J., Peisert H, Chassé T. Photo-oxidation and ozonization of poly(3-hexylthiophene) thin films as studied by UV/VIS and photoelectron spectroscopy. *Polym. Degrad. Stab.* **95** (2010) 818-825.

[19] Manceau M, Rivaton A, Gardette J-L, Guillerez S, Lemaître N. The mechanism of photo- and thermooxidation of poly(3-hexylthiophene) (P3HT) reconsidered. *Polym. Degrad. Stab.* **94** (2009) 898-907.

[20] Caronna T, Forte M, Catellani M, Meille S V. Photodegradation and photostabilization studies of poly(3-butylthiophene) in the solid state. *Chem. Mater.* **94** (1997) 991-995.

[21] Ljungqvist N, Hjertberg T. Oxidative degradation of poly(3-octylthiophene). *Macromol.* **28** (1995) 5993-5999.

[22] López-Elvira E, Escasaín E, Baró A, Colchero J, Palacios-Lidón E. Wavelength dependence of nanoscale photodegradation in poly(3-octylthiophene) thin films. *Polym. Degrad. Stab.* **96** (2011) 1279-1285.

[23] Bjerring M, Nielsen J S, Siu A, Nielsen N C, Krebs F C. An explanation for the high stability of polycarboxythiophenes in photovoltaic devices–A

solid-state NMR dipolar recoupling study. *Sol. Energy Mater. Sol. Cells* **92** (2008) 772-784.

[24] Manceau M, Helgesen M, Krebs F C. Thermo-cleavable polymers: Materials with enhanced photochemical stability. Polym. Degrad. Stab. **95** (2010) 2666-2669.

[25] McCullough R D, Lowe R D, Jayaraman M, Anderson D L. Design, synthesis, and control of conducting polymer architectures: Structurally homogeneous poly(3-alkylthiophenes). J. Org. Chem. **58** (1993) 904-912.

[26] Aoyama Y, Hatakeyama K, Mukai T, Koizumi H. Electronic properties of poly[3-(1,1-dimethylpropyl)thiophene] and poly(3-cyclohexyl thiophene). *Bull. Chem. Soc. Jpn.* **86** (2013) 51-56.

[27] Hatakeyama K, Koizumi H, Ichikawa T. Stability of a conductive state of Poly(3-alkoxythiophene)s. *Bull. Chem. Soc. Jpn.* **82** (2009) 202-205.

[28] Tromholt T, Madsen V. M., Carlé J.E., Helgesen M, Krebs F. C.. Photochemical stability of conjugated polymers, electron acceptors and blends for polymer solar cells resolved in terms of film thickness and absorbance. *J. Mater. Chem.* **22** (2012) 7592-7601.

[29] Hintz H, Egelhaaf H.-J., Lüer L, Hauch J, Peisert H, Chassé T. Photodegradation of P3HT – A systematic study of environmental factors. *Chem. Mater.* **23** (2011) 145-154.

[30] Madsen M. V., Tromholt T, Böttiger A, Andreasen J. W., Norrman K, Krebs F. C.. Influence of processing and intrinsic polymer parameters on photochemical stability of polythiophene thin films. *Polym. Degrad. Stab.* **97** (2012) 2412-2417.

[31] Hapke B, Francis G. Spectral properties of condensed phases of disulfur monoxide, polysulfur oxide, and irradiated sulfur. *Icarus* **79** (1989) 47-55.

[32] Koeckelberghs G, Vangheluwe M, Samyn C, Persoons A, Verbiest T. Regioregular poly(3-alkoxythiophene)s: Toward soluble, chiral conjugated polymers with a stable oxidized state. *Macromol.* **38** (2005) 5554-5559.

[33] Chemical Society of Japan. Chemistry of active oxygen species. KIKAN KAGAKU SOSETSU. Japan: Scientific Societies Press **7** (1990) 3-28.

[34] Liu C C, Yang C-M, Liu W-H, Liao H-H, Horng S-F, Meng H-F. Interface effect of oxygen doping in polythiophene. *Synth. Met.* **159** (2009) 1131-1134.

5. Summary and future guideline

Recently, in terms of the world environmental preservation, the expectation for power generation by renewable energy has been dramatically increasing. Especially, solar cell has a big advantage because of infinite solar energy, and inorganic solar cells have already began to contribute to our society. In contrast, organic solar cell is still the research stage. One of the most researched organic solar cells for commercialization is polymer solar cells (PSCs) using poly(3-hexylthiophene) (P3HT). This is because the fabrication of PSCs is wet process and printable. In fact, large-scale production research of PSCs has been progressed. Furthermore, power conversion efficiencies of PSCs has been improved in the recent decade. On the other hand, PSCs degrades during illumination, and the degradation problem prevents commercialization. The research about degradation is mainly investigated by physical approach such as hole trap by ESR and current-voltage measurementin a complete device. In contrast, the physical phenomenon has not been investigated in connection with the molecular chemistry approach. Here, in this research, in order to further investigate the physical degradation phenomenon in the PSCs, I focused on the degradation of organic material and conducted the investigation of (1) the correlation between slightly photo-oxidized organic material and photovoltaic performance of PSCs, (2) the photo-oxidative another active species of P3HT, which caused the initial photooxidation, and (3) the differences in the photochemical behavior of the polythiophene derivatives whose side chain at reactive α-position was varied. Consequently, partial molecular scission of P3HT (~10 mol%), which was triggered by the $[O_2]^-$, was observed

even in the begining of initial photooxidation time, and the fragments by partial molecular scission of P3HT and these oxides in polythiophene itself prevented good packing state (crystallinity) of P3HT and remained some amorphous state, which decreased the hole mobility and then increased the series resistance of the device. As the result, it is deduced that the device characteristics decreased. This material decomposition was suppressed by changing the reactive α-hydrogan of the side chain, whose result show the guideline of polymer molecular designing toward the photostable polythiophene derivatives.

So far, I focus on the organic material degradation and explain the phenomenon and mechanism including device. In contrast, in this paragraph, I will explain part of research guideline for photo-stable PSCs, as follows.

(i). Elucidation of further degradation mechanism in real device

P3HT molecular scission with complete device performance degradation are observed in spite of fully encapsulated PSCs. We are the first person to find out the phenomenon at this time, and we should search more detail phenomenon. For example, the molecular scission effect to real device performance (J_{sc}, FF and R_s may be related to the molecular scission), the degree of molecular scission in real device with gas atmosphere change (especially changing oxygen atmosphere from 0.1 ppm to 10 ppm), the degree of molecular scission in real device by changing endcap structure of polymer from Br- or CH_3- to hydrogen (C-Br bond may be easily disocciated and forms radical species by irradiation, which lead to molecular scission, and also CH_3 endcapping may have sterically-bulky and forms bad stacking, and may lead to the oxidation like P3DMPT in the result), the molecular scission effect to real device charge trap formation by TSC, ESR and CELIV measurement (small molecule probably may form trap state at the interface), the molecular scission effect to real device metal atoms

intrusion (P3HT become amorphous state a little by preventing small molecule from forming good packing state, and then metal atoms come more easily to intrude into the organic layer)、the molecular scission effect to the reorganization of BHJ state in the real device (BHJ structural change in P3HT/PCBM device may be triggered not only the thermal by irradiation but also restructured by the molecular scission. Especially, P3HT has a high T_g (over 150 ^{o}C)) and it is hard to think that the main reason of BHJ structural change is only thermal by irradiation because max temperature of the device can not rise to the high temperature (80 ^{o}C at best).

(ii). Synthesis of photostable polymer and photocrosslinkable polymer

The probability of photostable polymer with alkyl side chain are mentioned, and this phenomenon may be common thing among electroconductive polymer though the the detailed mechanism has not been cleared. Therefore, the design should be applied to the low bang gap, donor-acceptor based polymer. By changing the atom in the α-position of side chain, we can also change the π-electron state of ring (especially thiophene ring can easily be adjustable to electron donor unit or acceptor unit because thiophene ring itself has rich neutral π-electron). In addition, in order to prevent small molecule reorganization of BHJ structure, it is good idea to design photocrosslinkable polymer, which forms crosslink with each other or with PCBM by UV irradiation accompanied by consuming oxygen molecule. If this technology become available, we does not have to think about the BHJ structure destroy (by small molecule) and perhaps photobleaching because it become harder to intrude oxygen into the organic layer once rigid photocrosslink are made.

(iii). Adding a superoxide anion or a singlet oxygen quencher

The photoactive species (a superoxide anion or singlet oxygen) in the photooxidation of P3HT are mentioned. Therefore, the next step

is to add quencher of these photoactive species in organic layer, for example, superoxide dismutase, 5,5-Dimethyl-1-pyrroline N-oxide (DMPO) (spin trapping agent), paltimine acid ascorbyl, ascorbic acid, astaxanthine, β-carotene, and so on. Perhaps, some difficulties are the photooxidation of these quencher itself and become photoactive species. But, in some report, light screen chemicals, which can prevent the P3HT photooxidation, has already been mentioned in Macromolecules. Amazingly, in this report, adding amount of the chemicals is only ~3 mol%, and it may not only quench the photoactive species but also become good impurity and form the good BHJ structure. It may be believed the probability of these quencher for long term durability of PSCs.

Finally, the future expectation of PSCs are mentioned. If the long term durability of PSCs are realized and then become commercialized in the near future, PSCs are mainly used in doors. This is because PSCs is inherently very weak against direct sunlight as a weak point, but, as a strong point, power conversion efficience ability in doors, where light intensity is weak and incident light enters to device from an angle, is known to be higher than that of inorganic solar cells. In this case, I think we should apply PSCs to something which has large and flat area because of easy fabrication by solution process, as additional value like the architectual material combined with PSCs, for example, flat desk rack, flat floor board, flat panel, and a book cabinet. In addition, we should use these photovoltaic material in combination with rechargeable battery to use electrical power efficiently. As just described, I really expect PSCs to become one of providers of sustainable energy from the bottom of the heart.

Appendix

1. Material synthesize

All reactions were carried out in dried glassware. Flash chromatography was performed using flash silica gel 32-63 mm, 60 Å. H^1NMR and spectra were recorded on Bruker Avance 400 spectrometer using $CDCl_3$ solvent. The chemical shift values were given in a part per million (ppm) relative to internal tetramethylsilane (TMS) for H^1NMR. Data are reported as follows: chemical shifts in ppm (δ), multiplicity (singlet = s, doublet = d, triplet = t, quartet = q, quintet = p, multiplet = m, broad singlet = bs), coupling constants in Hz.

Dibrominated monomers of thiophene derivatives with different side chains (**3a,b**) were synthesized according to a similar route in the previous report. The procedure was shown in Scheme 2-1. One monomer (**1a**) synthesis scheme was omitted here but described in the subsequent detailed procedure.

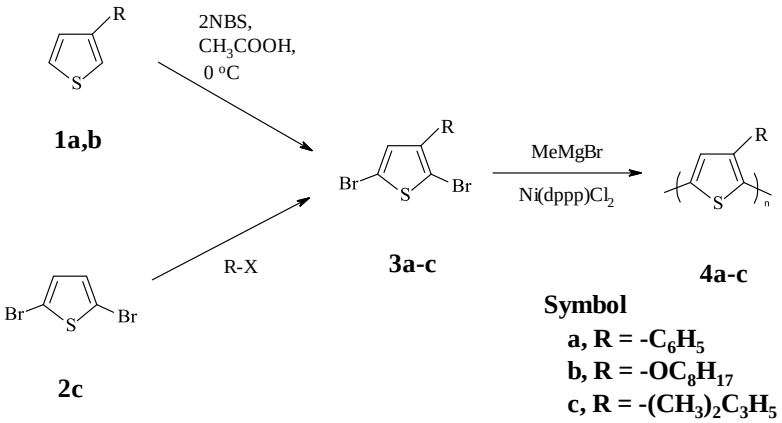

Scheme 1.1 *Synthetic scheme of polythiophene derivatives used in this research.*

All the polymer was prepared by polymerization of dibrominated monomer using the Grignard metathesis method (Scheme 1.1, detailed mechanism is shown in Scheme 1.2) [25,26].

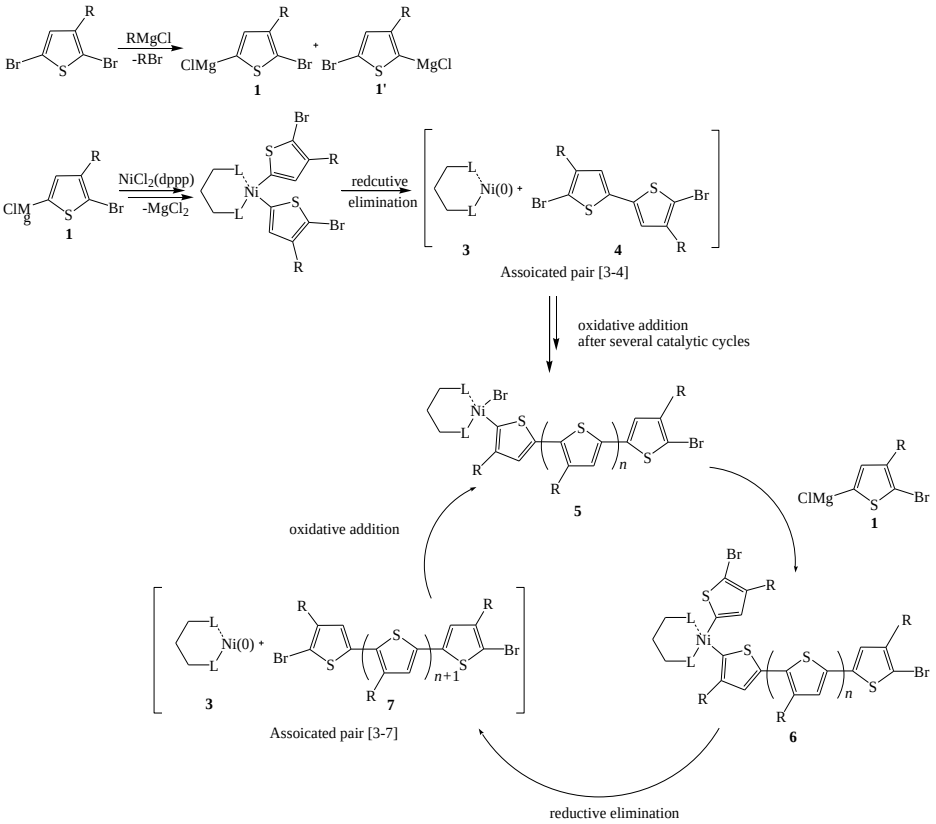

Scheme 1.2 *Mechanism of Grignard metathesis method for the synthesis of regio-regular poly(3-alkylthiophene).*

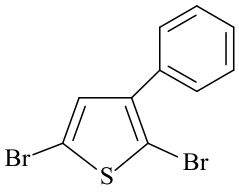

2,5-Dibromo-3-phenylthiophene (3a). 3-phenylthiophene was dibrominated with N-bromosuccinimide (NBS) in tetrahydrofuran (THF) to afford 2,5-dibromo-3-phenylthiophene at 0 ℃ under a nitrogen and dark atmosphere. NBS (1.09 g, 10.0 mmol) added THF solution (20 mL) was stirred for 10min and cooled to 0 ℃, and then 3-phenylthiophene (**2a,** 1.09 g, 4.0 mmol) dissolved in THF (5 mL) was added dropwise over 10 min. The mixture was stirred for some time with confirming new spot by the thin-layer chromatography (TLC) method. The developing solvent is hexane and ethyl acetate (20:1 ml%). The reaction was warmed to room temperature over 6 hours. The reaction mixture was added to a potassium hydroxide aqueous solution (1M, 100 mL), and then extracted by chloroform. The solution was washed with saturated sodium hydrogen carbonate solution.. The solvent was removed by rotary evaporation. The product was subjected to flash chromatography (hexane and ethyl acetate (20:1 ml%), and then subjected to liquid chromatography to purify the monomer. The product **3a** was collected as a yellow oil (125 mg, 90% yield). 1H NMR (400MHz, CDCl3) δ 7.48 (d, 2H, *J* = 8.0 Hz), δ 7.42 (t, 2H, *J* = 7.8 Hz), δ 7.36 (t, 1H, *J* = 8.0 Hz), δ 7.02 (s, 1H, *J* = 16.5 Hz). 13C NMR: (400MHz, CDCl3) δ 138.3 (t, *J* = 30.2 Hz), 129.5 (t, *J* = 5.5 Hz), 120.8 (t, *J* = 243.5 Hz), 111.7, 109.7 (t, *J* = 5.8 Hz), 106.7, 105.7, 104.5, 102.2, 101.2 (t, *J* = 5.8 Hz),

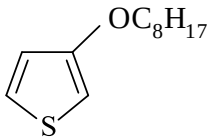

3-octyloxythiophene (1b). 3-methoxythiophene (2.57 g, 9.0 mmol),1-octanol (2.57 g, 9.0 mmol) and sodium hydrogen sulfate (2.57 g, 9.0 mmol) in dehydrated toluene (10 mL) was heated to reflux for 3h. The solvent was removed by rotary evaporation. The solution was washed with saturated sodium hydrogen carbonate solution. The mixture was then subjected to reduced-pressure distillation and purified. The product **1b** was collected as a colorless oil (125 mg, 90% yield). 1H NMR (400MHz, CDCl3) δ 7.18 (s, 1H), δ 6.72 (d, 1H, *J* = 3.0 Hz), δ 6.15 (s, 1H), δ 3.91 (t, 2H, *J* = 8.0 Hz), δ 1.75 (bm, 2H), δ 1.45-1.25 (br, 10H), δ 0.88 (t, *J* = 7.0

Hz, 3H). 13C NMR: (400MHz, CDCl3) δ 155.8 (t, *J* = 30.2 Hz), 129.5 (t, *J* = 5.5 Hz), 119.3 (t, *J* = 243.5 Hz), 99.7 (t, *J* = 5.8 Hz), 37.7 (t, *J* = 26.7 Hz), 31.6, 28.9, 22.6, 22.3 (t, *J* = 3.6 Hz), 14.0 (d, *J* = 3.6 Hz).

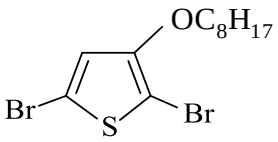

2,5-Dibromo-3-octyloxythiophene (3b). 3-octyl oxythiophene was dibrominated with N-bromo succinimide (NBS) in tetrahydrofuran (THF) to afford 2,5-dibromo-3-octyloxythiophene at 0 ℃ under a nitrogen and dark atmosphere. NBS (1.09 g, 10.0 mmol) added THF solution (20 mL) was stirred for 10min and cooled to 0 ℃, and then 3-octyloxythiophene (**2a,** 1.09 g, 4.0 mmol) dissolved in THF (5 mL) was added dropwise over 10 min. The mixture was stirred for some time with confirming new spot by the thin-layer chromatography (TLC) method. The developing solvent is hexane and ethyl acetate (20:1 ml%). The reaction was warmed to room temperature over 6 hours. The reaction mixture was poured into a potassium hydroxide aqueous solution (1M, 100 mL), and then extracted by chloroform. The solution was washed with saturated sodium hydrogen carbonate solution. The solvent was removed by rotary evaporation. The product was subjected to flash chromatography (hexane and ethyl acetate (20:1 ml%), and then subjected to liquid chromatography to purify the monomer. The product **3b** was collected as a yellow oil (125 mg, 90% yield). 1H NMR (400MHz, CDCl3) δ 6.88 (s, 1H), δ 3.99 (t, 2H, *J* = 8.0 Hz), δ 1.77 (bm, 2H), δ 1.45-1.25 (br, 10H), δ 0.80 (t, *J* = 7.0 Hz, 3H). 13C NMR: (400MHz, CDCl3) δ 155.8 (t, *J* = 30.2 Hz), 129.5 (t, *J* = 5.5 Hz), 119.3 (t, *J* = 243.5 Hz), 99.7 (t, *J* = 5.8 Hz), 37.7 (t, *J* = 26.7 Hz), 31.6, 28.9, 22.6, 22.3 (t, *J* = 3.6 Hz), 14.0 (d, *J* = 3.6 Hz).

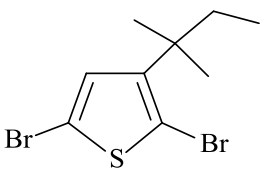

2,5-Dibromo-3-(1,1-dimethylpropyl)thiophene (3c). 2-chloro-2-methylbutane (17 g, 160 mmol) and $AlCl_3$ (21.3 g, 160mmol) in CS_2 solution (100 mL) was cooled to 0 ℃. 2,5-dibromothiophene (32.3 g, 133mmol) dissolved in 20mL of CS_2 solution were added dropwise to the solution and stirred ar room temparature. The mixture was

stirred for 24h and then heated to reflux for 1h. the reaction solution was poured into hydrogen chloride solution (2M, 200mL), and then extracted with CS_2. The obtained organic layer was washed with saturated aqueous potassium hydrocarbon solution, and then with water. The solvent was removed by rotary evaporation. The product was washed with hexane. The product **3c** was collected as a red-brown crystal (125 mg, 90% yield). It indicates the products may contain some oligomers due to the strong Lewis acid, $AlCl_3$. 1H NMR (400MHz, CDCl3) δ 6.80 (s, 1H), δ 1.75 (q, 2H, *J* = 5.8 Hz), δ 1.60 (s, 6H), δ 1.00 (t, 3H, *J* = 7.0 Hz). 13C NMR: (400MHz, CDCl3) δ 140.1 (t, *J* = 30.2 Hz), 129.5 (t, *J* = 5.5 Hz), 125.3 (t, *J* = 8.5 Hz), 119.7 (t, *J* = 5.8 Hz), 31.6, 28.9, 22.6, 22.3 (t, *J* = 3.6 Hz), 14.0 (d, *J* = 3.6 Hz).

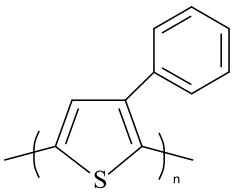

Poly(3-phenylthiophene) (4a). 3a (1.50 g, 4.7 mmol) added dehydrated THF solution (30 mL) was stirred for 10 min, and then 3.0M methyl grignard (1.57 ml, 4.7 mmol) dissolved in THF solution was added dropwise over 10 min. The mixture was heated to reflux with stiring for 3h. Then, the solution was cooled to room temperature and $NiCl_2$(dppp) [dppp = 1,3-bis(diphenylphosphino)propane] (25.5 mg, 0.047 mmol) was added. The mixture was heated to reflux with stiring for 24h. The reaction mixture was added to a potassium hydroxide aqueous solution (1M, 100 mL), and then extracted by chloroform. The solution was washed with saturated sodium hydrogen carbonate solution.. The solvent was removed by rotary evaporation, and condensed solution was added dropwise to cooled methanol (500 mL). The solid product was washed with hexane by soxhlet washing for 24h, and then subjected to soxhlet extraction by using chloroform. The solid is dried in vacuum drier (80^{o}C) and a red brown powder was obtained with ca. 10 % yield. 1H NMR (400MHz, CDCl3) δ 7.49 (d, 2H), δ 7.43 (t, 2H), δ 7.36 (t, 1H), δ 7.10 (s, 1H). 13C NMR (400MHz, CDCl3) signal could not be detected (integrated for 24h). Regio-regularity > 95%. GPC (Waters Co., LTD.): Mw = 1.59 kg/mol, Mw/Mn = 1.39.

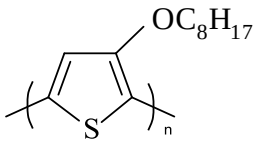

Poly(3-octyloxythiophene) (4b). 3b (3.09 g, 8.1 mmol) added dehydrated THF solution (50 mL) was stirred for 10 min, and then 3.0M methyl grignard (2.7 ml, 8.1 mmol) dissolved in THF solution was added dropwise over 10 min. The mixture was heated to reflux with stiring for 3h. Then, the solution was cooled to room temperature and $NiCl_2$(dppp) [dppp = 1,3-bis(diphenylphosphino)propane] (44.0 mg, 0.08 mmol) was added. The mixture was heated to reflux with stiring for 24h. The reaction mixture was added to a potassium hydroxide aqueous solution (1M, 100 mL), and then extracted by chloroform. The solution was washed with saturated sodium hydrogen carbonate solution. The solvent was removed by rotary evaporation, and condensed solution was added dropwise to cooled methanol (500 mL). The solid product was washed with hexane by soxhlet washing for 24h, and then subjected to soxhlet extraction by using chloroform. The solid is dried in vacuum drier (80^{o}C) and a dark blue powder was obtained with ca. 16 % yield. 1H NMR (CDCl3) δ 6.80 (s, 1H), δ 4.00 (t, 2H), δ 1.80 (q, 2H), δ 1.40 (broad, 10H), δ 0.95 (t, 3H). 13C NMR (400MHz, CDCl3) signal could not be detected (integrated for 24h). Regio-regularity > 95%. GPC (Waters Co., LTD.): Mw = 12.0 kg/mol, Mw/Mn = 1.72

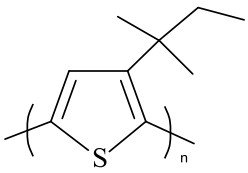

Poly3-[(1,1-dimethylpropyl)thiophene] (4c). 3c (1.09 g, 10.0 mmol) added dehydrated THF solution (20 mL) was stirred for 10 min, and then methyl grignard (1.09 g, 4.0 mmol) dissolved in THF (5 mL) solution was added dropwise over 10 min. The mixture was heated to reflux with stiring for 3h. Then, the solution was cooled to room temperature and $NiCl_2$(dppp) [dppp = 1,3-bis(diphenylphosphino)propane] (0.05 mmol) was added. The mixture was heated to reflux with stiring for 24h. The reaction mixture was added to a potassium hydroxide aqueous solution (1M, 100 mL), and then extracted by chloroform. The solution was washed with saturated sodium hydrogen carbonate solution. The solvent was removed by rotary evaporation, and condensed solution was added dropwise to cooled

methanol (500 mL). The solid product was washed with hexane by soxhlet washing for 24h, and then subjected to soxhlet extraction by using chloroform. The solid is dried in vacuum drier (80^{o}C) and a brown powder was obtained with ca. 10 % yield. 1H NMR (CDCl3) δ 6.80 (s, 1H), δ 1.60 (s, 6H), δ 1.35 (q, 2H), δ 1.00 (t, 3H). 13C NMR (400MHz, CDCl3) signal could not be detected (integrated for 24h). Regio-regularity > 95%. GPC: Mw = 11.4 kg/mol, Mw/Mn = 2.30.

2. Experimental figures

Table S1. *Series resistance (Rs) estimated by I-V curves of the ITO/PEDOT:PSS/P3HT:PCBM/Al device. Before fabrication of the organic film, the blended solution was irradiated for (—) 0, (—) 20, (—) 40, and (—) 60 min in air using simulated solar light (AM 1.5 G) at an intensity of 100 mW/cm^2. Obviously, Rs value increases with irradiation time.*

Time (min)	Rs (Ωcm^2)
0	5.606
20	13.10
40	25.94
60	43.15

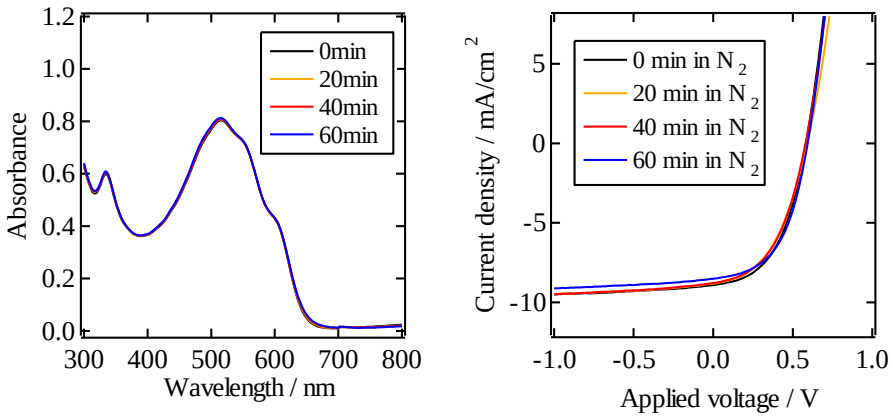

Figure S1. *UV-vis spectra of P3HT:PCBM organic films and I-V curves of the device characteristics of the ITO/PEDOT:PSS/P3HT:PCBM/Al device. Before fabrication of the organic film, the blended solution was irradiated for (—) 0, (—) 20, (—) 40, and (—) 60 min in nitrogen using simulated solar light (AM 1.5 G) at an intensity of 100 mW/cm^2. In contrast to the changes in Figures 1 and 4, the observed spectra changed only slightly.*

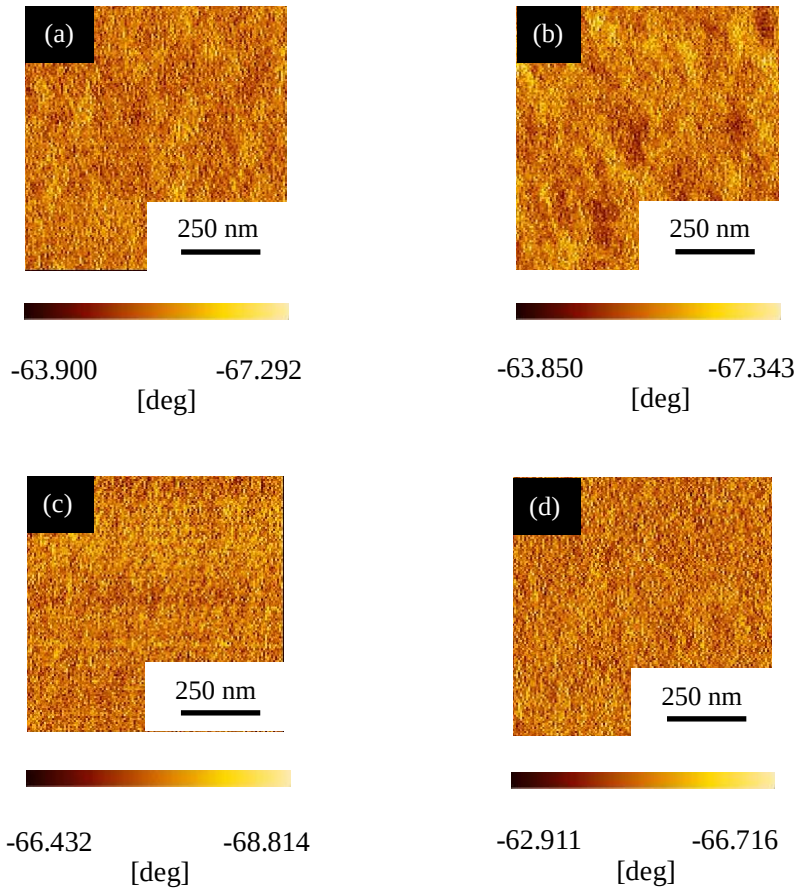

Figure S2. *AFM phase images of P3HT:PCBM organic films. Before fabrication, the blended solution was irradiated for (a) 0, (b) 20, (c) 40, and (d) 60 min in air using simulated solar light (AM 1.5 G) at an intensity of 100 mW/cm2. Note that a phase segregation and P3HT fibril structure were not observed.*

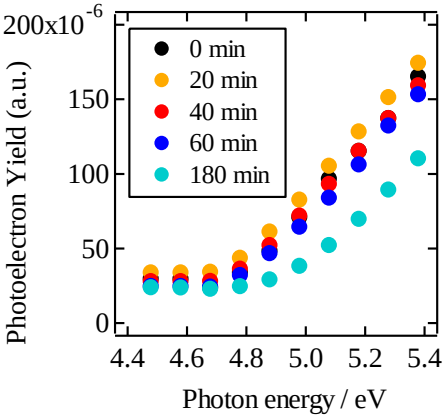

Time (min)	Voc (eV)
0	4.72
20	4.72
40	4.75
60	4.80
180	4.94

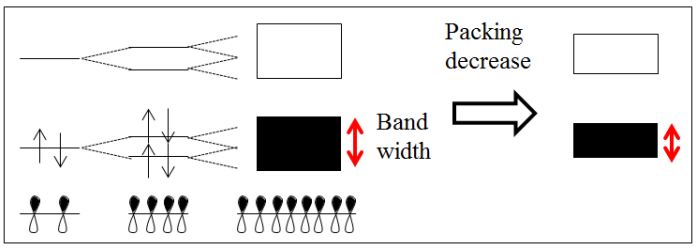

Figure S3. *Ionic potential of P3HT:PCBM organic films, and calculated* V_{oc} *by using the values. Before fabrication, the blended solution was irradiated for (a) 0, (b) 20, (c) 40, and (d) 60 min in air using simulated solar light (AM 1.5 G) at an intensity of 100 mW/cm2. Note that the band width decrease was formed by P3HT chain packing decrease (π-orbital overlapping decrease)*

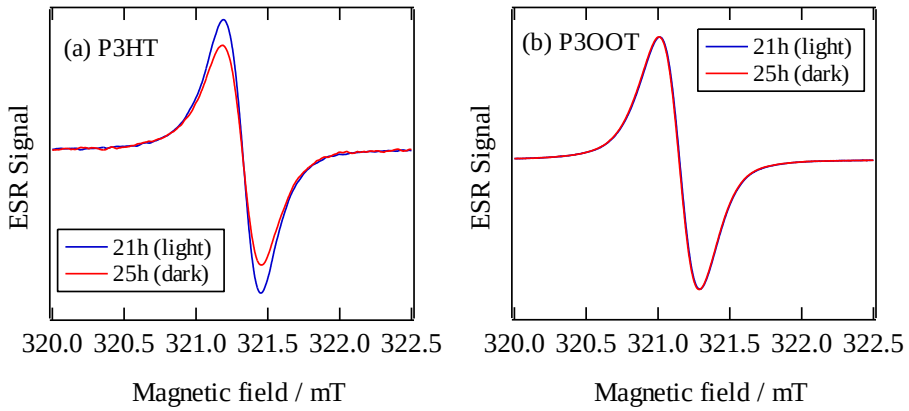

Figure S4. *ESR spectra of (a) P3HT and (b) P3OOT films of (—) after 21 h light irradiation and (—) after 25 h (after 4 h under the dark condition followed by 21 h light irradiation).*

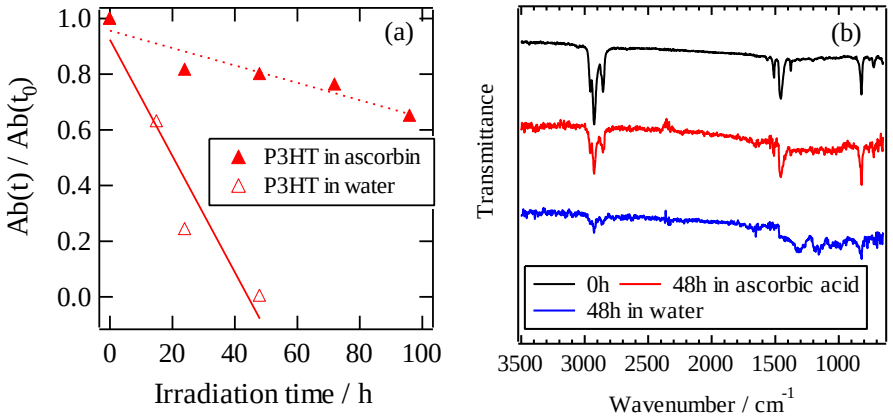

Figure S5. *(a) Normalized UV-visible absorption peaks of P3HT (at 530 nm) film in ascorbic acid solution (▲) or in water (△) during AM 1.5G light irradiation. (b) FT-IR (ATR) spectra of P3HT films of (—) 0 h, (—) after 48 h irradiation in ascorbic acid solution, and (—) after 48 h irradiation in water.*

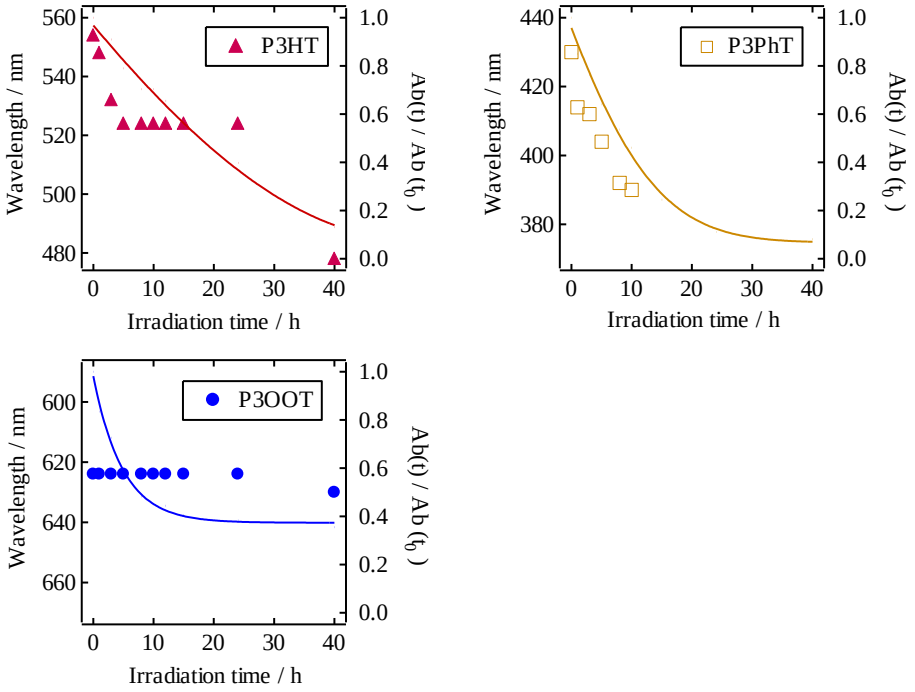

Figure S6. *Changes of UV-visible absorption peaks (left axis) and normalized UV-visible absorption (right axis) of P3HT(▲,-), P3PhT(□,-) and P3OOT(●,-) films during AM1.5G light irradiation. Note that only P3OOT does not show blueshift (may not show molecular scission).*

List of publications

1. **Electronic properties of poly[3-(1,1-dimethylpropyl)thiophene] and poly(3-cyclohexylthiophene)**
   Yoshinori Aoyama, Kouji. Hatakeyama, Takuma. Mukai, Hitoshi. Koizumi
   Bulletin Chemical Society of Japan, 86, 51-56 (2013)

2. **Direct effect of partially photooxidized poly(3-hexylthiophene) on the device characteristics of a bulk heterojunction solar cell**
   Yoshinori Aoyama, Toshihiro Yamanari, Yosei Shibata, Noboru Ohashi, Yasumasa Suzuki, Junji Mizukado, Hiroyuki Suda, Yuji Yoshida
   Solar Energy Materials and Solar Cells, 120, 584-590 (2014)

3. **Initial photooxidation mechanism leading to reactive radical formation of polythiophene derivatives**
   Yoshinori Aoyama, Toshihiro Yamanari, Takurou N. Murakami, Tatsuya Nagamori, Kazuhiro Marumoto, Hiroto Tachikawa, Junji Mizukado, Hiroyuki Suda, Yuji Yoshida
   Chemical Physics Letters, submitted

4. **Photo-induced oxidation of polythiophene derivatives: Dependence on side chain structure**
   Yoshinori Aoyama, Toshihiro Yamanari, Nagatoshi Koumura,

Hiroto Tachikawa, Masaru Nagai, Yuji Yoshida
Polymer Degradation and Stability, 98, 899-903 (2013)

5. **Structural analysis of P3HT photo-oxidation by MALDI-TOF MS**
   Junji Mizukado, Yasumasa Suzuki, Liang Chen, Yoshinori Aoyama, Toshihiro Yamanari, Hiroaki Sato, Hiroyuki Suda, Yuji Yoshida
   In preparation

6. **A study for superoxide radical anion generation and involvement in photo-oxidation of poly (3-hexylthiophene) in chlorobenzene solution**
   Liang Chen, Junji Mizukado, Shuzo Kutsuna, Yoshinori Aoyama, Hiroyuki Suda, Yuji Yoshida
   In preparation

7. **Conductivity degradation analysis of P3HT/PCBM BHJ organic film dependent on P3HT molecular chain scission by photoirradiation**
   Yoshinori Aoyama, Olivier Douhéret, Philippe Leclère, Junji Mizukado, Tetsuhiko Miyadera, Hiroyuki Suda, Roberto Razzaroni, Yuji Yoshida
   In preparation

Conferences

1. (International) Y. Aoyama, T. Yamanari, N. Koumura, H. Tachikawa, Y. Yoshida. ”Photo-induced degradation of polythiophene derivatives and its dependence on the structures of their side chains”, Photovoltaic Science and Engineering Conference 21 (PVSEC 21), Fukuoka, Japan, 2011/12/2 (*poster presentation*)

2. (Domestic) Y. Aoyama, T. Yamanari, N. Koumura, H. Tachikawa, Y. Yoshida. ”Photo-induced degradation of polythiophene derivatives and its dependence on the structures of their side chains”, 61st the society of polymer science japan annual meeting (SPSJ 61st), Pacifico Yokohama, Japan, 2012/5/30 (*oral communication*)

3. (International) Y. Aoyama, T. Yamanari, T. Murakami, K. Marumoto, T. Nagamori, Y. Yoshida "Initial reaction of the photo-oxidation of polythiophene derivatives for organic photovoltaics", the 2012 Global Organic Photovoltaic Conference (GOPV2012), Suzhou Institute of Nano-Tech and Nano-Bionics (SINANO), Suzhou, China, 2012/09/10 (*poster presentation*)

4. (Domestic) Y. Aoyama, T. Yamanari, T. Murakami, K. Marumoto, T. Nagamori, Y. Yoshida "Initial reaction of the photo-oxidation of polythiophene derivatives", the annual meeting on Photochemistry 2013, Tokyo Institute of Technology, Tokyo, Japan, 2012/09/12 (*oral communication*)

5. (International) Y. Aoyama, T. Yamanari, T. Murakami, K.

Marumoto, T. Nagamori, Y. Yoshida " Initial reaction of the photo-oxidation of polythiophene derivatives", 7th Asian Photochemistry Conference (APC2012), Icho Kaikan, Osaka University, Osaka, Japan, 2012/11/13 (*poster presentation*)

6. (International) Y. Aoyama, T. Yamanari, Y. Shibata, N. Ohashi, Y. Suzuki, J. Mizukado, and Y. Yoshida" Direct effect of photooxidized poly(3-hexylthiophene) on the device characteristics in bulkhetero junction solar cell", Seventh International Conference on Molecular Electronics and Bioelectronics (M&BE7), Fukuoka International Congress Center, Fukuoka, Japan, 2013/3/19 (*poster presentation*)

7. (Domestic) Y. Aoyama, T. Yamanari, Y. Shibata, N. Ohashi, Y. Suzuki, J. Mizukado, and Y. Yoshida" Direct effect of photooxidized poly(3-hexylthiophene) on the device characteristics in bulkhetero junction solar cell", 62nd the society of polymer science japan annual meeting (SPSJ 62nd), Kyoto International Conference Center, Japan, 2013/5/31 (*oral English communication*)

8. (Domestic) Y. Aoyama, T. Yamanari, and Y. Yoshida" Direct effect of photooxidized poly(3-hexylthiophene) on the solar cell device characteristic", 4th symposium in Tokyo university of science, Akihabara Convention Hall, Japan, 2014/1/22 (*poster presentation*)

9. (Domestic) Y. Aoyama, O. Douheret, P. Leclere, J. Mizukado, T. Miyadera, H. Suda, R. Razzaroni, Y. Yoshida " Conductivity degradation analysis of BHJ organic film dependent on P3HT molecular chain scission", annual Hokkaido meeting by Chemical Society of Japan, Hokkaido University, Japan, 2014/1/29 (*poster presentation*)

Acknowledgement

This thesis composes of research conducted on photooxidation of polythiophene derivatives and polythiophene used solar cells during 2011 – 2014 at the advanced low cost processing team in Research Center for Photovoltaic Technologies (RCPVT) of National Institute of Advanced Industrial science and Technology (AIST). The reported results are archived through interaction and collaboration with a number of colleagues to whom I am sincerely grateful.

Late in 2011, I was a master student of Hokkaido University. I asked Yuji Yoshida, who is both Professor of Tokyo institute of Technology and leader of RCPVT, whether to start working with organic solar cells or not as a Ph.D student. He kindly accepted me and became my supervisor. I am thankful for all the great discussions and some kinds of opportunities such as using a lot of experimental machines in AIST, working with AIST researchers, and studying abroad.

The work together with colleagues at RCPVT has been essential for many of the results in this thesis. When I started to work in 2011, I had no previous backgroud about organic solar cells. Dr. Toshihiro Yamanari, Dr. Masaru Nagai, Dr. Takaya Itou, Dr. Sasaki Kenich, Mrs. Yuka Yoshinuma, Mr. Yuuki Sugimoto, and other colleagues (polymer team members) had taught me the polymer solar cells and discussed with me, for which I am very grateful. Furthermore, Dr. Tetsuya Taima, Dr. Tetsuhiko Miyadera, Dr. Noboru Ohashi, Mr. Hiroyuki Ogou, Dr. Takaniro Kono, Dr. Zippen Wang, Dr. Yosei Shibata and other colleagues (small molecule team) had taught me how to use machines and sometimes discussed with me. I want to say thank

you for all members. In addition, Dr. Nagatoshi Koumura, Dr. Takurou Murakami, and Dr. Yu Uemura (Dye-sensitized team) had mainly gave me english instruction, for example, writing, speaking, oral presentation in conference, and how to spend a time in europe study abroad, for which I am very grateful.

The help from Prof. Hiroto Tachikawa (Hokkaido univ.) is also very grateful. He supported my experiment by using DFT cauculation, which was strong support. In addition, I would like to thank to Prof. Kazuhiro Marumoto and Mr. Tatsuya Nagamori (Tsukuba univ.) for LESR measurement support. Also, I particularly wish to thank Dr. Junji Mizukado (Research Institute for Innovation in Sustainable Chemistry (ISC) of AIST) for excellent collaboration, for stimulating discussions reviewing from polymer chemistry, for how to think and progress research with members, for english writing, and sometimes a lot of encouragement. He often treated me from our student view and had a friendly talk with me. I appreciate his great consideration for my Ph. D life.

Also, I should not omit acknowledgement Prof. Loberto Razzaroni, Dr. Philippe Leclere, Dr. Olivier Douheret, Mr. David Moreman, Mrs. Laurie letertre, Mrs. Marie-Sophie Renoirt, and Mrs Chinh NGO, Dr. Jenifier-Rubio Magnieto (UMONS and MateriaNova in Belgium) for all the discussions, for the much appericiated practical advices around this work, and for the enjoyable life in Belgium.

Finally, my family and my friends have always been important for me. Thank you for all members.

January 10, 2014
Yoshinori Aoyama